creative commons
COMMONS DEED

저작자표시-비영리-변경금지 2.0 대한민국

이용자는 아래의 조건을 따르는 경우에 한하여 자유롭게

- 이 저작물을 복제, 배포, 전송, 전시, 공연 및 방송할 수 있습니다.

다음과 같은 조건을 따라야 합니다:

저작자표시. 귀하는 원저작자를 표시하여야 합니다.

비영리. 귀하는 이 저작물을 영리 목적으로 이용할 수 없습니다.

변경금지. 귀하는 이 저작물을 개작, 변형 또는 가공할 수 없습니다.

- 귀하는, 이 저작물의 재이용이나 배포의 경우, 이 저작물에 적용된 이용허락조건을 명확하게 나타내어야 합니다.
- 저작권자로부터 별도의 허가를 받으면 이러한 조건들은 적용되지 않습니다.

저작권법에 따른 이용자의 권리는 위의 내용에 의하여 영향을 받지 않습니다.

이것은 이용허락규약(Legal Code)을 이해하기 쉽게 요약한 것입니다.

Disclaimer

dCollection

공학박사학위논문

융합 디지털 트윈을 위한 물리-데이터 기반 모델의 통계적 모델 보정 및 갱신 방법 연구

Investigation on Statistical Model Calibration and Updating of Physics and Data-driven Modeling for Hybrid Digital Twin

2022 년 02 월

서울대학교 대학원

기계항공공학부

김 원 곤

융합 디지털 트윈을 위한 물리-데이터 기반 모델의 통계적 모델 보정 및 갱신 방법 연구

Investigation on Statistical Model Calibration and Updating of Physics and Data-driven Modeling for Hybrid Digital Twin

지도교수 윤 병 동

이 논문을 공학박사 학위논문으로 제출함

2021 년 10 월

서울대학교 대학원

기계항공공학부

김 원 곤

김 원 곤의 공학박사 학위논문을 인준함

2021 년 12 월

위 원 장 : 김 윤 영 (인)

부위원장 : 윤 병 동 (인)

위 원 : 김 도 년 (인)

위 원 : 이 호 원 (인)

위 원 : 윤 헌 준 (인)

Abstract

Investigation on Statistical Model Calibration and Updating of Physics and Data-driven Modeling for Hybrid Digital Twin

Wongon Kim
Department of Mechanical and Aerospace Engineering
The Graduate School
Seoul National University

Digital Twin technology, a virtual representation of the physical entity, has been explored toward providing a solution that could support engineering decisions, such as design, manufacturing, and system health management. Digital twin approaches can be divided into three categories: 1) data-driven, 2) physics-based, and 3) hybrid approaches. The hybrid digital twin is recognized as a promising solution for reliable engineering decisions based on the observed data because it utilizes both the data-driven and physics-based models to overcome the disadvantages of these two approaches. However, the applicability of the digital twin approach has been limited by a lack of prior information. The prior information includes the statistics of model input parameters, required information for (data-driven, physics-based, and hybrid)

modeling, and prior knowledge about system failure.

Now, a question of fundamental importance arises how to help decision-making using a digital twin under a given insufficient prior information. Statistical model calibration and updating can be used to validate the digital twin analysis under insufficient prior information. In order to build a hybrid digital twin under insufficient prior information, this doctoral dissertation aims the investigation on three co-related research areas in model calibration and updating:

Research Thrust 1 – Data-driven dynamic model updating for anomaly detection with an insufficient prior information

Research Thrust 2 – A new calibration metric formulation considering statistical correlation

Research Thrust 3 – Hybrid model calibration and updating considering system failure

A sufficient prior knowledge such as observed data in various conditions, geometry, material properties, and operating conditions for data-driven / physics-based modeling are required to build a valid digital twin model. However, the prior information for modeling is hard to obtain for complex engineering system. Research Thrust 1 proposes Data-driven dynamic model updating for anomaly detection with insufficient prior knowledge. The time-frequency domain features are extracted from the observed signal using signal pre-processing. The state-space model is driven by a numerical algorithm for subspace state-space system identification (N4SID) to predict the extracted features under different operating conditions. In the model, the operating

condition is defined as a parameterized input signal of a system model. Next, the input signal parameters are updated to minimize the prediction error that quantify the discrepancy between the target observed signal and reference model prediction.

Optimization-based statistical model calibration (OBSMC) can be applied to estimate unknown input parameters of the digital twin. In OBSMC, the unknown statistical parameters of input variables associated with a digital twin model are inferred by maximizing the statistical similarity between predicted and observed output responses. A calibration metric is defined as the objective function to be maximized that quantifies statistical similarity. Research Thrust 2 proposes a new calibration metric: Marginal Probability and Correlation Residual (MPCR), to improve the accuracy and efficiency of model calibration considering statistical correlation. The foundational idea of the MPCR is to decompose a multivariate joint probability distribution into multiple marginal probability distributions while considering the statistical correlation between output responses.

In order to diagnose and predict the system failure of a complex engineering system without prior knowledge about system failure using the digital twin, uncertainties in manufacturing and test conditions must be taken into account. Research Thrust 3 proposed a hybrid digital twin approach for estimating fatigue crack initiation and growth considering those uncertainties. The proposed approach for estimating fatigue crack initiation and growth is based on two techniques; (i) statistical model calibration and (ii) probabilistic element updating. In statistical model calibration, statistical parameters of input variables that indicate uncertainties in manufacturing and test conditions are estimated based on the observed response related to the crack initiation condition. Further, probabilistic analysis using estimated statistical

parameters can predict possible critical elements that indicate crack initiation and growth. In probabilistic element updating procedures, the possible crack initiation and growth element is updated based on the Bayesian criteria using observed responses related to the crack growth condition.

Keywords: Digital Twin
Model Validation & Verification
Optimization-based Statistical Model Calibration
Parameter Estimation

Student Number: 2015-22710

Table of Contents

List of Tables

List of Figures

Nomenclatures

$\hat{\mathbf{Y}}_{\text{pre}}$	predicted (model) output response
$\mathbf{Y}_{\text{obs}}$	observed (experimental) output response
$\mathbf{X}$	model input variables
$\boldsymbol{\theta}$	calibration parameters
$\boldsymbol{\theta}^{\text{U}}$	upper bound of calibration parameter
$\boldsymbol{\theta}^{\text{L}}$	lower bound of calibration parameter
ρ	Pearson correlation coefficient
μ_i	mean of the *i*-th model input variable
σ_i	standard deviation of the *i*-th model input variable
m_i	mean of the *i*th observed output response
M_i	mass of *i*-th lumped mass
C_i	damping coefficient of *i*-th lumped damper
K_i	stiffness of *i*-th lumped stiffness
cv_{ij}	The *i* row *j* column components of the covariance matrix
f_{CM}	calibration metric
JL	joint likelihood metric
ML	marginal likelihood metric
MM	moment matching metric
MPCR	marginal probability correlation residuals
MPR	marginal probability residuals
CCR	correlation coefficient residuals
s	phase modulation parameter
P	amplitude modulation parameter
L_2	L_2-norm

σ_t	time delay parameter of impulse force
E_b	Young's modulus of beam
ρ_b	density of beam
$u(t)$	pseudo excitation force
A	system matrix
B	input matrix
C	output matrix
D	feedthrough matrix
[X]	state vector
[U]	input vector
σ_n	standard deviation of the measurement noise
T	large time scale
t	small time scale
$Y(t, f)$	time-frequency feature using short time Fourier transform
$\boldsymbol{Y}_N$	observed response related to crack initiation
$\boldsymbol{Y}_F$	observed response related to crack growth
$\widehat{\boldsymbol{Y}}_{DT}$	predicted (model) output response by data-driven twin
$\widehat{\boldsymbol{Y}}_{PT}$	predicted (model) output response by physics-based twin
L	likelihood function
e_i	i-th candidate element
K_i	Bayes factor calculation at i-th iteration
$\boldsymbol{\Delta Y}_{\mathrm{F}}$	observed response transition during crack growth
$\boldsymbol{\gamma}_k$	parameter noise at k-th time step
$\mathbf{Q}_k$	parameter noise covariance matrix at k-th time step
$[\boldsymbol{f}]_{k+1}$	input excitation time history from time t_1 to t_{k+1}
$\boldsymbol{u}_0$	initial nodal displacement

$\dot{\boldsymbol{u}}_0$	initial velocity vector
$\boldsymbol{v}_{k+1}$	measurement noise at $k+1$-th time step
$\mathbf{R}_{k+1}$	measurement noise covariance matrix at $k+1$-th time step
$\boldsymbol{P}^{-}_{\boldsymbol{\theta y},\boldsymbol{k+1}}$	estimated parameter response cross-covariance matrix at $k+1$-th time step
$\boldsymbol{P}^{-}_{\boldsymbol{y},\boldsymbol{k+1}}$	the estimated response covariance matrix

Chapter 1

Introduction

1.1 Motivation

A digital twin connects physical entities in the real world and a computational model in the virtual world using the observed response from a real system to help make an engineering decision for design, maintenance, and control. However, the applicability of the digital twin approach has been limited by a lack of data and computational power until the last few years. Today, sensor and data acquisition and data processing systems are getting more reliable and affordable. Thus, the digital twin approach has gained more attention for design, control, and maintenance of physical entities.

In digital twin approaches, the simulation model must be improved using the observed response. Simulation models used in digital twin approaches can be categorized into 1) data-driven and 2) physics-based models. Data-driven models, such as classical machine learning [1]–[3] and deep-learning using neural networks [4], [5] have been proposed to diagnose and design of the system using an experimentally observed response. Data-driven models rest on past experimental

data to predict the performance or condition of the engineered system. However, the methods require enough data to predict the performance or condition of the engineered system of interest. Further, the results of data-driven models are less interpretable than those of physics-based models. Physics-based models, such as finite element-based models [6]–[10] and dynamic system models [11], have been used to simulate the physical process of system behavior. However, due to the uncertainties in modeling and simulation, it is challenging to predict system behavior with high accuracy using physics-based models. In addition, the expensive computational cost is a constraint of physics-based models. The hybrid digital twin approach uses both data-driven and physics-based models simultaneously to capitalize on the advantages of each method while minimizing the disadvantages of each method.

It requires sufficient prior information to build valid digital twin model. The prior information includes 1) required information for (data-driven, physics-based, and, hybrid) modeling, 2) the statistics of model input variables, and 3) prior knowledge about system failure.

Even though the IoT sensor and data-acquisition system getting affordable, most of the data from the system are unlabeled and not informative for training the data-driven model. And the physics-based model with a lack of information such as geometry, operating condition, and test condition is in-valid as a digital twin. So, the digital twin method with insufficient prior information for modeling is required. And the input variables in digital twin models have a certain amount of physical uncertainty, such as inherent variability in material properties and manufacturing tolerances. A digital twin model that uses a deterministic form fails to analyze an

engineered system accurately. The effects of physical uncertainty thus have to be taken into account to improve the predictive capability of digital twins. To conduct accurate statistical analysis considering the uncertainty, the statistical information of physical uncertainty should be appropriately estimated. The various physical status of the system should be identified and represented by the digital twin. However, the prior knowledge of system failure, such as the failure location and severity, is quite uncertain and unidentifiable. So, the statistical and probabilistic prognostics and diagnostics of system failure using the digital twin method are required.

To deal with those issues, many research efforts have been made to develop digital twin approach with insufficient prior information. However, there is still a great need for a hybrid digital twin approach to elaborate on analyzing the engineering system. First, whereas a significant number of studies have focused on the improvements of data-driven modeling using imbalanced data set such as auto-encoder [12] and physics-guided machine learning [13], [14], relatively little attention has been paid to investigating model updating. Model updating can improve the accuracy of a digital twin for target engineered system. And updated model and prediction results can be used to detect anomaly conditions. The data-driven model with a large number of parameters is not efficient for model updating. So, the efficient model updating method with insufficient prior information needs to be researched. Second, many research focusing on the statistical model calibration to estimate the statistical parameter of model input variables [15]–[23]. Optimization-based statistical model calibration is formulated as an unconstrained optimization problem that infers the unknown statistical parameters of input variables associated with a digital twin model by maximizing the statistical similarity

between predicted and observed output responses [20], [23]–[25]. A calibration metric is defined as the objective function to be maximized that quantifies statistical similarity. A critical challenge in formulating a calibration metric is appropriate considering the statistical correlation in output responses. Third, the digital twin needs to be updated under system failure without prior information about system failure. And updating accuracy under system failure is sensitive to uncertainties in manufacturing and test conditions. So, the uncertainties have to be taken into account to update the digital twin under system failure. However, probabilistic analysis considering the uncertainty needs expensive computational cost. Therefore, the above three technical challenges should be properly addressed to realize digital twin in reality successfully.

1.2 Research Scope and Overview

This doctoral dissertation aims at advancing three essential and co-related research areas in statistical model calibration & updating for hybrid digital twin: (1) Research Thrust 1 – Data-driven Dynamic Model Updating for Anomaly Detection ; (2) Research Thrust 2 – A New Calibration Metric that Considers Statistical Correlation; and (3) Research Thrust 3 – Hybrid Model Calibration and Updating For Estimating System Failure. The research scope in this doctoral dissertation is to develop technical advances in the following three research thrusts:

Research Thrust 1: Data-driven Dynamic Model Updating for Anomaly Detection

Research Thrust 1 proposes Data-driven dynamic model updating for anomaly detection with insufficient prior knowledge. The time-frequency domain features are extracted from the observed response using signal pre-processing. The state-space dynamic model is driven by the system identification method, a numerical algorithm for subspace state-space system identification (N4SID). In the model, the operating condition is defined as a parameterized input excitation force of the dynamic model. Next, the amplitude and phase modulation parameter of excitation force are updated to minimize the prediction error that can quantify the discrepancy between the reference model prediction and target observed response in different operating condition and system state. An optimization-based parameter tuning was originally applied to estimate the operating condition of the engineering system. Health indices, such as time delay of operation, prediction error by anomaly system operation, can be derived from the digital twin analysis using the proposed method.

Research Thrust 2: A New Calibration Metric that Considers Statistical Correlation

In optimization-based statistical model calibration, a calibration metric, which is defined as an objective function to be minimized (or to be maximized), is used to quantify the statistical dissimilarity (or similarity) between the predicted and observed output responses. If the statistical correlation between multivariate output

responses is not properly considered, some calibration parameters could converge to physically unreasonable values, even if the optimal set of the calibration parameters is mathematically valid. Research Thrust 2 proposes a new calibration metric considering statistical correlation: Marginal Probability and Correlation Residual (MPCR). The foundational idea of the MPCR is to decompose a multivariate joint probability distribution into multiple marginal probability distributions, while considering the statistical correlation between output responses. The MPCR has favorable properties, such as normalization, boundedness, and marginalization. Two mathematical and two engineering examples are presented to demonstrate the effectiveness and potential benefits of the MPCR.

Research Thrust 3: Hybrid Model Calibration and Updating considering System Failure

Maintaining high predictive capability of a digital twin model under system failure is of great concern to the engineers who make design decisions at the early stages of product development. The predictive capability of the digital twin approach is improved by considering uncertainties in manufacturing and test conditions. Research Thrust 3 proposed hybrid digital twin approach for estimating system failure considering the uncertainties. The proposed approach for estimating system failure is based on two techniques; (i) statistical model calibration and (ii) probabilistic element updating. In statistical model calibration, statistical parameters of input variables are estimated based on the observed response related to the failure initiation condition. Further, probabilistic analysis using estimated statistical

parameters can predict possible critical elements that indicate failure location and severity. In probabilistic element updating procedures, the possible failure location and growth element is updated based on the observed response related to the failure severity condition.

As shown in Figure 1-1, valid hybrid digital twin can be formulated using proposed methods in this doctoral dissertation. The data-driven and physics-based model can be calibrated and updated with insufficient prior knowledge using proposed methods. The egineering decisions such as design, diagnostics, prognostics and control of the system can be made with valid hybrid digital twin analysis.

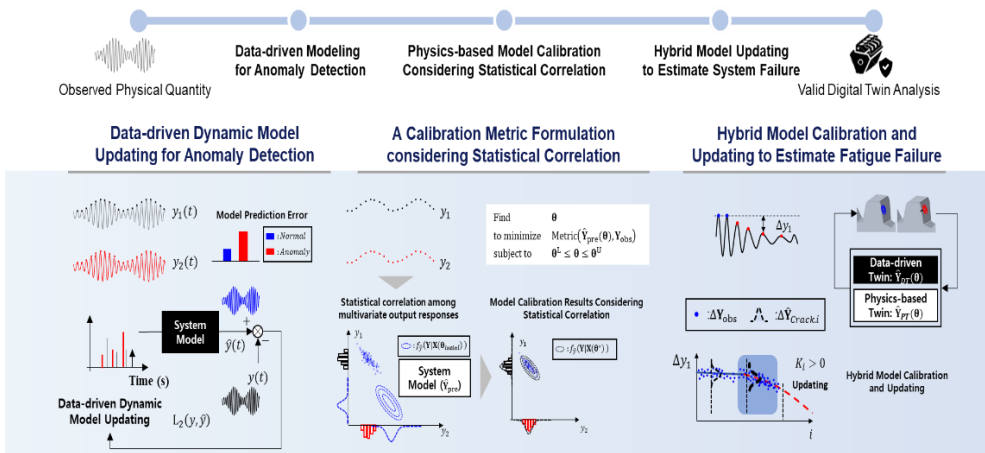

Figure 1-1 Proposed hybrid digital twin framework

1.3 Dissertation Layout

This doctoral dissertation is organized as follows. Chapter 2 reviews the current state of knowledge regarding digital twin and statistical model calibration. Chapter 3 presents an data-driven model updating for anomaly detection with an insufficient

prior information for modeling (Research Thrust 1). Chapter 4 propose a new calibration metric considering statistical correlation: Marginal Probability and Correlation Residuals (MPCR) (Research Thrust 2). Chapter 5 addresses hybrid digital twin approach to estimate the system failure and severity. Finally, Chapter 6 summarizes the doctoral dissertation with its contributions and suggests future research directions.

Chapter 2

Literature Review

To provide readers with sufficient background information, this chapter is designated to present the literature reviews of the knowledge within the scope of this doctoral dissertation: (1) Digital Twin Formulation: 1) Data-driven, 2) Physics-based and 3) Hybrid Digital Twin; (2) Digital Twin Calibration & Updating; Literatures on each of these aspects are discussed in subsection and challenges are address. Since this doctoral dissertation focuses on how to calibrate and update the hybrid digital twin under in-sufficient prior knowledge, perspectives of data-driven and physics-based digital twin model are not reviewed here in detail.

2.1 Digital Twin Formulation

A digital twin is numerical model in virtual world to mimic and simulate the physical system in real world as shown in Figure 2-1. A conventional simulation model with non-real time modeling data gives a weak engineering intuition to an engineer. On the other hand, the digital twin which mimics operating systems using real time gives a strong engineering decision support in real time. Depending on the given prior information, digital twin can be formulated in various type :1) Data-driven, 2)

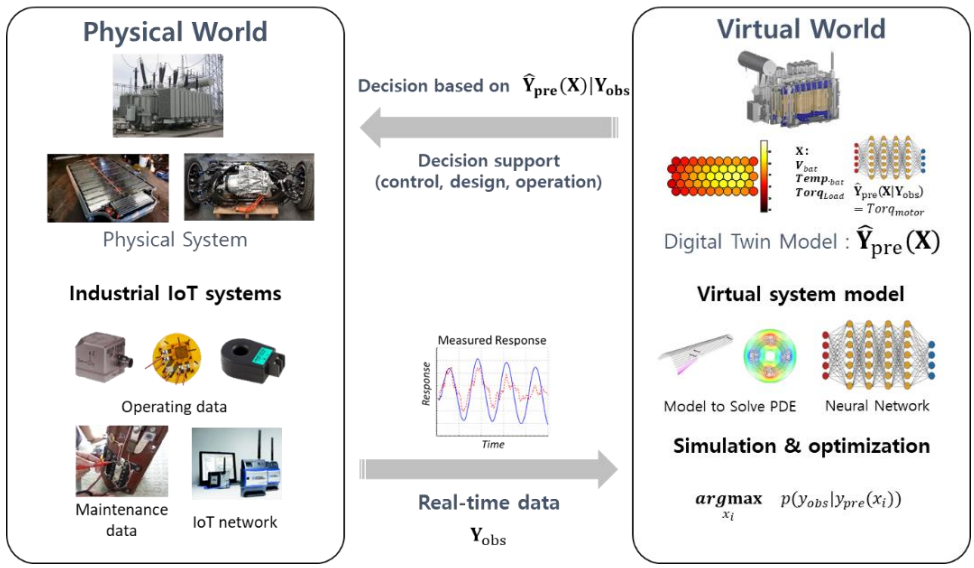

Figure 2-1 Digital twin for engineering decision support

Physics-based and 3) Hybrid digital twin. The characteristics and example of each method will be briefly explained in following subsection.

2.1.1 Data-driven Digital Twin

The data-driven digital twin is statistically trained and validated using machine learning & deep-learning method. As shown in Figure 2-2, the data-driven model have a pros and cons. Further, the data-driven digital twin is widely applicable for various fields. Meraghni et al. (2021) proposed a deep-learning based digital twin framework for proton exchange membrane fuel cell remaining useful life prediction. The stacked de-noising auto encoders are proposed to capture the degradation behavior of fuel cell [26]. Wang et al. (2020) proposed a digital twin approach for visualized weld joint growth monitoring and penetration control. Convolutional neural network model estimate the welding quality and geometry using the

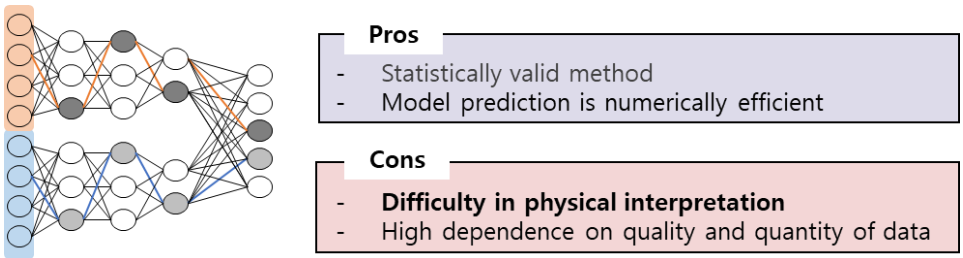

Figure 2-2 Pros and Cons of data-driven digital twin approach.

information available directly from sensors including weld pool images, arc images, welding current and arc voltage [27].

To train the data-driven model, sufficient data including the status and label of the target system is required. However, it is suffer from lack of the data and information in most engineering system. To overcome those situation, many research focusing on the transfer-learning and data-augmentation [4], [12], [28]–[31].

Transfer learning is a set of methods that enhance learning target domain based upon previously acquired knowledge in source domain. Here, knowledge is transferred from source domain to another target domain in order to reduce the amount of data or time needed to train a machine learning algorithm. Xu et al. (2019) proposed a digital-twin for fault diagnosis using deep transfer learning [4]. The proposed method combines advantages of both deep learning and transfer learning. It trains the deep-learning model to extract high level knowledge in the source domain where there is a huge amount of data available, and then transfer it to the target domain which has different data distributions. Li et al. (2021) proposed the wind turbine fault diagnosis based on transfer learning and convolutional auto encoder with small-scale data [12]. The convolutional auto encoder network with

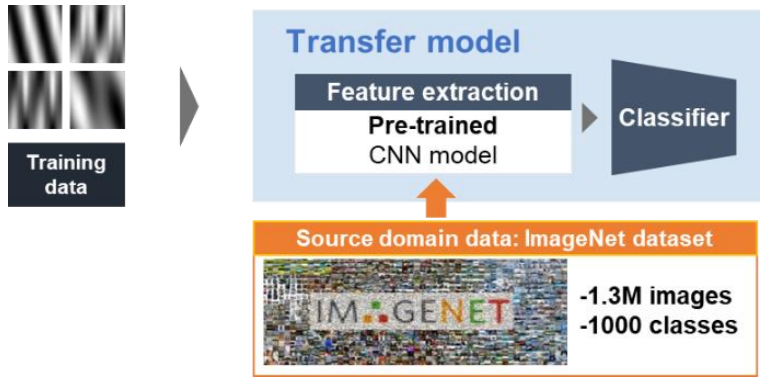

(a) Convolution-neural network based transfer learning

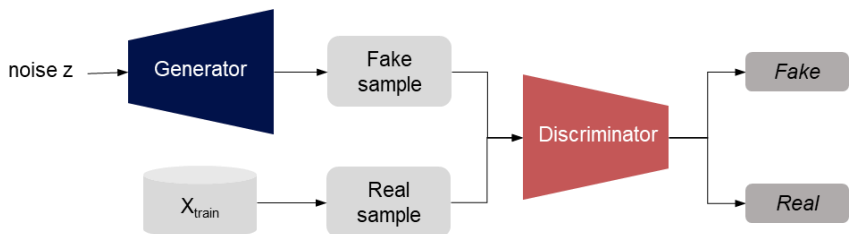

(b) Generative adversarial network based data-augmentation

Figure 2-3 Examples of data-driven digital twin: (a) transfer learning, (b) data-augmentation.

parameter-based transfer learning is proposed. Parameter-based transfer learning employs a neural network to transfer knowledge between domains by sharing parameters and fine tuning.

The data-driven model trained with small number of training data can suffer from over-fitting and invalid model prediction. To overcome the lack of the data, data-augmentation method applied to increase the training data. There are various augmentation method including data driven and physics based method. Data driven method includes traditional signal processing (e.g. additional Gaussian noise, signal

translation, amplitude shifting and time stretching) and deep learning based data-augmentation (e.g. generative adversarial network) [28]–[30]. Generative adversarial networks (GANs) have been proved to be able to produce artificial data that are alike the real data, and have been successfully applied to various image generation tasks as a useful tool for data augmentation. Shao et al. (2019) developed auxiliary classifier GAN to learn from mechanical sensor signals and generate realistic one-dimensional raw data [29]. K. Yu et al. (2020) proposed a multi-stage semi-supervised learning (SSL) approach for fault diagnosis of rolling bearing using data augmentation and metric learning [30]. In the proposed SSL, small number of labeled data were randomly augmented using 7 traditional signal processing augmentation strategies. Then, semi-supervised learning using clustering were conducted to diagnose the bearing faults.

However, the data-driven model with insufficient information still require enough data and prior information about data. And It is hard to explain the analysis results and ensure the prediction accuracy in unknown operating and exploration domains.

2.1.2 Physics-based Digital Twin

A physics-based digital twin – such as a finite element model or a system dynamic model – has been widely used for design and control. Figure 2-4 shows pros and cons of physics-based digital twin. Physics-based model analysis is less dependent on data and is physically interpretable. Guivarch et al. (2019) applied multibody simulation to digital twin modeling of a helicopter [32]. Jain et al. (2019) proposed a dynamic model of a distributed photovoltaic energy conversion unit (PVECU); the error residual was calculated to diagnose the PVECU [33]. However, a physical

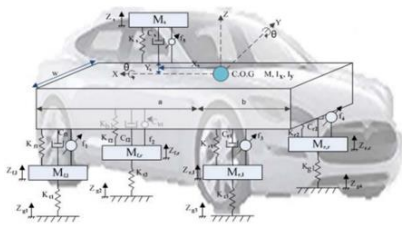

Pros

- Health state w/ physical meaning
- Less dependence on data

Cons

- **Invalid physical** assumption
- Simulation is numerically expensive

Figure 2-4 Pros and Cons of physics-based digital twin approach.

digital twin model can be invalid due to improper physical assumptions. Further, physics-based model analysis is often numerically expensive for complex and large-scale engineered systems.

As the relevant physical phenomena taking place in an engineered system become more complex, a physics-based model needs to be more sophisticated. However, it is not easy to fully characterize the physics in the real system using physics-based model due to limited resources (e.g., time, budget, and computation costs). To overcome those situation, many research focusing on the model verification & validation (V&V) and model refinement (including non-linear analysis).

V&V activities include model verification and model validation. According to the ASME and AIAA guides [34], [35], model verification is defined as the process of determining whether a model's implementation accurately represents the developer's conceptual description of the model. Model validation is defined as the process of determining the degree to which a model is an accurate representation of the real phenomenon from the perspective of the intended uses of the model. It is

important that the model validation is including both a process of assessing the accuracy of a computational model and a process of improving the model based on the validation results.

For the model calibration, deterministic methods were proposed in several studies [36], [37]. Although the deterministic methods effectively reduce the discrepancy between observed and predicted responses, deterministic adjustment of model parameters can significantly degrade the predictive capability of the digital twin in statistical sense [35], [38]. Recently, for this reason, statistical methods have received significant attention [39]–[41]. However, it is hard to conduct statistical model validation because of several existing issues, including uncertainty quantification, uncertainties in model variables and statistical model validation, etc. Statistical methods are superior to deterministic methods since they attempt to enhance the digital twin's predictive capability by thoroughly addressing uncertainties in a real system and digital twin. The sources of uncertainties in digital twin should be properly investigated in the statistical model validation.

In most engineering problems, the sources of uncertainties can be divided into three sources: (1) physical, (2) modeling, and (3) statistical uncertainties [42]–[44]. The physical uncertainty comes from inherent uncertatinty in physical quantities, whereas the modeling uncertainty is from inadequate or erroneous models. The statistical uncertainty is attributed to the lack of prior information about uncertainties. In principle, the existence of these uncertainties in engineering systems can be either recognized, unrecognized or a combination of both. Numerous studies attempted to effectively incorporate various aspects of uncertainty in statistical model validation.

Figure 2-5 describes a framework of statistical model validation, which consists of the sequentially-executed three procedures: 1) model calibration, 2) validity check, and 3) model refinement. Statistical model calibration refers to an activity that infers the statistical parameters of unknown model input variables. Validity check is an activity to quantitatively determine the degree of the validity of a digital twin model by comparing the observed output response with predicted ones. Representative methods for validity check includes generalized u-pooling method considering correlation [45], [46] and Bayesian hypothesis test [47]. If validity check turns out to be invalid, model refinement should be performed by revisiting the physical behavior of a digital twin model [24], [25]. The uncertainties of output response propagated from the aleatory uncertainties are quantified in forward problem. And to reduce uncertainty in epistemic variable, the unknown statistical parameters are

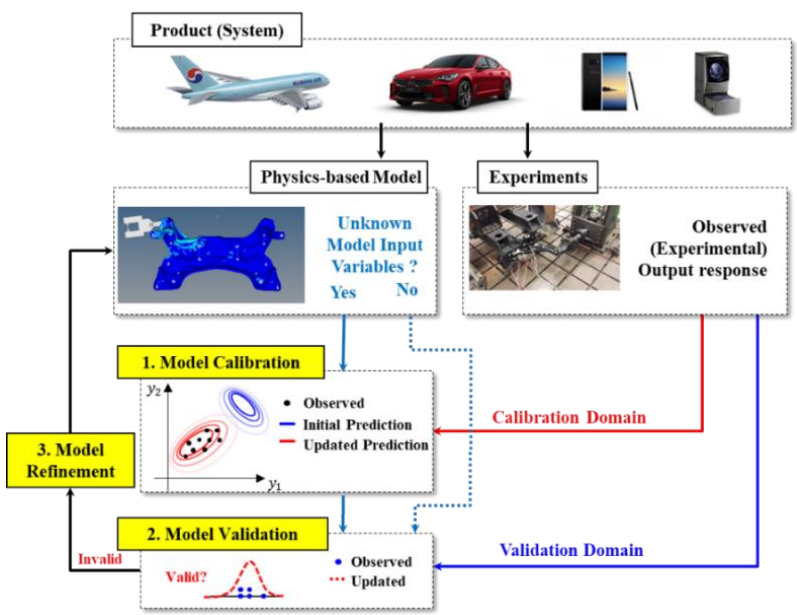

Figure 2-5 Framework of statistical model verification and validation

inferred using inverse problem which is statistical model calibration.

2.1.3 Hybrid Digital Twin

To overcome the disadvantages of data-driven and physics-based approaches, the hybrid digital twin simultaneously utilizes both the physics-based and the data-driven model. Li et al. (2017) proposed a hybrid digital twin using an airplane wing finite element model and a Bayesian network approach, considering uncertainty sources such as material properties and manufacturing tolerance in the system [48]. Roohi et al. (2019) proposed state estimation approaches using state observers for assessment of instrumented wood-frame buildings [49]. Wang. B et al. (2021) suggested data-driven digital twin of proton exchange membrane fuel cells to overcome the computation cost of multi-physics-analysis as shown in Figure 2-6 (a) [50]. The previous hybrid digital twin approach uses the predicted data from a physics-based model as training data for a data-driven model to overcome a lack of data. However, an invalid physics-based model prediction that is based on unknown input variables and invalid assumptions can result in poor data-driven model performance.

To overcome this problem in the hybrid digital twin model, statistical model updating can be a good strategy for improvement. Xia et al. (2021) proposed hybrid digital twin approach which is digital twin-assisted deep transfer learning as shown in Figure 2-6 (b) [51]. In this work, the de-noising auto-encoder is pre-trained using the data generated from physics-based model and update the model using transfer learning method. Yu et al. (2021) proposed hybrid digital twin model based on nonparametric Bayesian network and real-time model updating based on the Gaussian particle filter and dirichlet process mixture model [52].

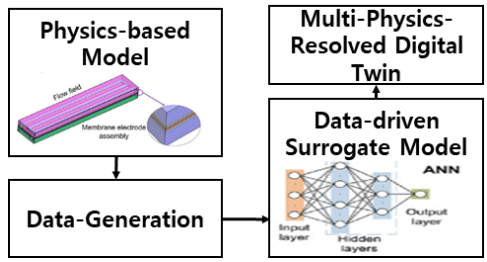

(a)

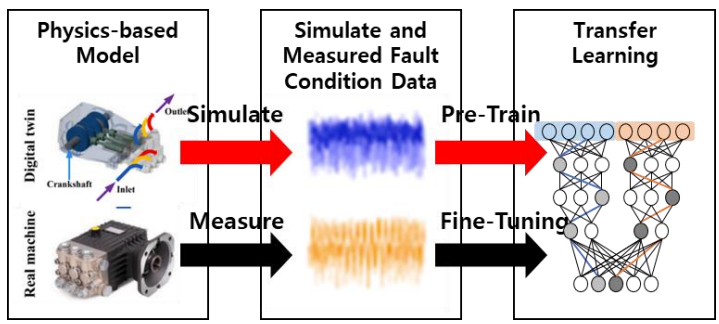

(b)

Figure 2-6 Examples of hybrid digital twin: (a) Multi-Physics-Resolved digital twin, (b) Intelligent fault diagnosis of machinery

However, the computation cost to update the large number of parameter in data-driven model of hybrid digital twin is expensive for real-time updating and prediction. And the updated results such as parameter variation in network, prediction error are not physically interpretable.

2.2 Digital Twin Calibration & Updating

Compared with conventional simulation models, a distinct characteristic of a digital twin is its ability to update predicted performances simultaneously with a real system change. The system change can be reflected in digital twin by calibrating digital twin

input parameters and updating digital twin model structure. Statistical model calibration and updating is thus of great importance as a strategy to improve the predictive capability of a digital twin model [15], [17], [20]–[23], [53], [54]. Representative methods for statistical model calibration and updating include optimization-based statistical model calibration approaches [20], [23], [24] and parameter estimation using Kalman/ Particle based filter [55]. These methods were developed with different backgrounds and philosophies. The characteristics and example of each method will be briefly explained in following subsection.

2.2.1 Optimization-based Statistical Model Calibration

From the frequentist perspective, a PDF is an effective way to statistically characterize the inherent variability in input variables and output responses. The PDF can be parameterized by statistical parameters. For instance, a normal distribution is fully characterized by the mean and standard deviation. In practice, however, some statistical parameters are unknown due to a lack of data. Therefore, optimization-based statistical model calibration inversely estimates the unknown statistical parameters, which are defined as calibration parameters, by maximizing the agreement (or minimizing the disagreement) between the two probability distributions of the predicted and observed output responses.

Optimization-based statistical model calibration can be formulated as a design problem without constraint function as:

$$\underset{\boldsymbol{\theta}}{\text{Minimize}} \text{ or } \underset{\boldsymbol{\theta}}{\text{Maximize}} \; f_{\text{CM}}\left(\widehat{\mathbf{Y}}_{\text{pre}}(\boldsymbol{\theta}), \mathbf{Y}_{\text{obs}}\right) \tag{2.1}$$

where $\boldsymbol{\theta}$ denotes a calibration parameter vector; and $f_{\mathrm{CM}}\left(\widehat{\mathbf{Y}}_{\mathrm{pre}}(\boldsymbol{\theta}), \mathbf{Y}_{\mathrm{obs}}\right)$ denotes a calibration metric, which is defined as an objective function to be maximized or minimized. The lower and upper bounds of the calibration parameters, denoted by $\boldsymbol{\theta}^{\mathrm{L}}$ and $\boldsymbol{\theta}^{\mathrm{U}}$, can be determined based on prior information. Calibration metrics can quantify statistical similarity or dissimilarity between the predicted and observed output responses. To find the optimal set of the calibration parameters, a sequential quadratic programming, genetic algorithms, or another advanced optimization solver can be used as a searching algorithm [23], [56]. Selecting a proper optimizer is important to improve the accuracy of optimization-based statistical model calibration. There might be several local minimums in a solution space because of the nonlinearity between the input variables and output responses. As such, a global optimization solver such as a genetic algorithm and multi-start gradient method is preferred. Figure 2-7 describes the procedure for optimization-based statistical model calibration, which is summarized as follows:

- Step 1. Identify the unknown input variables that contribute significantly to the output response. The number of calibration parameters in an unconstrained optimization problem can be reduced through variable screening.

- Step 2. Assume the probability distribution type of each model input variable identified in Step 1. The type of the probability distribution can be decided based on prior information such as an expert's opinion.

- Step 3. Initialize the calibration parameters $\boldsymbol{\theta}_{i=1}$ and their lower and upper

bounds $\boldsymbol{\theta}^{L}$ and $\boldsymbol{\theta}^{U}$.

- Step 4. Perform uncertainty propagation (UP) analysis to probabilistically quantify the uncertainties in the output response that are propagated from the variability in the model input variables through a CAE model. Since a common challenge in UP analysis is a multidimensional integration to quantify the probabilistic nature of the output responses, many research efforts have been made to develop UP methods, such as 1) sampling methods, 2) expansion methods, 3) response surface approximate methods, and 4) approximate integration methods. Applying sampling methods directly would be not affordable due to its considerable computational cost. However, once an accurate surrogate model is available, the Monte Carlo simulation can be applied to the accurate surrogate model to perform the uncertainty propagation with affordable computational burden. Since UP analysis is required for every iteration in optimization-based statistical model calibration, an appropriate method should be selected with consideration of accuracy and efficiency.

- Step 5. Calculate the calibration metric to quantify the statistical similarity (or dissimilarity) between the observed and predicted output responses.

- Step 6. Update the calibration parameters until the calibration metric is maximized or minimized. If the convergence criterion is satisfied, stop the iteration; otherwise set *i=i+1* and repeat Steps 4 to 6.

In optimization-based statistical model calibration, a calibration metric, which is defined as an objective function to be minimized (or to be maximized), is used to quantify the statistical dissimilarity (or similarity) between the predicted and

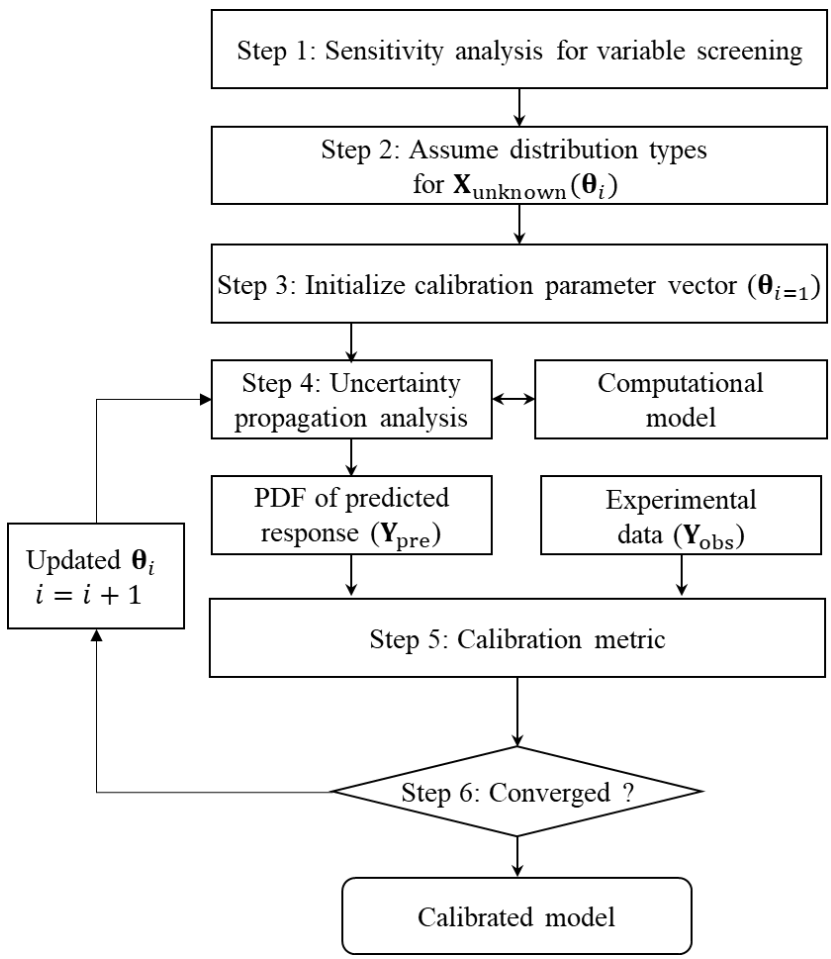

Figure 2-7 Procedure for optimization-based statistical model calibration

observed output responses. This implies that the effectiveness of optimization-based statistical model calibration strongly depends on how the calibration metric is formulated. If a calibration metric is not well-defined, optimization-based statistical model calibration could fail to accurately infer the calibration parameters. There have been several calibration metrics proposed in the literature, including the marginal likelihood (ML) metric [53], the joint likelihood (JL) metric [17], the moment matching metric [57], and statistical distance based metrics [58]. Since optimization-based statistical model calibration inversely estimates the calibration parameters by maximizing the agreement (or minimizing the disagreement) between the two probability distributions of the predicted and observed output responses, the calibration metric should be carefully formulated to properly account for the information obtained from the output responses. It has been reported that the use of multiple output responses as additional information can improve identifiability in statistical model calibration, thereby better inferring the calibration parameters [59], [60]. It is worth pointing out that the statistical correlation between multivariate output responses is not to be overlooked in optimization-based statistical model calibration [46]. Based on the authors' experiences, if the statistical correlation between multivariate output responses is not properly considered, some calibration parameters could converge to physically unreasonable values, even if the optimal set of the calibration parameters is mathematically valid. In other words, neglecting the statistical correlation might lead to arriving at a physically unreasonable solution in optimization-based statistical model calibration. For the ML metric, since multivariate output responses are assumed to be statistically independent of each other, the ML metric cannot consider the statistical correlation between them. The statistical distance-based metrics such as the Bhattacharyya distance and

Mahalanobis distance have the limitation similar to the likelihood metric, including un-boundedness and joint PDF modeling issues. Even though the moment matching and JL metrics are able to quantify the statistical correlation for the purpose of model calibration, those metrics have their own limitations that will be discussed in Section 4. This drives research interest in developing a new calibration metric that is able to consider the statistical correlation between multivariate output responses.

2.2.2 Parameter Estimation using Kalman/ Particle filter

To update the digital twin model using the observed time varying (dynamic) signal with a physics-based model, parameter estimation is conducted using an Kalman-based filter. The model parameter $\boldsymbol{\theta}$ is modeled as a Gaussian Markov process as:

$$\boldsymbol{\theta}_{k+1} = \boldsymbol{\theta}_k + \boldsymbol{\gamma}_k \tag{2.2}$$

where $\boldsymbol{\gamma}_k$ denotes parameter noise that follows a normal distribution with zero mean and covariance ($\mathbf{Q}_k$). The system model output is modeled as

$$\mathbf{y}_{k+1} = \boldsymbol{h}_{k+1}(\boldsymbol{\theta}_k, [\boldsymbol{f}]_{k+1}, \boldsymbol{u}_0, \dot{\boldsymbol{u}}_0) + \boldsymbol{v}_{k+1} \tag{2.3}$$

where h_{k+1} is the k+1-th time step acceleration response function of the proposed dynamic model; $[\boldsymbol{f}]_{k+1}$ denotes the input excitation time history from time t_1 to t_{k+1}. The terms $\boldsymbol{u}_0$ and $\dot{\boldsymbol{u}}_0$ are the initial nodal displacement and velocity vector, respectively. The initial condition is assumed as at rest (that is, $\boldsymbol{u}_0 = \dot{\boldsymbol{u}}_0 = 0$). Further, $\boldsymbol{v}_{k+1}$denotes measurement noise, which follows a normal distribution with zero mean and covariance ($\mathbf{R}_{k+1}$). The initial model parameter and covariance matrix is assumed as

$$\widehat{\boldsymbol{\theta}}^{+}{}_{0} = E[\boldsymbol{\theta}_0] \tag{2.4}$$

$$\boldsymbol{P}^{+}_{\boldsymbol{\theta},\mathbf{0}} = \mathbf{E}[(\boldsymbol{\theta}_0 - \widehat{\boldsymbol{\theta}}_0)(\boldsymbol{\theta}_0 - \widehat{\boldsymbol{\theta}}_0)] \tag{2.5}$$

The prior parameter and covariance matrix is estimated as

$$\widehat{\boldsymbol{\theta}}^{-}{}_{k+1} = \widehat{\boldsymbol{\theta}}^{+}{}_{k} \tag{2.6}$$

$$\boldsymbol{P}^{-}_{\boldsymbol{\theta},\boldsymbol{k+1}} = \boldsymbol{P}^{+}_{\boldsymbol{\theta},\boldsymbol{k+1}} + \mathbf{Q}_{\boldsymbol{k}} \tag{2.7}$$

The response sensitivity with respect to the parameter is calculated as

$$\mathbf{C}_{k+1} = \frac{\partial \boldsymbol{h}_{k+1}(\boldsymbol{\theta}_k, [\boldsymbol{f}]_{k+1})}{\partial \boldsymbol{\theta}^{\boldsymbol{T}}} \tag{2.8}$$

where the response sensitivity can be calculated using finite difference methods. The Kalman gain matrix is calculated as

$$\mathbf{K}_{k+1} = \boldsymbol{P}^{-}_{\boldsymbol{\theta y},\boldsymbol{k+1}}\left(\boldsymbol{P}^{-}_{\boldsymbol{y},\boldsymbol{k+1}}\right)^{-1}$$
$$\text{where } \boldsymbol{P}^{-}_{\boldsymbol{\theta y},\boldsymbol{k+1}} = \boldsymbol{P}^{-}_{\boldsymbol{\theta},\boldsymbol{k+1}}\mathbf{C}^{T}_{k+1},\ \boldsymbol{P}^{-}_{\boldsymbol{y},\boldsymbol{k+1}} = \mathbf{C}_{k+1}\boldsymbol{P}^{-}_{\boldsymbol{\theta},\boldsymbol{k+1}}\mathbf{C}^{T}_{k+1} + \mathbf{R}_{k+1} \tag{2.9}$$

where $\boldsymbol{P}^{-}_{\boldsymbol{\theta y},\boldsymbol{k+1}}$ denotes the estimated parameter response cross-covariance matrix; $\boldsymbol{P}^{-}_{\boldsymbol{y},\boldsymbol{k+1}}$ denotes the estimated response covariance matrix. The posterior parameter is estimated as

$$\boldsymbol{\theta}^{+}_{\boldsymbol{k+1}} = \boldsymbol{\theta}^{-}_{\boldsymbol{k+1}} + \mathbf{K}_{\boldsymbol{k+1}}(\boldsymbol{y}_{\boldsymbol{k+1}} - \widehat{\boldsymbol{y}}_{\boldsymbol{k+1}}) \tag{2.10}$$

where $\boldsymbol{y}_{\boldsymbol{k+1}}$ and $\widehat{\boldsymbol{y}}_{\boldsymbol{k+1}}$ denote the observed and predicted output response at t_{k+1}, respectively. The posterior covariance matrix is estimated as

$$\boldsymbol{P}^{+}_{\boldsymbol{\theta},\boldsymbol{k+1}} = (\boldsymbol{I} - \mathbf{K}_{\boldsymbol{k+1}}\mathbf{C}_{\boldsymbol{k+1}})\boldsymbol{P}^{-}_{\boldsymbol{\theta},\boldsymbol{k+1}} \tag{2.11}$$

The Particle-filter is sampling based method using Monte-Carlo simulation. The sets of parameter is sampled based on given parameter noise and the variation of output response ($\hat{\boldsymbol{y}}_{\boldsymbol{k+1}}$) is estimated with sample points. The most probable and possible parameter ($\boldsymbol{\theta}_{\boldsymbol{k+1}}^{+}$) is resampled based on the weight calculation using observed response ($\hat{\boldsymbol{y}}_{\boldsymbol{k+1}}$). And the covariance of matrix of parameter is updated.

The parameter estimation using Kalman/ Particle based is efficient and straight forward. There are several study to enhance the Kalman filter approach for digital twin updating and calibration. Branlard et al. (2020) proposed the Augmented Kalman filter with a reduced mechanical model to estimate tower loads on a land-based wind turbine [55]. The approach combines a mechanical model and a set of measurements to estimate responses that are not available in the measurements, such as wind speed, thrust, tower position, and tower loads.

The input-excitation ($\boldsymbol{f}$) can be estimated using the system matrixes and Kalman based filter approaches. Azam et al. (2015) proposed a dual Kalman filter approach for input and state estimation using output-only measurements [61]. Shrivastava et al. (2019) applied the joint-input state estimation method for estimation of unbalance parameters of rotor-bearing systems [62].

However, The parameter estimation using Kalman/ Particle based filter approach require proper dynamics model and estimation accuracy is affected by the covariance matrix of the measurement and parameter noise (Q, R). Also the input excitation of the system is hard to measure for most engineering case study. So, It is hard to apply the method for digital twin updating with an insufficient prior information. This drives research interest in developing a new data-driven dynamic

model updating that is able to apply without prior information such as dynamic model, input excitation and statistical information of noise.

2.2.3 Summary and Discussion

Whereas significant efforts have been made to develop digital twin with enough data and prior information about system, relatively little attention has been paid to investigating hybrid digital twin approach with an insufficient prior information. In the small number of existing works based on data-driven and hybrid approaches, it is assumed that lack of data or imbalanced data sets.

However, it should be noted that the characteristics of the system may change corresponding system failure or operating condition, thereby resulting in invalid model prediction by a transition of the observed output response. Therefore, an model calibration and updating considering system failure and anomaly condition must be developed to help engineering decisions using digital twin analysis.

Chapter 3

Data-driven Dynamic Model Updating for Anomaly Detection with an Insufficient Prior Information

The data-driven digital twin is statistically trained and validated using the machine learning & deep-learning method. The data-driven digital twin can be used for real-time analysis because of its efficiency. Further, the data-driven digital twin is widely applicable for various fields because of its flexibility. To train the data-driven model, sufficient data, including the status and label of the target system, is required. However, it suffers from a lack of data and information in the most engineering system.

Whereas significant efforts have been made to enhance the data-driven model with imbalanced and insufficient data set (i.e., transfer-learning or data-augmentation), relatively little attention has been paid to investigating data-driven dynamic model updating method. In the small amount of existing works based on the Kalman/Particle filter based model updating, it is assumed that the observable

operation condition and valid physics-based model. However, it should be noted that the prior knowledge for physics-based modelling is not available for complex engineering system.

The chapter thus proposes data-driven dynamic model updating for anomaly detection with insufficient prior knowledge. The time-frequency domain features are extracted from the observed response using signal pre-processing. The state-space model is driven by numerical algorithm for subspace state-space system identification (N4SID) to predict the extracted features under different operating condition. In the model, the operating condition that arises from the operation are defined as a parameterized input excitation force of a system model. Next, the phase and amplitude modulation of input excitation force are updated to minimize the prediction error that quantify the discrepancy between the observed and predicted time- and frequency-domain features. An optimization-based parameter tuning was originally applied to estimate operating condition of engineering system. Using the proposed method, health indices, such as time delay of operation, prediction error by anomaly system operation can be derived from the digital twin analysis.

The remainder of Chapter 3 is organized as follows. Section 3.1 describes the target system which is suffering from lack of prior knowledge for digital twin. Section 3.2 address the data-driven dynamic model updating to detect anomaly condition with insufficient data. In Section 3.3, numerical and engineering example are demonstrated. Finally, the conclusions of this work are provided in Section 3.4.

3.1 System Description of On-Load Tap Changer

Power transformers are essential equipment for the transmission and distribution of alternating electric current. Power transformers are made up of several key components, including the core, winding, bushing and an on-load tap changer (OLTC). The voltage ratio between the input and the output voltage of the power transformer is decided by the winding turns ratio. An OLTC is a sequential shift mechanism that allows the variable turns ratio to be selected to regulate the output voltage of the power transformer. The turn ratio is decided by the OLTC connecting to one of a number of access points (known as taps) along either the primary or secondary winding. The OLTC mechanically changes the turn ratio without stopping the operation of the power transformer. Figure 3-1 shows the internal components of a widely used three-phase OLTC, specifically, the MR-MIII 350. The OLTC mechanically operates 10-15 times per day. Due to its frequent operation, it is vulnerable to mechanical faults. Mechanical faults cause other electrical and thermal faults. To prevent OLTC failure, time-based maintenance is typically carried out. The maintenance overhaul of an OLTC should be conducted after 6-7 years of operation or 20,000-100,000 iterations of the tap changing operation. However, the traditional time-based overhaul strategy can cause unnecessary inspection costs, and can lead to human error, such as incorrect assembly or visual inspection error. To overcome the disadvantages of time-based maintenance, several studies have been carried out to diagnose OLTC health using measurable data without the need for overhaul. These studies have examined the 1) OLTC vibration signal [63]–[67], 2) OLTC motor current [68], [69], 3) High Frequency Current Transformer (HFCT) sensor signal for Partial Discharge (PD) measurements [63], and 4) Dynamic

Resistance Measurement (DRM) [70].

Erbrink et al. (2010) showed that the electrical and mechanical health state transition of an OLTC results in variation in DRM. However, the DRM is not measurable during power-transformer operation [70]. Seo et al. (2017) proposed a joint measurement system that simultaneously observes three types of measurable data during power transformer operation: 1) the HFCT signal from the grounding cable, 2) the OLTC motor current, and 3) the vibration signal [68]. Further, Seo et al. (2018) applied the Savitzky-Golay filter to extract health features from PD measurements and the vibration envelope signal [63]. However, the complementary effect of each type of data is not shown in this previous study. For reasons outlined herein, the study described in this paper focuses on using the vibration signal to estimate the mechanical state of an OLTC.

The vibration signal is caused by the OLTC's sequential mechanical operation. Mechanical faults of an OLTC can be detected using the vibration signal. Rivas et al. (2010) showed that the characteristics of the vibration signal, such as its magnitude and time of burst signal, depend on the mechanical health state of the OLTC, such as spring looseness, damaged tap selector contacts, or a broken output contact bar [71]. Qingmin et al. (2012) proposed a Hidden Markov Model based fault diagnosis model using frequency domain features from the vibration signal [67]. Duan et al. (2016) applied Empirical Mode Decomposition to fault/normal vibration signals of an OLTC to extract health features and calculated the Lorenz information measure to show the difference between a faulty and normal-state signal [65]. Liu et al. (2017) applied variational mode decomposition to extract features and trained a relevance vector machine diagnostic model [72]. Yang et al. (2019) applied dynamic

time warping for mechanical fault diagnosis of an OLTC [73]. Signal processing and statistical diagnostic methods were applied to experimentally observed fault and normal-state vibration signals in these previous studies.

In most previous studies, artificial faults were applied to the OLTC in experimental conditions to create a fault vibration signal. However, this approach can require significant experimental costs and effort to derive artificial faults. Further, performing experiments to create a fault vibration signal is not possible during power transformer operation. Thus, most real-world applications suffer from a lack of fault vibration signal data. Statistical diagnostic methods, such as machine-learning and deep-learning with insufficient fault signals, cannot guarantee accuracy and efficiency. In the study described in this paper, to overcome this problem, we

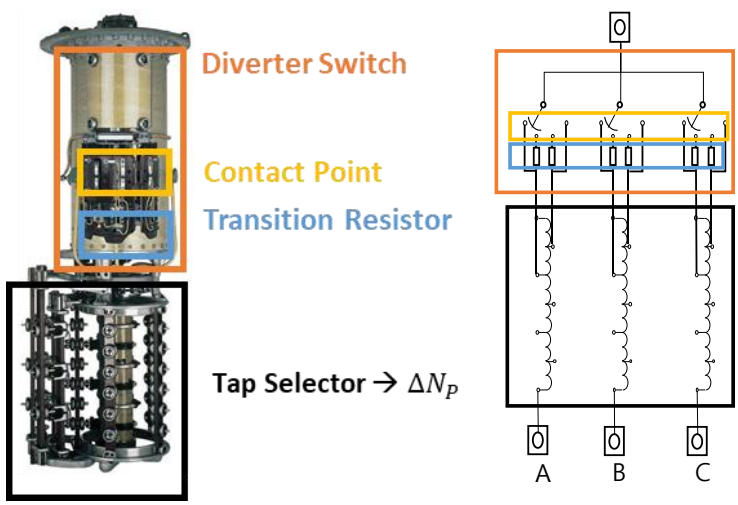

(a) (b)

Figure 3-1 The internal components of an OLTC : (a) MR-MIII 350 and (b) general schematic representation

propose a digital twin approach for mechanical state estimation of an OLTC. The mechanical state of an OLTC affects the vibration signal in both the time and frequency domains. The proposed digital twin approach can infer the transition of the health state of an OLTC using the features in the time-frequency domain of an observed vibration signal. The proposed method consists of 1) pre-processing of the vibration signal to extract features in time-frequency domain, 2) OLTC digital twin modeling to simulate the vibration signal, and 3) model updating using observed features in the time-frequency domain to infer the mechanical operating condition and health state of the OLTC.

Figure 3-2 (a) shows the OLTC's operation and vibration signal when operating in three phase diverter switch. The operation sequence of the internal components, such as tap selectors and contact points in the diverter switch, causes a burst vibration signal. The OLTC operates 10-15 times per day, which – over time – causes mechanical faults in the OLTC, such as spring failure, contact point wear, incomplete contact of the tap-selector, and time delay of the switching sequence. In turn, those mechanical faults result in electrical and thermal faults in the OLTC. Figure 3-2 (b) shows a schematic representation of the time delay of diverter switch operation between phases, which causes circular current. The mechanical faults can cause delays in the tap-selector and diverter-switch operation that result in a severe circular current. Using the observed vibration signal, the delay of the diverter switch and tap changer operation can be quantified. In this paper, we propose a digital twin approach to estimate the mechanical state of an OLTC using its vibration signal.

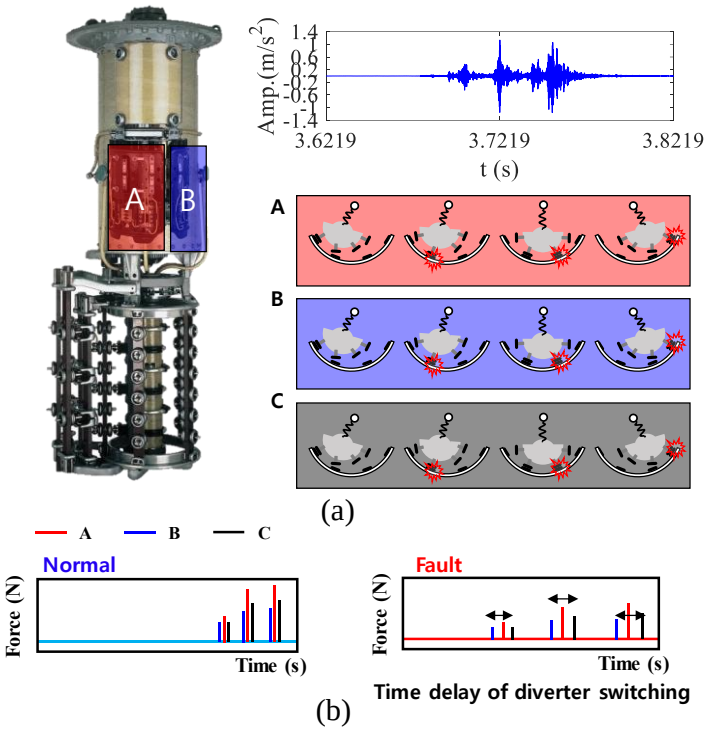

Figure 3-2 OLTC operation sequence: (a) Schematic representation of diverter switch operating sequence and (b) the time delay of the diverter switch operation

3.2 Data-driven Dynamic Model Updating for Anomaly Detection with an Insufficient Prior Information

The following section outlines the proposed digital twin approach. Figure 3-3 describes the procedure for the proposed digital twin approach. The proposed method consists of 1) pre-processing the response using minimum entropy deconvolution (MED) filtering to extract the impulsive target system operation response and short-time Fourier transform (STFT) to extract the time-frequency

domain features, 2) target system dynamic model formulation using numerical algorithm for subspace state-space system identification (N4SID), and 3) optimization-based model updating using time-frequency domain features to infer the OLTC's operating condition. This method is applicable to all sequential operating OLTCs that generate a vibration signal. The mechanical state of the OLTC, including spring force magnitude and time delay between diverter contact and the tap selector can be analyzed from the updated input parameters.

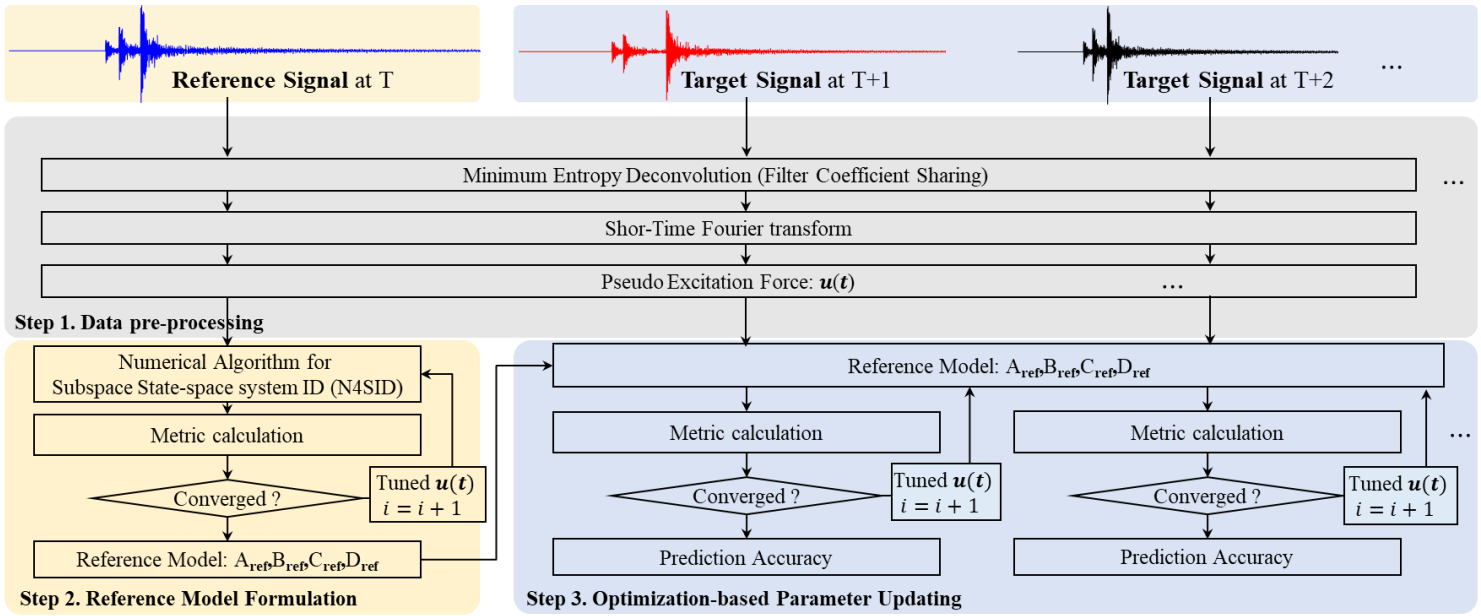

Figure 3-3 Procedure for the proposed digital twin approach to estimate the mechanical health state of target system.

3.2.1 Preprocessing of Vibration Signal

Measurement of the vibration signal is available during power transformer operation. The observed vibration signal during power transformer operation includes vibration from sources such as 1) vibration due to the mechanical OLTC operation, 2) vibration from the electromagnetic force of the winding and core, and 3) external noise. To diagnose the OLTC using the vibration signal, the mechanical vibration from the OLTC operation should be extracted from the raw vibration signal. The mechanical vibration from OLTC operation is caused by impulsive force during OLTC operation. In 1978, Wiggins proposed a minimum entropy deconvolution (MED) method that derives a linear filter to minimize entropy of a signal [74]. MED filtering is widely used to extract an impulsive signal to diagnose mechanical components, such as gears [75] and bearings [76]. In this study, we applied MED filtering to extract the impulsive vibration from OLTC operation.

The vibration signal can be analyzed in both the time and frequency domains using STFT and Wavelet Transform (WT). The OLTC health state affects the vibration in both the time and frequency domains [65], [73]. Further, the mechanical health information of the OLTC temporarily is concentrated in the vibration signal during tap-selector and diverter switch operation. Park et al. (2019) found that the "WT process requires lengthy computational time…"(p. 253) and proposed using the variance of energy residual for gear fault detection based on the STFT [77]. In our approach, STFT is applied to extract vibration features in the time-frequency domain. Discrete-time STFT for a discrete vibration signal can be mathematically formulated as:

$$\mathrm{Y}(t,f) = \sum_{\tau=-\infty}^{\infty} y[\tau]w[\tau - t]e^{-jf\tau} \tag{3.1}$$

where *t* and *f* denote the time step and frequency, respectively; $w(\tau)$ is the window function; $y(\tau)$ denotes vibration signal at time step τ ; and $\mathrm{Y}(t,f)$ denotes amplitude in time step *t* and frequency *f*. In this study, a uniform window is applied because the vibration signal from the OLTC is an impulsive and transient signal. The length of widow can be adjusted depending on the signal acquisition condition. STFT with high frequency and time resolution is computationally expensive. The STFT for the predicted vibration signal is required for every update iteration. Thus, the resolution of the STFT should be properly selected to consider computational cost. The numerical options of STFT, such as window and overlap size, are discussed in Section 3.3.

To formulate state space model simulating the vibration signal, the input signal of the system is required. To extract the pseudo OLTC input excitation force, the STFT signal is marginalized as:

$$\overline{\mathrm{Y}}(t) = \int_{f_{min}}^{f_{max}} \mathrm{Y}(t,f)\, df \tag{3.2}$$

where f_{min} and f_{max} denote the minimum and maximum frequency value of the STFT signal, respectively. To extract operating features that occurred during an operation sequence, the peaks of marginalized STFT signals ($d_{\mathrm{j}} = \{\overline{\mathrm{Y}}_j, \mathrm{t_j}\}$) are find using peak finding algorithm. The initial input excitation force is defined as:

$$u_{\text{intial}} = \begin{cases} \frac{\overline{Y}_j}{\max(\overline{Y}_j)} & t = t_j \\ 0 & t \neq t_j \end{cases} \tag{3.3}$$

where $\overline{Y}_j, t_j$ denote amplitude, time of peaks in marginalized STFT signal, respectively. The normalized initial input excitation force have amplitude values from 0 to 1.

3.2.2 Reference Model Formulation using N4SID

This study applied a simplified, state space model formulation method using numerical algorithm for subspace state-space system identification (N4SID) to simulate the vibration signal of an OLTC. Liu et al. (2019) proposed a simplified FE model that requires 48.8 seconds to run the simulation while requiring a lot of unknown model parameters (i.e., spring constant, contact model parameters, material properties) [78]. In contrast, the proposed state space model requires only a few milliseconds to simulate the given force parameter. The state space model can be generally formulated as:

$$\begin{aligned} [\dot{\boldsymbol{X}}] &= \boldsymbol{A}[\boldsymbol{X}] + \boldsymbol{B}[\boldsymbol{U}] \\ Y_{pre} &= C[X] + D[U] \end{aligned} \tag{3.4}$$

where *A*, *B*, *C*, and *D* denote system, input, output and feedthrough matrix, respectively. The X, Y_{pre} and U denote state, output, and input vector, respectively. The matrix can be derived physically using Finite Element Method [78] and lumped dynamic model [79]. However, it requires prior knowledge of the system such as geometry, material properties and operating condition. It is not easy to get

prior knowledge with respect to various OLTC and power transformer. To build the valid state space model, we applied the N4SID method. In N4SID method, it requires 3 assumptions as:

1) Assumption 1: States visit every dimension.
2) Assumption 2: Persistently exciting inputs.
3) Assumption 3: No linear state feedback

The N4SID method requires the sets of input and output vectors as:

$$U_p = U_{0|k-1} = \begin{bmatrix} u(0) & u(1) & \cdots & u(N-1) \\ u(1) & u(2) & \cdots & u(N) \\ \vdots & & \ddots & \vdots \\ u(k-1) & u(k) & \cdots & u(k+N-2) \end{bmatrix} \tag{3.5}$$

$$Y_p = Y_{0|k-1} = \begin{bmatrix} y(0) & y(1) & \cdots & y(N-1) \\ y(1) & y(2) & \cdots & y(N) \\ \vdots & & \ddots & \vdots \\ y(k-1) & y(k) & \cdots & y(k+N-2) \end{bmatrix} \tag{3.6}$$

where U_p and Y_p denote past input and past output matrix, respectively. where N is assumed large integer. The past data matrix is formulated as:

$$W_p = \begin{bmatrix} U_{0|k-1} \\ Y_{0|k-1} \end{bmatrix} \tag{3.7}$$

Similarly, the future output and input matrix defined as:

$$U_f = U_{k|2k-1} = \begin{bmatrix} u(k) & u(k+1) & \cdots & u(k+N-1) \\ u(k+1) & u(k+2) & \cdots & u(k+N) \\ \vdots & & \ddots & \vdots \\ u(2k-1) & u(2k) & \cdots & u(2k+N-2) \end{bmatrix} \tag{3.8}$$

$$Y_f = Y_{k|2k-1} = \begin{bmatrix} y(k) & y(k+1) & \cdots & y(k+N-1) \\ y(k+1) & y(k+2) & \cdots & y(k+N) \\ \vdots & & \ddots & \vdots \\ y(2k-1) & y(2k) & \cdots & y(2k+N-2) \end{bmatrix} \tag{3.9}$$

The future input-output relationship can be expressed as:

$$Y_f = O_k X_f + \Psi_k U_f \tag{3.10}$$

were O_k and Ψ_k denote observability, block Toeplitz matrix, respectively. Those matrices can be derived from state space representation as:

$$O_k = \begin{bmatrix} C \\ CA \\ \vdots \\ CA^{k-1} \end{bmatrix} \quad \Psi_k = \begin{bmatrix} D & 0 & \cdots & 0 \\ CB & D & \cdots & 0 \\ \vdots & & \ddots & \vdots \\ CA^{k-2}B & \cdots & CB & D \end{bmatrix} \tag{3.11}$$

The combined data matrix can be decomposed into L (lower triangular matrix) and Q (orthogonal matrix) as:

$$\begin{bmatrix} U_f \\ W_p \\ Y_f \end{bmatrix} = \begin{bmatrix} L_{11} & 0 & 0 \\ L_{21} & L_{22} & 0 \\ L_{31} & L_{32} & 0 \end{bmatrix} \begin{bmatrix} Q_1^T \\ Q_2^T \\ Q_3^T \end{bmatrix} \tag{3.12}$$

where the L_{ij} *(i,j=1,2,3)* are blocks of lower triangular matrix. The L_{33} should be zero, because all the inputs of both past and future times are zero and the outputs were 0 in the past time. The three equations can be obtained from above equations as:

$$U_f = L_{11} Q_1^T \tag{3.13}$$

$$W_p = L_{21} Q_1^T + L_{22} Q_2^T \tag{3.14}$$

$$Y_f = L_{31}Q_1^T + L_{32}Q_2^T \tag{3.15}$$

Then, the output matrix can be derived as:

$$\begin{aligned} Y_f &= L_{31}L_{11}^{-1}U_f + L_{32}L_{22}^{\#}(W_p - L_{21}L_{11}^{-1}U_f) \\ &= (L_{31} - L_{32}L_{22}^{\#}L_{21})L_{11}^{-1}U_f + L_{32}L_{22}^{\#}W_p \end{aligned} \tag{3.16}$$

where $L_{22}^{\#}$ denote pseudoinverse of L_{22} because L_{22} is rank deficit. From the equation (3.8), (3.9) and assumption 2 and 3, the following equation derived as:

$$O_k X_f = L_{32}L_{22}^{\#}W_p = U_1\Sigma_1 V_1^T \tag{3.17}$$

where the U_1, V_1 and Σ_1 are singular value decomposition of $L_{32}L_{22}^{\#}W_p$. The results can be split between O_k and X_f as:

$$\begin{aligned} X_f &= T^{-1}\Sigma_1^{1/2}V_1^T \\ O_k &= U_1\Sigma_1^{1/2}T \end{aligned} \tag{3.18}$$

Based on the series of states (X_f) and the input-output data (U_f, Y_f), we can form the following 4 matrices (A,B,C and D) as:

$$\begin{bmatrix} A & B \\ C & D \end{bmatrix} = \begin{bmatrix} X_{k+1} \\ Y_k \end{bmatrix} \begin{bmatrix} X_k \\ U_k \end{bmatrix}^T \left(\begin{bmatrix} X_k \\ U_k \end{bmatrix} \begin{bmatrix} X_k \\ U_k \end{bmatrix}^T \right)^{-1} \tag{3.19}$$

where X_k, Y_k and U_k are the series of state, output and input data at time k to $k+N-2$. X_{k+1} is the series of state at time $k+1$ to $k+N-1$. For valid model formulation, accurate output and input data is required. However, the input excitation force cannot be measured for OLTC vibration signal. So we proposed pseudo input excitation force using pre-processing. Figure 3-4 (a) shows an initial pseudo excitation force.

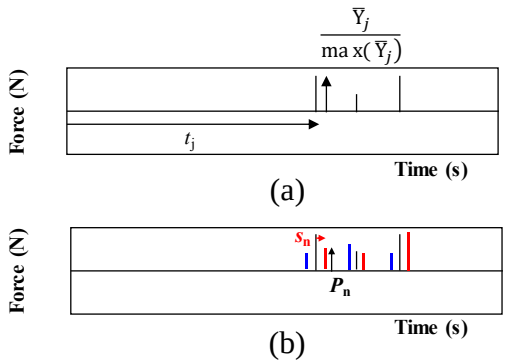

Figure 3-4 Model Input: (a) Initial pseudo input excitation force, (b) the parameter of input signal

However, the operating condition can be varying for each operation. So, optimization –based tuning is applied for reference model formulation and operating condition estimation using reference model.

3.2.3 Optimization-based Parameter Updating

The optimization-based parameter updating is applied to update the input excitation force using the observed vibration signal. In this approach, the parameters of input force are updated to minimize the L_2-norm error of the frequency and time domain features of signal. The optimization-based tuning is defined as:

$$\underset{\boldsymbol{\theta}}{\text{minimize}} \quad L_2(\boldsymbol{\theta}) \tag{3.20}$$

where $\boldsymbol{\theta}$ denotes an updating parameter vector; and $\boldsymbol{\theta}$ includes the set of parameters, such as phase modulation (s_n) and amplitude modulation (P_n) parameters of *n*-th impulse input; Figure 3-4 (b) represents the parameter of input excitation

force. $L_2\left(Y(t,f), \hat{Y}(t,f|\boldsymbol{\theta})\right)$ denotes the L_2 norm metric value using observed and time-frequency features. The L_2 norm metric is formulated as:

$$L_2 = \frac{\iint \left\| Y(t,f) - \hat{Y}(t,f|\boldsymbol{\theta}) \right\| dtdf}{\iint \| Y(t,f) \| dtdf} \tag{3.21}$$

where $Y(t,f)$, $\hat{Y}(t,f|\boldsymbol{\theta})$ denote the amplitude of Discrete-time STFT of observed and predicted signal, respectively. To solve the optimization problem, sequential quadratic programming, genetic algorithms, or another advanced optimization solver can be used as a searching algorithm. There might be several local minimums in a solution space because of the discrete signal. As such, a global optimization solver, such as a genetic algorithm (GA), and a multi-start gradient method are preferred. In this study, GA is applied for the case study. The $\boldsymbol{\theta}$, which includes the phase and amplitude modulation parameters of the impulse input forces (s_n, P_n), is updated to estimate the operating condition of an OLTC using the observed signal at each operation. The updated model prediction accuracy and parameters can represent the mechanical health state and operating condition of the observed OLTC. To quantify the mechanical state of an OLTC, health indices – including time delay of operation – can be derived using updated model parameters. If enough data is observed from both faulty and healthy state vibration signals, data-driven approaches – including support vector machine and deep learning algorithms (including Convolution Neural Network, Recurrent Neural Network) – can be used to distinguish the faulty and healthy states of an OLTC. However, as we introduced, it is difficult to obtain faulty state OLTC vibration signals for an active power transformer to train or use a data-driven model. If the proposed indices accumulate data over time (i.e., until failure), the health indices can show degradation of the OLTC's mechanical state. Rule-based

diagnosis based on the observed health indices can also be proposed.

3.3 Case Study

In this section, numerical and engineering examples are demonstrated to verify the effectiveness of the proposed digital twin approach. In the numerical example, the sets of vibration signal are generated in normal and anomaly operating condition in different noise level using physics-based simulation model. And the analysis results are compared to identify the effectiveness of proposed method in different noise level. In engineering example, the proposed digital twin approach is applied to estimate the mechanical state of an observed OLTC, specifically an MR-MIII 350. The MR-MIII 350 is a three-phase OLTC made by Maschinenfabrik Reinhausen (MR).

3.3.1 Case Study 1: (Numerical) Vibration Analysis using Parameter Varying Cantilever Beam and Multi-DOF model

In this example, the sets of vibration signal are generated using numerical model. The physics-based model using a finite element (FE) method was constructed to perform dynamic analysis. Figure 3-5 shows a numerical model consists of Euler-Bernoulli beam and lumped parameter model and parameterized impulsive excitation force. The observed output response is acceleration at the six-th node of the beam element. Each mass (m_i) is loaded by the impulse force which defined by two parameters: amplitude (P_i) and time (t_i). Each mass is heated in three different

period and magnitude. To consider uncertain operating condition of OLTC, the three different period of impulse force are assumed to follow normal distributions ($t_i \sim N(\mu_i, \sigma_i)$, i=1,2,3). The statistical parameter vector of three different periods is that [μ_1, σ_1, μ_2, σ_2, μ_3, σ_3] = [0.04, 8e-04, 0.05, 8e-04, 0.06, 8e-04]. The model parameter is summarized in Table 3-1.

The large and small-time scale are assumed as day and second. The response is simulated for ten days and 0.2 seconds long vibration signal using Monter Carlo simulation. The vibration signal of anomaly operating condition is simulated with change of system parameter in large time scale. The standard deviation which indicates time delay of system operation is increased in anomaly operating condition.

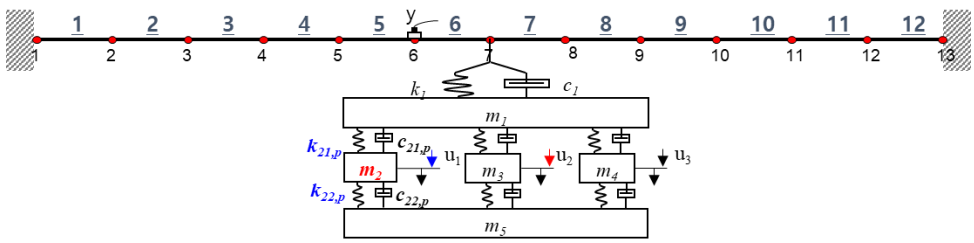

(a)

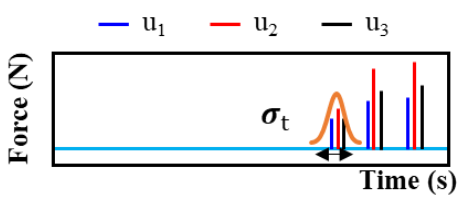

(b)

Figure 3-5 (a) The computational model for generating vibration signal and (b) parameterized impulsive excitation force

Table 3-1 Model Parameter (Normal Operating Condition)

Symbol	Quantity	Value
E	Young's Modulus of Beam	210 GPa
ρ	Density of Beam	7860 kg/m3
w	Width of Beam	0.1 m
t	Thickness of Beam	0.03 m
l	Length of Beam	1.2 m
M_1	Mass of m_1	$10^{0.5}$ kg
m_p	Mass of m_2, m_3, m_4	$10^{0.2}$ kg
M_5	Mass of m_5	$10^{0.5}$ kg
K_1	Stiffness of k_1	10^{10} N/m
k_p	Stiffness of $k_{21,p}$, $k_{22,p}$, $k_{31,p}$, $k_{32,p}$, $k_{41,p}$, $k_{42,p}$	10^7
C_1	Damping Coefficient of c_1	10^8 Ns/m
c_p	Damping Coefficient of $c_{21,p}$, $c_{22,p}$, $c_{31,p}$, $c_{32,p}$, $c_{41,p}$, $c_{42,p}$	10^5 Ns/m

Figure 3-6 (a) shows assumed system parameter and standard deviation in normal and anomaly operating condition in large time scale. To consider different sensor noise condition, white Gaussian with two different noise level is added in simulated response. The peak signal noise ratio (PSNR) is defined using ratio of maximum magnitude of signal to standard deviation of noise. Figure 3-6 (b) shows example of observed vibration signal with two different noise level.

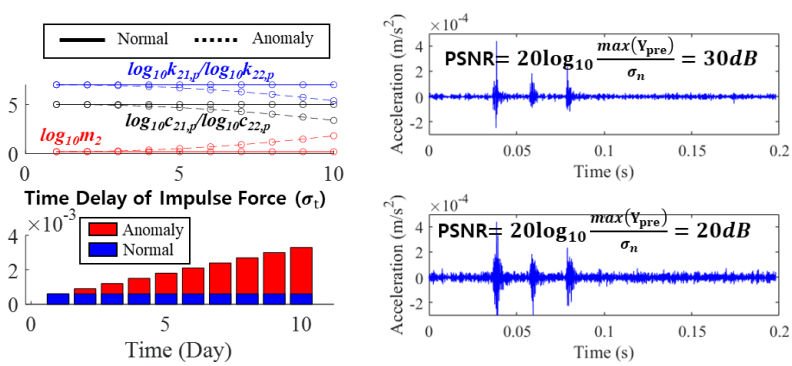

Figure 3-6 Uncertain operating and data measurement condition: (a) model parameter (b) measurement noise

The proposed digital twin approach is utilizing the system identification method to formulate reference dynamic model. Instead of data-driven method, the reference dynamic model can be formulated into simplified physics-based model because of in-sufficient prior information about geometry and modeling. To compare the effectiveness of the proposed method, the results using system identification method and simplified physics-based model are compared. The three degrees of freedom lumped parameter model is used to formulate the reference dynamic model as shown in Figure 3-7. To calibrate the model parameter of simplified model using observed vibration signal, the optimization-based model calibration is formulated as:

$$\underset{\boldsymbol{\theta}}{\text{minimize}} \quad L_2(\boldsymbol{\theta}) \tag{3.22}$$

where $\boldsymbol{\theta}$ denotes an updating parameter vector; and $\boldsymbol{\theta}$ includes the set of parameters, such as phase modulation (s_n) and amplitude modulation (P_n) parameters of *n*-th impulse input and mass, stiffness, and damping coefficients (m_i, c_i, and k_i) of simplified physics based model; The reference simulation model are formulated using observed signals in initial large time scale. The phase modulation (s_n) and amplitude modulation (P_n) are updated using targe signal in different time

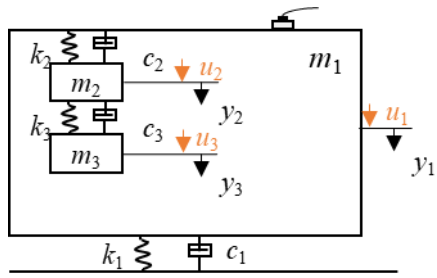

Figure 3-7 Simplified 3-DOF reference model

to minimize the L_2 norm metric.

Figure 3-8 shows the variation trend of L_2 norm error metric which indicates prediction error and estimated phase modulation parameter in large time scale. The analysis results using simplified physics based model shows larger prediction error in both anomaly and normal operating condition compared to the proposed method. And the differences between anomaly and normal operating condition cannot be identified in the results using simplified physics based model. On the other hand, the difference such as the increasing L_2 norm error metric in large time scale and the larger variation in phase modulation parameter for anomaly case can be

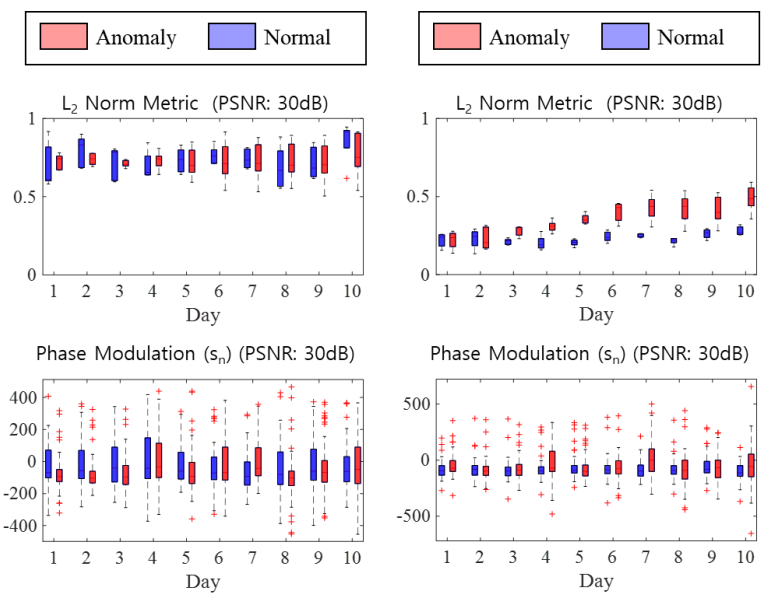

Figure 3-8 Analysis results in large time scale using different reference model formulation: (a) simplified physics-based model, (b) system identification methods

identified in the results using proposed method.

Figure 3-9 shows detailed analysis results in small time scale. The predicted response using simplified physics-based twin cannot represents frequency and time characteristic of the observed vibration signal. On the other hand, the predicted response using proposed method can represent frequency characteristics of observed response in normal condition. The updated response using reference model can represents the time delay of impulse response in anomaly case. The frequency modulation in anomaly condition can be identified in comparison of

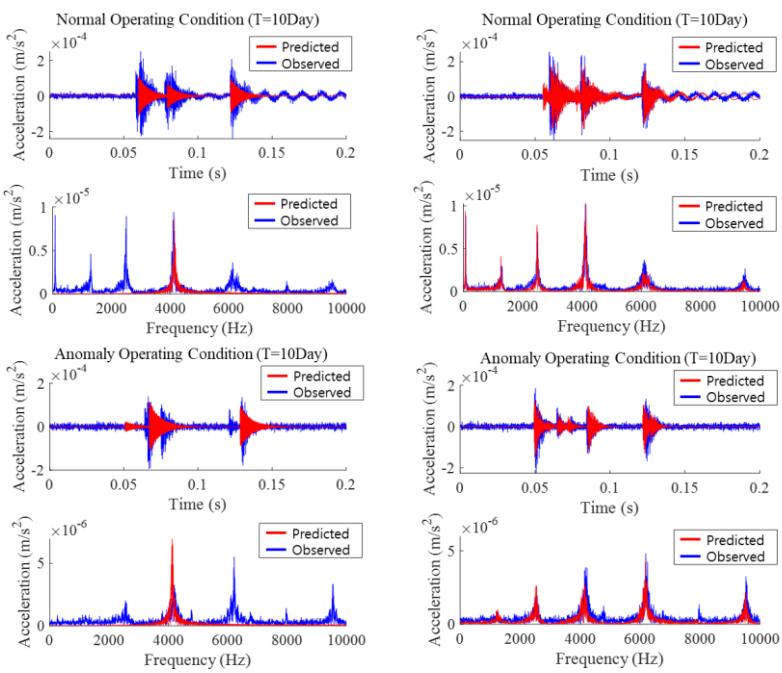

Figure 3-9 Detailed analysis results in small time scale using different reference model formulation: (a) simplified physics-based model (b) system identification methods

Table 3-2 Prediction accuracy & computational cost comparison between (a) simplified physics-based model and (b) system identification methods

	Computation Time (s)	Response Accuracy (%)
(Proposed) N4SID based Reference Model Formulation	716.54	87.00
In-valid Physics-based Reference Model Formulation	47.84	13.83

predicted response using reference model. Those modulation induce the increasing the L_2 norm error metric in time-frequency for anomaly operating condition.

Table 3-2 shows prediction accuracy & computational cost comparison between simplified physics-based model and proposed system identification methods. Even though, the proposed reference model formulation using system identification methods requires more computation cost than the in-valid physics-based model, the response prediction accuracy of the proposed method is higher than that of in-valid physics-based model.

The proposed digital twin approach is utilizing the optimization-based parameter updating to estimate uncertain input excitation force. Instead of the proposed method, the input excitation force can be estimated using joint-input state estimation method using the reference dynamic model from system identification method [79]. To compare the effectiveness of the proposed method, the estimated results using proposed method and joint-input state estimation method are compared.

Figure 3-10 shows analysis results using two method. The predicted response using both methods can represent characteristics of observed response in time and frequency domain in normal condition. However, the estimated force using joint-input state estimation method is non-informative because of overfitting problem. Even though, the model from system identification method has modelling error because of measurement noise and estimated inaccurate excitation force. The joint-input estimation method estimates the force magnitude at every time step to minimize prediction accuracy with model error and induces overfitting problem. On the other hand, the estimated force using proposed method can give an information such as the delay of operation and magnitude of impulse force.

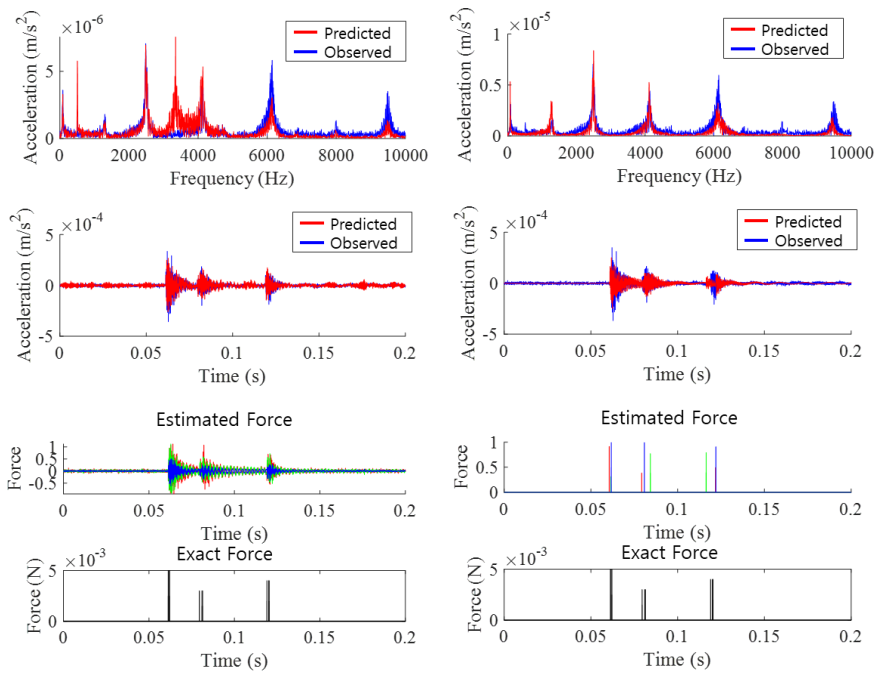

Figure 3-10 Analysis results and estimated excitation force: (a)optimization-based parameter updating and (b)Joint-input state estimation method

Table 3-3 Prediction accuracy & computational cost comparison between (a) optimization-based parameter updating and (b) Joint-input state estimation method

	Computation Time (s)	Response Accuracy (%)
(Proposed) Optimization-based Parameter Updating	52.22	71.28
Joint-Input State Estimation Method	1099.07	96.47

The proposed method is applied to observed vibration signals with the high noise level to identify the proposed method's effectiveness in different noise levels. As shown in Figure 3-11, even though prediction accuracy decreases because of high noise levels, the difference between normal and anomaly conditions can be identified even with a high noise level. It can be concluded that the proposed idea can be applied in different measurement noise conditions with insufficient prior information of modeling and operating condition.

Table 3-3 shows prediction accuracy & computational cost comparison between optimization-based parameter updating and joint-input state estimation method. Even though the response prediction accuracy of the joint input state

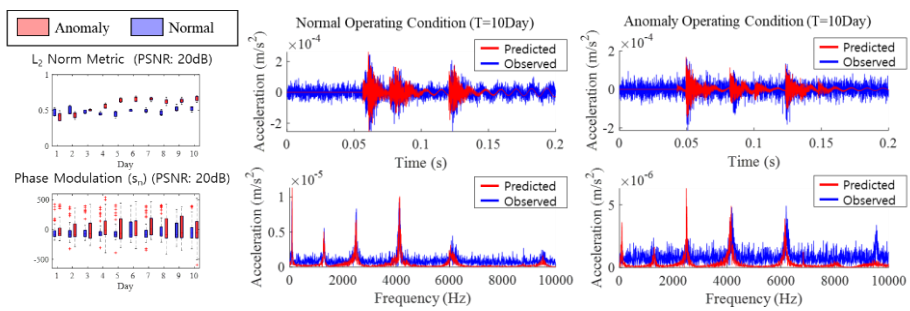

(a) (b)

Figure 3-11 Analysis results in large measurement noise: (a) simplified physics-based model (b) system identification methods

estimation is higher than that of proposed optimization-based parameter tuning, the required computation cost of the proposed methods is much less than that of joint input state estimation. And the estimated input force using the joint-input state estimation method is non-informative because of the overfitting problem. So, the proposed method can be more suitable in engineering examples with insufficient prior knowledge.

3.3.2 Case Study 2: Vibration Signal of On Load Tap Changer in Power Transformer

The proposed method was applied to an MR-MIII 350 model OLTC. The MR-MIII 350 is a 3-phase, oil-insulated OLTC with a tap selector. Figure 3-12 shows the experimental condition and the attached position of the accelerometer (PCB Piezotronics, 352C34). Study of the OLTC in active power transformer operation is limited. Thus, we measured two different power transformers. One was in-active; the other was an active power transformer. The active power transformer was changed only one tap level up and down at the 6th tap (tap changing sequence: 6th Tap → 7th Tap , 7th Tap → 6th Tap, 6th Tap → 5th Tap , 5th Tap → 6th Tap). The

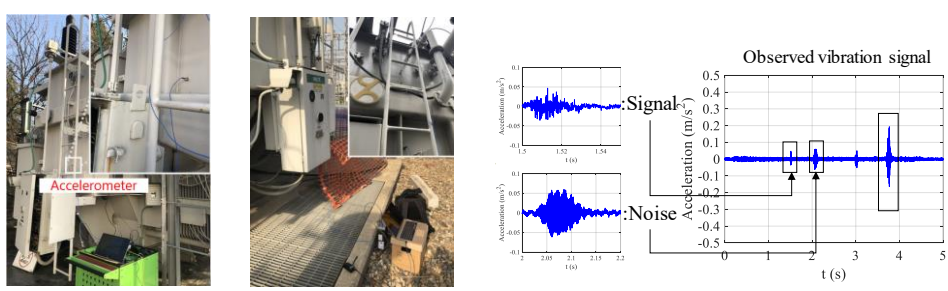

(a) (b) (c)

Figure 3-12 Experimental condition: (a) in-active and (b) active, and (c) observed vibration signal before filtering (in-active power transformer)

in-active power transformer was operated same sequence as active one. The vibration signal was measured at a sampling frequency of 10,240 Hz using DAQ (LMS SCADAS Mobile). The bursts of the vibration signal during tap change and diverter switching were caused by the OLTC operation sequence. A vibration signal caused by diverter switch operation with a 0.2-second time length was analyzed. The diverter switch operation generated the maximum amplitude burst signal. The signal is truncated by 0.1 seconds forward and 0.1 seconds backward, based on the maximum burst vibration signal. Figure 3-13 shows the measured original (raw) vibration signal when the tap changed from the sixth to the seventh tap position in the in-active and active power-transformer. The noise signal can be induced by external noise and vibration from the electromagnetic force of the winding and core.

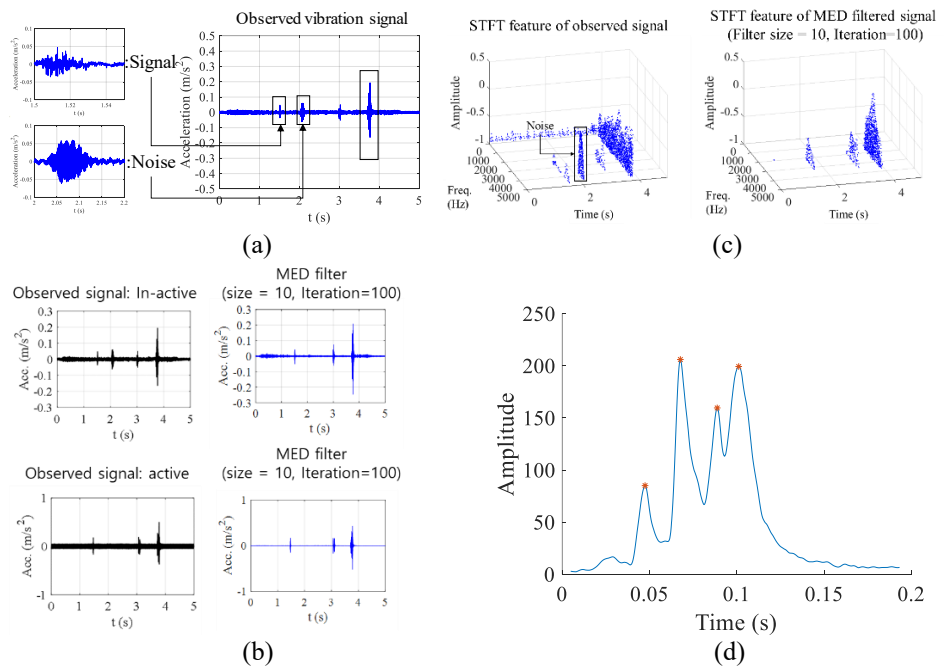

Figure 3-13 Observed vibration signal: (a) before filtering (in-active power transformer) (b) after filtering, (c) STFT feature, and (d) peaks in marginalized

STFT signal

An MED filter was applied to the measured raw vibration signal (sixth to seventh tap position) to extract the mechanical vibration from OLTC operation in both the active and non-active power transformers. As shown in Figure 3-13 (b), the MED filter can extract the vibration signal from OLTC operation, except the noise signal, both in the active and non-active settings. STFT with high resolution is computationally expensive; thus, for predicted signals, a uniform window size was defined as 400 sampling lengths. Figure 3-13 (c) shows the extracted time-frequency features of original and MED filtered signals. The extracted features from the original signal include noise components around 2 seconds and 4 kHz. The MED filters can extract the features from OLTC operation signal, except the features from the noise signal. The initial pseudo excitation force is defined using amplitude, time of peaks in marginalized STFT signal, as shown in Figure 3-13 (d).

Using a GA algorithm, the phase and amplitude modulation parameter were searched to minimize the L_2 norm metric using STFT features of the predicted signals by reference model. Figure 3-14 shows the variation trend of L_2 norm error metric and estimated phase modulation parameter in large time scale. The analysis results in active operating condition shows larger prediction error compared to the in-active case. Because the vibration signal includes the higher noise by vibration from the electromagnetic force of the winding and core. And the variation of estimated phase modulation is similar in both analysis results in active and in-active condition. Figure 3-15 shows detailed analysis results in small time scale. The predicted vibration signal can represent characteristics of observed response in time and frequency domain.

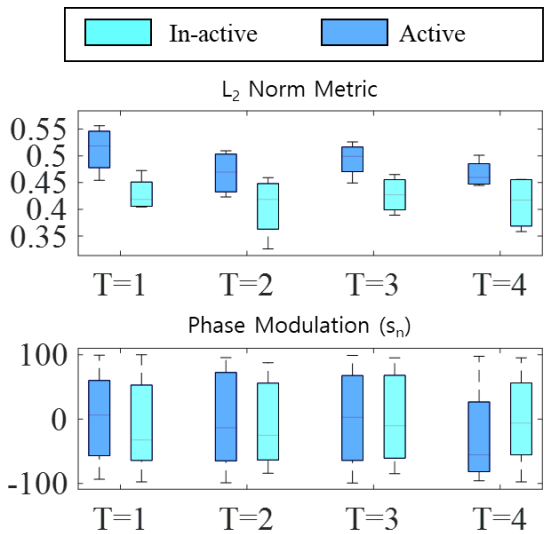

Figure 3-14 Analysis results in large time scale

To diagnose OLTC, Dynamic Resistance Measurement (DRM) can be measured in each phase during diverter switch operation [70], [80], [81]. The DRM represents the resistance transition in diverter switch operation. However, the DRM is only measurable in in-active power transformers one at a time for each phase. Here, we simultaneously measure dynamic resistance and vibration signal in an in-active power transformer one tap level up and down up (tap changing sequence: 16th Tap

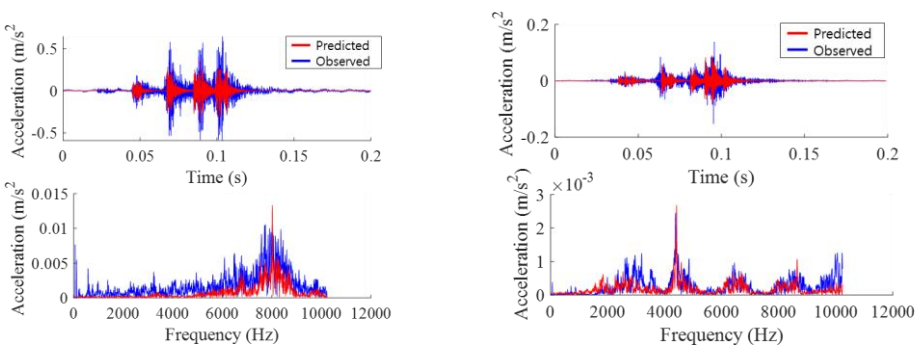

Figure 3-15 Detailed analysis results in small time scale: (a) In-active (b) Active

<=>17th Tap). Figure 3-16 shows the experimental conditions and a schematic representation of DRM measurement, the diverter switch operation sequence, and a DRM graph. When performing the DRM, the measurement system injects a DC current in each phase and records the transition of the current signal during the diverter switch operation. Each inflection point in the DRM graph indicates the contact point operation in the diverter switch that causes the impulsive vibration signal. To validate the proposed method, in this study, the model updating results were compared against estimated excitation force using proposed method.

Figure 3-17 shows the synchronization between the estimated excitation forces and the dynamic resistance for each phase. The estimated time of impulsive force using proposed method exhibits good agreement with the inflection point in the DRM graph. Based on the results, the variation of estimated phase modulation can

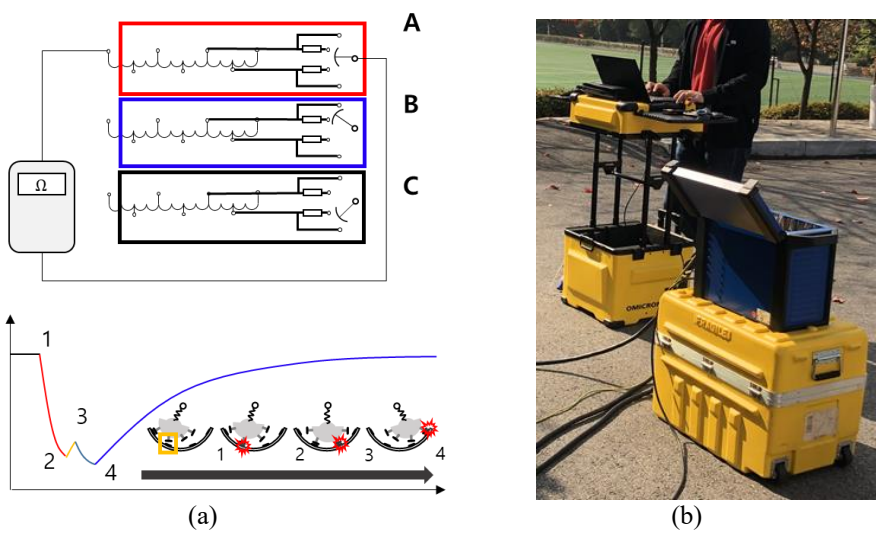

(a) (b)

Figure 3-16 (a) Schematic representation of diverter switch operation sequence and DRM graph and (b) Experimental condition

represent delay of diverter switch operation, which cause a circular current. The circular current degrades the transition resistor/reactor which makes an electrical fault or can even result in explosion of the OLTC.

3.4 Summary and Discussion

This study proposed a new digital twin approach for OLTC with an insufficient prior knowledge. The foundational idea of the proposed approach is to update a dynamic model using an observed vibration signal to estimate the uncertain operating condition and prediction error. Next, the health indices, such as time delay by switching fault, prediction error by system transition can be derived from the digital

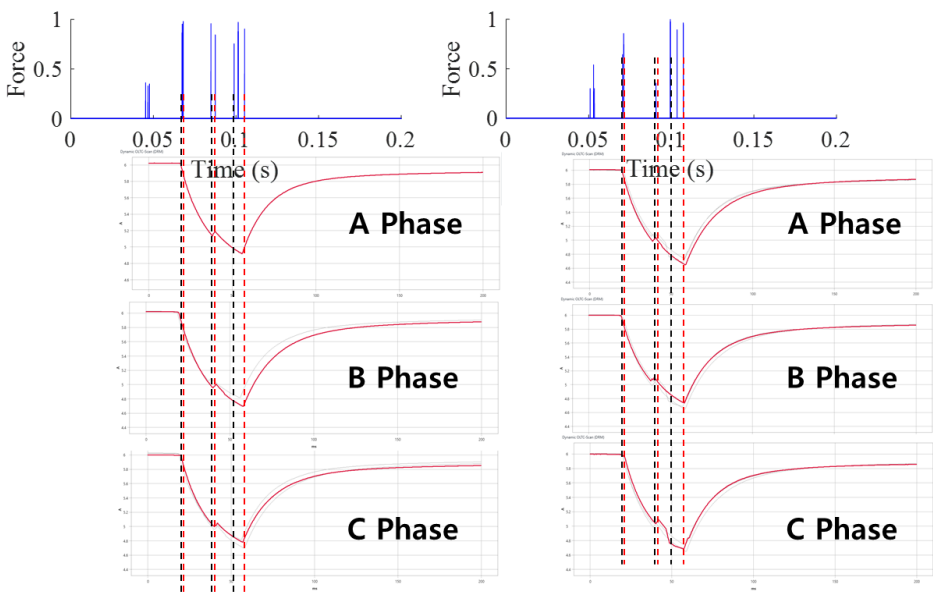

Figure 3-17 Synchronization between updated input forces and dynamic resistance : (a) 16→17Tap Changing Sequence, (b) 17→16Tap Changing Seq uence

twin analysis. The digital twin analysis results for numerical and engineering example were demonstrated to verify the effectiveness of the proposed approach. To validate the proposed method, the estimated parameters are compared with dynamic resistance measurement which represents actual OLTC working status. The physical health index can be calculated from the updated model parameter to estimate the time delay of the OLTC operation.

The proposed digital twin has many favorable properties as a diagnostic method, including 1) no need for accurate physics-based model, and 2) a physical health index that uses an updated model parameter. Previously studied statistical methods, such as deep learning and machine learning, require a known fault vibration signal. However, the proposed method only requires an understanding of the OLTC operation sequence. This method is much more efficient than the earlier in-valid finite element method. Finally, the physical health indices that represent the mechanical health state of an OLTC can be derived using the updated model parameter.

Sections of this chapter have been published or submitted as the following journal articles:

1) **Wongon Kim,** Sunuwe Kim, Jingyo Jeong, Hyunjae Kim, and Byeng D. Youn , "A Digital Twin Approach for On-Load Tap Changers with an Insufficient Prior Knowledge," *Mechanical Systems and Signal Processing*, submitted.

Chapter 4

A New Calibration Metric that Considers Statistical Correlation : Marginal Probability and Correlation Residuals

Chapter 3 was devoted entirely to the derivation of the data-driven dynamic model updating based on the system identification method by assuming that all the parameters are exactly determined. In other words, the loading parameters (i.e., t he time and amplitude of impulsive excitation force) and the system paramet ers (i.e., the material properties and the geometry) were considered to be deterministic. However, most input parameters in digital twin models have a certain amount of physical uncertainty, such as inherent variability in material properties and manufacturing tolerances, a digital twin model that uses a deterministic form fails to accurately analyze an engineered system. But, it is not easy to fully characterize the variability in the model input variables due to limited resources. Statistical model calibration is thus of great importance as a strategy to improve the

predictive capability of a digital twin model. Optimization-based statistical model calibration is formulated as an unconstrained optimization problem that infers the unknown statistical parameters of input variables associated with a digital twin model by maximizing statistical similarity between predicted and observed output responses. A calibration metric is defined as the objective function to be maximized that quantifies statistical similarity. One important challenge in formulating a calibration metric is how to properly consider the statistical correlation in output responses. Thus, this study proposes a new calibration metric, namely the Marginal Probability and Correlation Residuals metric. The foundational idea of the MPCR metric is to decompose a multivariate joint probability distribution into multiple marginal probability distributions while considering the statistical correlation between output responses. The three-fold novel aspects of this study include:

- This study thoroughly examines what happens if the statistical correlation is neglected in model calibration. In addition, three existing calibration metrics (marginal likelihood, joint likelihood, and moment matching) are reviewed from the perspective of their ability to address the statistical correlation between multivariate output responses.

- The MPCR metric allows consideration of the statistical correlation effectively; thus physically reasonable solutions can be confined. Consequently, accurate optimization-based statistical model calibration is enabled.

- The MPCR metric has favorable properties including normalization, boundedness, and marginalization; thereby, limitations of three existing

calibration metrics are overcome in this method.

Chapter 4 is organized as follows. Section 4.1 addresses the statistical correlation issue in optimization-based statistical model calibration and presents the proposed MPCR metric and its favorable properties. Section 4.2 presents proposed method: marginal probability and correlation residuals (MPCR). Two mathematical examples and one engineering example are demonstrated in Section 4.3. Finally, the conclusions of this work are outlined in Section 4.4.

4.1 Statistical correlation issue in calibration metric formulation

Section 4.1 underscores the importance of considering the statistical correlation when formulating a calibration metric in optimization-based statistical model calibration. Section 4.1.1 explains what happens if the statistical correlation is neglected in model calibration. A brief review of existing calibration metrics - specifically in terms of the statistical correlation is provided in Section 4.1.2.

4.1.1 What happens if the statistical correlation is neglected in model calibration?

It is common that the predicted output response $\widehat{\mathbf{Y}}_{\text{pre}}$ can be represented as a function of the input variables $\mathbf{X}$ that are embedded in a CAE model. In this

subsection, the output response $\widehat{\mathbf{Y}}_{\text{pre}}$ is assumed to be obtained through a bivariate model. One response is a quadratic equation and the other is a linear equation as:

$$y_1 = ax_1^2 + bx_1 \tag{4.1}$$

$$y_2 = cx_1 + dx_2 \tag{4.2}$$

The quadratic equation can be linearized by using the Taylor series expansion, at least in the neighborhood of the mean value of $\mathbf{X}$, as:

$$y_1 \cong (2a\mu_1 + b)(x_1 - \mu_1) + a\mu_1^2 + b\mu_1 = (2a\mu_1 + b)x_1 - a\mu_1^2 \tag{4.3}$$

It is assumed that the two input variables follow normal distributions and are independent from each other; $x_1 \sim N(\mu_1, \sigma_1^2)$ and $x_2 \sim N(\mu_2, \sigma_2^2)$. Here, the means and standard deviations of the input variables, denoted by μ_1, μ_2, σ_1, and σ_2, are unknown; these form the calibration parameter set $\boldsymbol{\theta}$. Then, the statistical parameters of the predicted output responses can be expressed in terms of the statistical parameters of the input variables as:

$$\boldsymbol{\mu}_{\widehat{\mathbf{Y}}} = \{a\mu_1^2 + b\mu_1 \quad c\mu_1 + d\mu_2\}^{\mathrm{T}} \tag{4.4}$$

$$\mathbf{COV}_{\widehat{\mathbf{Y}}} = \begin{bmatrix} (2a\mu_1 + b)^2\sigma_1^2 & (2ac\mu_1 + bc)\sigma_1^2 \\ \text{sym.} & c^2\sigma_1^2 + d^2\sigma_2^2 \end{bmatrix} \tag{4.5}$$

where $\boldsymbol{\mu}_{\widehat{\mathbf{Y}}}$ and $\mathbf{COV}_{\widehat{\mathbf{Y}}}$ denote the mean vector and covariance matrix of the predicted output response, respectively. When the observed output responses $\mathbf{Y}_{\text{obs}}$ follow normal distributions, the statistical parameters of the observed output response includes the mean vector and covariance matrix, denoted by $\boldsymbol{\mu}_{\mathbf{Y}}$ and $\mathbf{COV}_{\mathbf{Y}}$, respectively, as:

$$\boldsymbol{\mu}_{\mathbf{Y}} = \{m_1 \quad m_2\}^{\mathrm{T}} \tag{4.6}$$

$$\mathbf{COV}_{\mathbf{Y}} = \begin{bmatrix} cv_{11} & cv_{12} \\ \text{sym.} & cv_{22} \end{bmatrix} \tag{4.7}$$

The calibration parameter set can be inferred by comparing the statistics of the predicted output responses with those of the observed output responses. This calibration procedure can be considered as an inverse problem, which can be formulated as nonlinear simultaneous implicit equations as:

$$a\mu_1^2 + b\mu_1 = m_1 \tag{4.8}$$

$$c\mu_1 + d\mu_2 = m_2 \tag{4.9}$$

$$(2a\mu_1 + b)^2\sigma_1^2 = cv_{11} \tag{4.10}$$

$$c^2\sigma_1^2 + d^2\sigma_2^2 = cv_{22} \tag{4.11}$$

$$(2ac\mu_1 + bc)\sigma_1^2 = cv_{12} \tag{4.12}$$

Technically, since four unknowns and four equations are involved in Eqs. (4.8) to (4.12), the calibration parameter set $\boldsymbol{\theta}$ can be found by solving these equations simultaneously. The solution of the mean values μ_1 and μ_2 can be obtained by simultaneously solving the quadratic equation in Eq. (4.8) and the linear equation in Eq. (4.9) as:

$$\mu_1 = \frac{-b \pm \sqrt{b^2 + 4am_1}}{2a} \tag{4.13}$$

$$\mu_2 = \frac{m_2}{d} + \frac{bc \pm c\sqrt{b^2 + 4am_1}}{2ad} \tag{4.14}$$

There are two pairs of solutions for the mean values μ_1 and μ_2. These mean values obtained from Eqs. (4.13) and (4.14) are the mathematically valid solutions; however, it is not guaranteed that every solution is physically reasonable. Examples of physically unreasonable solutions of the calibration parameter include those with biased mean values or a large standard deviation. In addition, the existence of two

pairs of solutions implies that an optimization algorithm could lead to different solutions depending on the initial guess (the starting value) of the calibration parameters, rather than the physically reasonable solution. It is thus required to confine one pair of solutions for the mean values μ_1 and μ_2 for the CAE model. This solution conformity issue can be resolved by additionally considering Eq. (4.12). It is worth pointing out that Eq. (4.12) corresponds to the statistical correlation between the bivariate output responses. The value of the statistical correlation cv_{12} between the bivariate output responses can confine the solution of the calibration parameter μ_1, as:

$$\mu_1 = \frac{1}{2ac}\left(\frac{cv_{12}}{\sigma_1^2} - bc\right) \tag{4.15}$$

It can thus be concluded that the consideration of the statistical correlation helps provide a physically reasonable solution to statistical model calibration. In other words, ignoring the statistical correlation in Eq. (4.12) could result in an inaccurate solution. This drives research interest in developing a calibration metric that considers the statistical correlation between multivariate output responses.

4.1.2 Comments on existing calibration metrics in terms of the statistical correlation

This subsection briefly summarizes three existing calibration metrics in terms of the statistical correlation between multivariate output responses, including: (i) the marginal likelihood metric [53], (ii) the joint likelihood metric [59], and (iii) the moment matching metric [57].

First, the marginal likelihood metric is formulated as:

$$\mathrm{ML}(\boldsymbol{\theta}|\mathbf{Y}) = -\sum_{i=1}^{d}\sum_{j=1}^{n} \log_{10}\ f_{\hat{\mathbf{y}}_i}\left(y_{i,j}\middle|\boldsymbol{\theta}\right) \tag{4.16}$$

where **Y** is the *d*-dimensional observed (experimental) multivariate output response of an *n*-sample size; $y_{i,j}$ is the component of **Y**; the indices *i* and *j* represent the dimension and sequence of the sample, respectively; and $f_{\hat{\mathbf{y}}_i}$ denotes the marginal probability density function of the *i*th-dimensional predicted (model) output response. In the ML metric, it is assumed that multivariate output responses are statistically independent from each other . This implies that the ML metric neglects the statistical correlation between output responses.

Second, the joint likelihood is formulated as:

$$\mathrm{JL}(\boldsymbol{\theta}|\mathbf{Y}) = -\sum_{j=1}^{n} \log_{10}\ f_{\hat{\mathbf{y}}}\left(y_{1,j}, y_{2,j}, \dots, y_{d,j}\middle|\boldsymbol{\theta}\right) \tag{4.17}$$

where $y_{d,j}$ denotes a d-dimensional multivariate observed output response at the jth sampling sequence; and $f_{\hat{\mathbf{y}}}$ denotes the joint PDF of the d-dimensional multivariate predicted output response. It should be noted that the calculation of the JL metric requires the modeling of the joint PDF at every iteration of the optimization-based statistical model calibration. Copula, Nataf distribution, and kernel density estimation (KDE) can be used to estimate the joint PDF of the predicted output response [82], [83]. Even though the joint PDF contains the information on the statistical correlation, the estimation of the joint distribution can be inaccurate and less inefficient than that of the marginal PDF because of the curse of dimensionality. The curse of dimensionality means that a (nonparametric) density

estimator converges more slowly to the true PDF as the dimension increases due to data sparseness. Nagler et al. showed that a kernel density estimator requires 50 observations to accurately estimate an underlying univariate distribution, while 106 observations are required for a ten-dimensional multivariate joint PDF [84]. This indicates that – to accurately estimate the joint PDF – the required sample size for sampling-based uncertainty propagation (e.g., Monte Carlo simulation) increases rapidly as the dimension of the output response increases. Furthermore, the value of the JL metric is not bounded; thereby, it could have a numerically infinite value. If a calibration metric has an infinite value in optimization-based statistical model calibration, a gradient information-based searching algorithm would give an error at the starting point because it is impossible to calculate the numerical gradient.

Third, the moment matching metric (MM) [57] quantifies the difference between the statistical moments obtained by experiments and prediction. The moment matching metric is formulated as the weighted sum of the two functional:

$$\mathrm{MM}(\mathbf{y}, \hat{\mathbf{y}}(\boldsymbol{\theta})) = \boldsymbol{w}_{mean}\left\|\boldsymbol{\mu}_y - \boldsymbol{\mu}_{\hat{y}}\right\|_2^2 + \boldsymbol{w}_{cov}\left\|\boldsymbol{w}_v\left(\Delta Cov(\mathbf{y}, \hat{\mathbf{y}})\right)\boldsymbol{w}_v^{\boldsymbol{T}}\right\|_F^2 \qquad (4.18)$$

where $\boldsymbol{\mu}_y$ and $\boldsymbol{\mu}_{\hat{y}}$ denote the mean vector of the observed and predicted output responses, respectively; $\Delta\mathrm{Cov}(\mathbf{y}, \hat{\boldsymbol{y}})$ denotes the covariance matrix difference between the observed and predicted output responses; and w denotes the weighting vector ($\boldsymbol{w}_{mean}$ and $\boldsymbol{w}_{cov}$) and matrices ($\boldsymbol{w}_v$) that depend on the test data. In Eq. (4.18), the first term on the right-hand side is the 2-norm of the mean vector difference, while the second term is the Frobenius norm of the covariance matrix difference. This means that the second term on the right-hand side in Eq. (4.18) is in

charge of handling the statistical correlation between multivariate output responses. The advantage of the moment matching metric is that it can be efficiently calculated. However, due to experimental errors or lack of data, it is not guaranteed that the sample mean and standard deviation are not the true value. This implies that simply minimizing the mean vector and covariance matrix differences may lead to an inaccurate result. In addition, the weighting vector and matrix should be carefully chosen when the multivariate output responses have a different unit and scale. If the observed output responses have the same unit, the weighting matrix and vector can be set as an identity matrix and a ones-vector [57].

Therefore, it can be concluded from this brief review of existing calibration metrics that a calibration metric should be carefully formulated to properly quantify the statistical correlation between multivariate output responses; otherwise, it could give a poor calibration result. To overcome the limitations of existing calibration metrics, this study proposes a new calibration metric, this new metric is described in Section 4.2.

4.2 Proposed Method: Marginal probability and correlation residuals (MPCR)

The foundational idea of the MPCR metric is to decompose a multivariate joint probability distribution into multiple marginal probability distributions while considering the statistical correlation between the multivariate output responses. The MPCR metric is formulated as the sum of two normalized functionals, the Marginal

Probability Residual (MPR) and the Correlation Coefficient Residual (CCR):

$$\mathrm{MPCR} = \frac{1}{2}\sum_{i=1}^{d} \mathrm{MPR}_i + \frac{1}{d-1}\sum_{j<k}^{d} \mathrm{CCR}_{j,k}, \qquad (0 < \mathrm{MPCR} < 2d) \tag{4.19}$$

where d denotes the dimension of the multivariate output response. The value of the MPCR metric ranges from 0 to 2d.

In Eq. (4.19), the MPR_i quantifies the statistical difference between the predicted and observed output responses by using the marginal PDFs of the ith output response, which is formulated as:

$$\mathrm{MPR}_i = \int_{lb}^{ub} \left| f_{\hat{y}_i}(y|\boldsymbol{\theta}) - f_{y_i}(y) \right| dy, \qquad (0 < \mathrm{MPR}_i < 2)$$
$$\{ub \quad lb\} = \{\ \max(\hat{y}_{i,:}, y_{i,:}) \quad \min(\hat{y}_{i,:}, y_{i,:})\ \} \tag{4.20}$$

where $f_{\hat{y}_i}$ and f_{y_i} denote the marginal PDFs of the predicted and observed output responses, respectively; and y_i denotes the ith output response. The physical meaning of the MPR_i is a residual between the areas of the marginal PDFs of the ith predicted and observed output responses. The integration ranges from the lower to the upper bounds can be decided based on the min-max value of the output responses. The value of the MPR_i is bounded from 0 to 2. Figure 4-1 describes $f_{\hat{y}_i}$ and f_{y_i} for before and after calibration. To evaluate the MPR_i, marginal PDF estimation and numerical integration are required. In this study, KDE, which is a non-parametric PDF estimation method, is incorporated into the univariate PDF modeling. The Gaussian kernel is used as a basis function and the bandwidth is calculated by using the estimator proposed by Silverman [85].

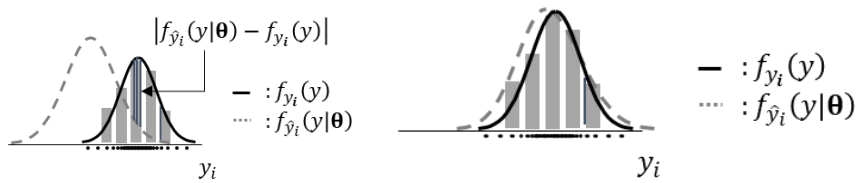

Figure 4-1 Marginal PDFs of the predicted and observed output responses: (a) before calibration and (b) after calibration

Compared to joint probability distributions, marginal probability distributions can be accurately modeled with computationally affordable efforts. However, the marginal probability distribution cannot capture the statistical correlation between the multivariate output responses. The $\mathrm{CCR}_{j,k}$ in Eq. (4.19) allows the MPCR metric to consider the statistical correlation, which is formulated as:

$$\mathrm{CCR}_{j,k} = \left|\rho_{\mathrm{pre}}\left(\hat{y}_{j,k}\middle|\boldsymbol{\theta}\right) - \rho_{\mathrm{obs}}(y_{j,k})\right|, \qquad (0 < \mathrm{CCR}_{j,k} < 2) \tag{4.21}$$

where $\rho_{\mathrm{pre}}\left(\hat{y}_{j,k}\middle|\boldsymbol{\theta}\right)$ and $\rho_{\mathrm{obs}}(y_{j,k})$ denote the correlation coefficients between the jth and kth output responses from model prediction and experimental observation, respectively. The correlation coefficient can be calculated as:

$$\rho\left(y_{j,k}\right) = \frac{1}{\sigma_{y_j}\sigma_{y_k}} E\left[\left(y_j - \mu_{y_j}\right)\left(y_k - \mu_{y_k}\right)\right] \tag{4.22}$$

The physical meaning of the CCR is the absolute difference between the correlation coefficients between the jth and kth output responses from the model prediction and the experimental observation. This implies that the value of $\mathrm{CCR}_{j,k}$ is bounded from 0 to 2. In this study, the formulation of the Pearson correlation coefficient was used to quantify the statistical correlation between the multivariate output responses.

The MPCR metric has many favorable properties as a calibration metric, such as (i) marginalization, (ii) normalization, and (iii) boundedness. First, the MPCR metric decomposes a multivariate joint probability distribution into multiple marginal probability distributions. The estimation of the marginal PDFs does not suffer from the curse of dimensionality, even for high-dimensional multivariate output responses. Second, $\sum_{i=1}^{d} \mathrm{MPR}_i$ is bounded from 0 to $2d$ and $\sum_{j<k}^{d} \mathrm{CCR}_{j,k}$ is bounded form 0 to $d(d-1)$, where d is the dimension of the multivariate output responses. To normalize the MPR and CCR, they are divided by 2 and $(d-1)$, respectively. Due to normalization, the MPCR metric can provide an accurate calibration result even when the multivariate output responses have a different unit and/or scale. Third, since the value of the MPCR metric is bounded from 0 to $2d$, the MPCR metric can directly describe the statistical similarity or dissimilarity between the predicted and observed output responses. For instance, if the value of the MPCR metric is close to 0, it can be concluded that the two probability distributions of the predicted and observed output responses are perfectly matched to each other. Conversely, if the value of the MPCR metric is close to $2d$, the two probability distributions do not coincide with each other.

The following section will demonstrate three case studies to show the outstanding performances of the proposed MPCR metric, as compared to existing calibration metrics, with respect to its ability to effectively consider the statistical correlation between multivariate output responses in optimization-based statistical model calibration.

4.3 Case Studies

In this section, two mathematical and two engineering examples are demonstrated to verify the effectiveness of the proposed MPCR metric. Here, the multi-start method, which is global optimization algorithm using multiple start points, was used as an optimizer. The initial points were sampled by using Latin hypercube sampling (LHS). The sequential quadratic programing was applied to all the initial points for each method. The computational cost and accuracy of each calibration metric are compared in each case study.

In the first mathematical example, the correlated bivariate output responses are considered to investigate the statistical correlation; in the second mathematical example, the correlated multivariate output responses are considered to investigate the curse of dimensionality. The first engineering example considers modal analysis of a beam structure with uncertain rotational stiffness boundary conditions to investigate scale issue. The second engineering example considers crashworthiness of vehicle side impact to demonstrate the effectiveness of the proposed method in a high dimensional and nonlinear problem. The calibration parameters of the input variables were inversely inferred by using optimization-based statistical model calibration. For the JL metric, the multivariate KDE and Gaussian copula are used to model the joint PDF; here, the former is called the JL_{KDE} and the latter is called the JL_{Copula}. The results are compared, with consideration of calibration metric properties.

4.3.1 Mathematical example 1: Bivariate output responses (Statistical correlation issue

In this example, the bivariate output responses are considered; one is a quadratic equation and the other is a linear equation. The functional relations between the input variables and the output responses are defined as:

$$\begin{aligned} \hat{y}_1(x) &= \mathbf{b}_1\mathbf{X} + \mathbf{X}^{\mathbf{T}}\mathbf{H}_1\mathbf{X} \\ \hat{y}_2(x) &= \mathbf{b}_2\mathbf{X} \end{aligned} \tag{4.23}$$

where $\mathbf{X}=[x_1\ x_2]^T$; $\mathbf{b_1}$=[1 0]; $\mathbf{H_1}$=[0.2 0; 0 0]; and $\mathbf{b_2}$=[1 -2]. The notions **b** and **H** are linear coefficients and Hessian matrices, respectively. Here, the input variables **X** are assumed to follow normal distributions. Then, the statistical parameters (the mean and standard deviation) of the input variables are assigned to be calibration parameters in the optimization-based statistical model calibration. The true statistical parameter vector of the input variables, denoted by $\boldsymbol{\theta}^*$, is that $[\mu_1, \sigma_1, \mu_2, \sigma_2]$= [-6, 0.2, -3, 0.2]. The observed bivariate output responses are given with 100 samples, as shown in Figure 4-2.

The number of runs for the Monte Carlo simulation (MCS) was 10,000 in this example. The marginal PDFs of the predicted output responses after optimization-

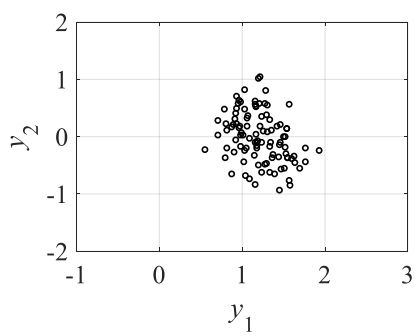

Figure 4-2 Observed correlated bivariate output responses (mathematical example 1)

based statistical model calibration are estimated by using the KDE with 10,000 samples, as shown in Figure 4-3. For each of the calibration metrics, the marginal PDFs of the predicted output responses after optimization-based statistical model calibration are in a very good agreement with the histograms of the observed ones. However, it is worth pointing out that even though the marginal PDFs of the predicted output responses are well matched with the histograms of the observed ones, the marginal PDFs of the input variables calibrated by the ML are invalid, as shown in Figure 4-4. This implies that the ML was failed to correctly infer the mean values of the input variables in Eq. (4.23). The other calibration metrics (the MPCR, the MM, the JL_{KDE}, and the JL_{Copula}), which are formulated considering statistical correlation, gave the valid results. This is attributed to the fact that optimization-based statistical model calibration inversely estimates the calibration parameters by maximizing the agreement (or minimizing the disagreement) between the two probability distributions of the predicted and observed output responses.

The joint PDF contours of the predicted output response calibrated by the MPCR and ML were drawn in Figure 4-5, respectively. The joint PDF contours were obtained by using the multivariate KDE from 10,000 samples. The scatters indicate the observed output response. It is interesting that the predicted output response calibrated by the ML exhibits totally opposite statistical correlation, as compared to the observed one. This is because the ML is formulated with an assumption that the bivariate output responses are not statistically correlated to each other. It can be thus concluded that even though the predicted marginal PDF of the output response after calibration matches well with the observed one, inaccurate solutions could be obtained if the statistical correlation between the output responses is not properly

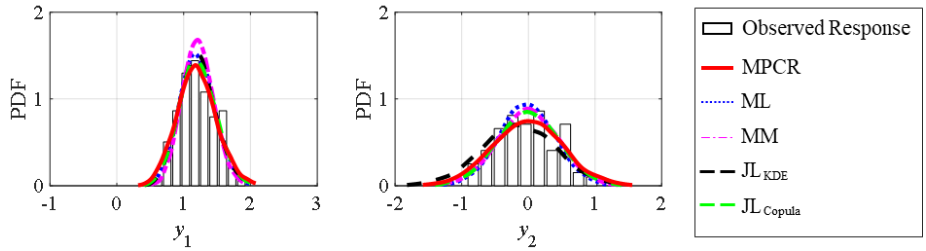

Figure 4-3 Calibrated marginal PDFs of the output responses (mathematical example 1)

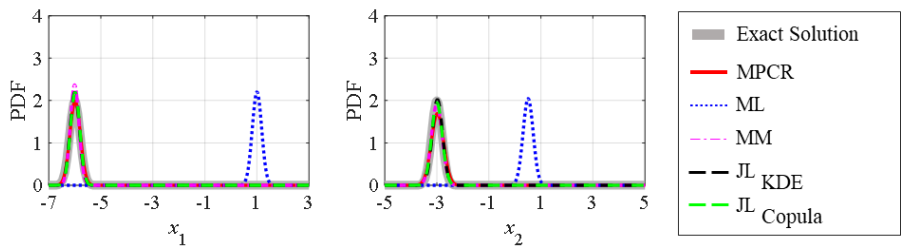

Figure 4-4 Calibrated marginal PDFs of the input variables (mathematical example 2)

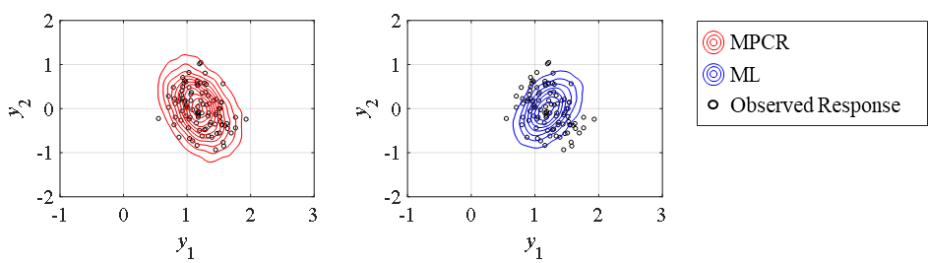

Figure 4-5 The joint PDFs of the output responses calibrated by the MPCR and ML

considered in formulating a calibration metric.

Table 4-1 summarizes the estimated calibration parameters, relative errors, iterations, and function calls for optimization-based statistical model calibration. Except for the ML, the relative errors of the estimated calibration parameters are below 10 % which are acceptable. It is worth noticing that the iteration and function

Table 4-1 The estimated statistical parameters, relative errors, iterations, and function calls (Mathematical example 1)

Calibration metric		Calibration parameters				Iterations	Function calls
		μ_1	σ_1	μ_2	σ_2		
Exact solution		-6.00	0.20	-3.00	0.20	-	-
MPCR	Estimate	-6.03	0.18	-3.03	0.22	22	142
	Error (%)	0.53	-9.11	1.16	8.28		
ML	Estimate	1.03	0.19	0.50	0.19	54	290
	Error (%)	-117.09	-4.94	-116.56	-6.59		
MM	Estimate	-6.03	0.16	-3.04	0.20	26	181
	Error (%)	0.50	-19.76	1.24	-1.59		
JL (KDE)	Estimate	-6.03	0.19	-3.03	0.19	21	171
	Error (%)	0.46	-7.40	1.04	-4.89		
JL (Gaussian copula)	Estimate	-6.02	0.19	-3.03	0.20	22	143
	Error (%)	0.37	-6.71	1.18	1.36		

MPCR: Marginal probability correlation residual
ML: Marginal likelihood metric
MM: Moment matching metric
JL: Joint likelihood metric
Error $= 100 \times (s - \hat{s})/s$ (%), s is the exact value and $\hat{s}$ is an estimate

calls for calibration using the ML is the highest; even its accuracy is poor. In general, the computational cost of optimization-based statistical model calibration is proportional to the function calls. Since each function call requires UP analysis, therefore, it can be concluded that the proposed MPCR is efficient as well as accurate for optimization-based statistical model calibration in the first mathematical example.

4.3.2 Mathematical example 2: Multivariate output responses (Curse of dimensionality issue)

The first example considered two correlated output responses. However, when the output responses are involved more, the curse of dimensionality issue could arise in optimization-based statistical model calibration. The second mathematical example thus considers five correlated output responses to investigate the curse of dimensionality issue; all the functional relations between the input variables and output responses are linear equations as:

$$\hat{y}_i(x) = \mathrm{c}_i + \mathbf{b}_i\mathbf{X} \quad (i = 1, 2, \dots, 5) \tag{4.24}$$

where $\mathbf{X}=[x_1\ x_2\ x_3\ x_4\ x_5]^{\mathrm{T}}$; $\mathbf{b}_1$=[0 9 3 -8 -2]; $\mathbf{b}_2$=[5 -1 3 3 9]; $\mathbf{b}_3$=[9 -6 8 5 0]; $\mathbf{b}_4$=[-5 -6 7 5 -2]; $\mathbf{b}_5$=[-2 8 1 4 2]; and $[\mathrm{c}_1\ \mathrm{c}_2\ \mathrm{c}_3\ \mathrm{c}_4\ \mathrm{c}_5]$ = [2 7 8 2 2]. The notations **b** and c are linear coefficients and constants, respectively. Here, the input variables **X** are assumed to follow normal distributions. Then, the statistical parameters (the mean and standard deviation) of the input variables are assigned to be calibration parameters in optimization-based statistical model calibration. The true statistical parameter vector of the input variables, denoted by $\boldsymbol{\theta}^*$, is that $[\mu_1, \sigma_1, \mu_2, \sigma_2, \mu_3, \sigma_3, \mu_4, \sigma_4, \mu_5, \sigma_5]$ = [2, 0.5, 4, 0.3, 1, 0.6, 5, 0.7, 2, 0.4].

To investigate how the curse of dimensionality affects optimization-based statistical model calibration, the number of runs for the MCS varies from one hundred to ten thousands in this example. The marginal PDFs of the predicted output responses after optimization-based statistical model calibration are estimated by using the KDE with 10,000 samples, as shown in Figure 4-6. For the remaining four different calibration metrics excepting the ML, the marginal PDFs of the predicted output responses after optimization-based statistical model calibration are in a good

agreement with the histograms of the observed ones.

As shown in Figure 4-7, the marginal PDFs of the input variables calibrated by the ML are inaccurate regardless of the MCS sampling size; this is, because it does not consider the statistical correlation between the multivariate output responses. It is worth noting that the calibration results of the JL_{KDE} become increasingly accurate, as the number of MCS runs is increased. This is due to the curse of dimensionality that causes the inaccurate estimation of the joint PDF when the number of runs for the MCS is relatively small. In general, because of data sparseness, the multivariate KDE requires larger sample sizes, as the dimension of the output responses increases.

On the other hand, the number of MCS runs has little influence on the marginal PDFs of the input variables calibrated by the MPCR and JL_{Copula}, as shown in Figure 4-7. The MPCR metric does not suffer from the curse of dimensionality, since it incorporates the univariate KDE into the modeling of the marginal PDF. Even though JL_{Copula} requires joint PDF modeling, it is known that the Gaussian copula does not suffer from the curse of dimensionality. However, use of the Gaussian copula will cause the improper modeling of the joint PDF when the assumed distribution of the input variable differs from the true distribution.

The joint PDF contours of the first and second predicted output responses (y_1-y_2 and y_4-y_5) after calibration when the number of MCS runs is 10,000 were drawn in Figure 4-8. The joint PDF contours were obtained by using the multivariate KDE from 10,000 samples. The scatters indicate the observed output response. It is interesting that the predicted output responses calibrated by the ML exhibit totally opposite statistical correlation, as compared to the observed one. It can be concluded

from the results that the proposed MPCR can improve the accuracy of optimization-based statistical model calibration even for a high-dimensional problem.

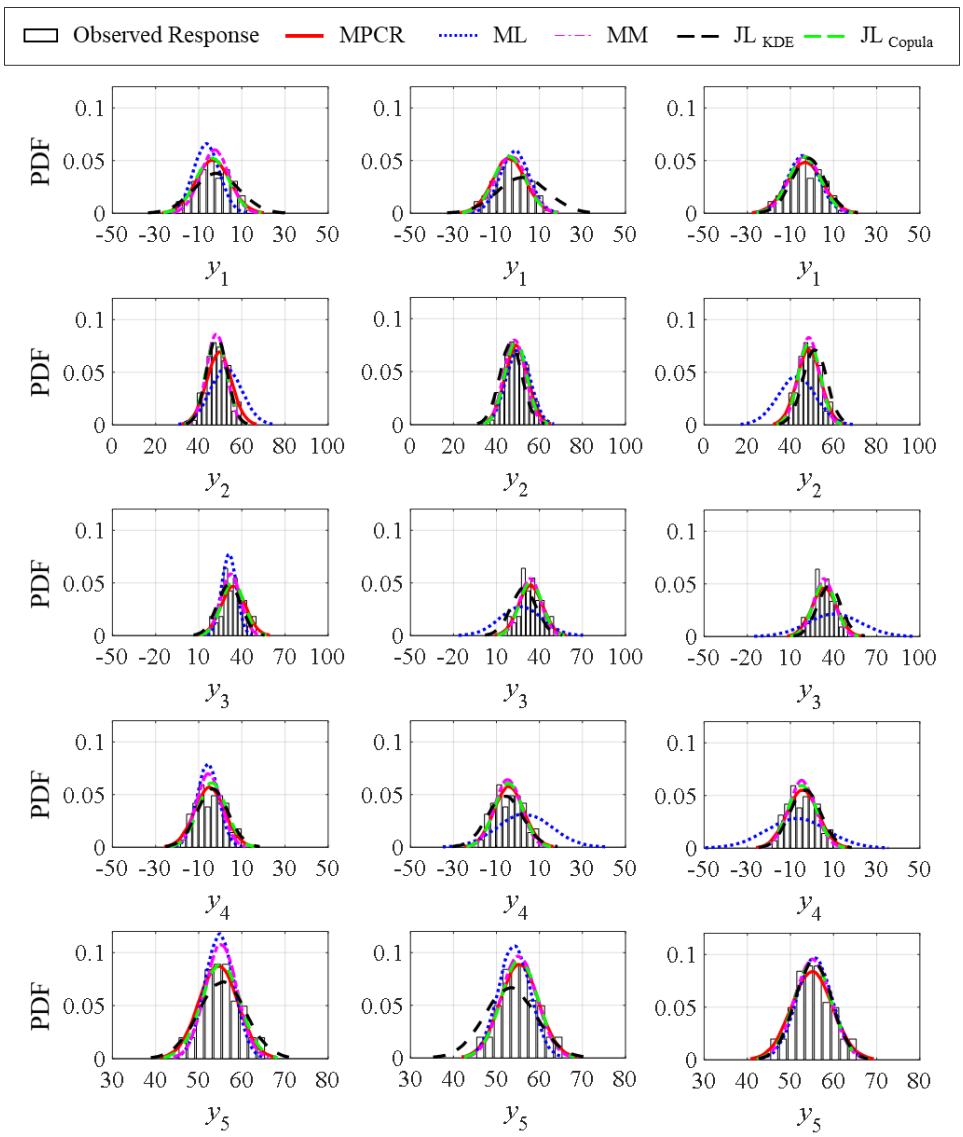

Figure 4-6 Calibrated marginal PDFs of the output response with the number of MCS runs of: (a) 100, (b) 1,000, and (c) 10,000 (mathematical example 2)

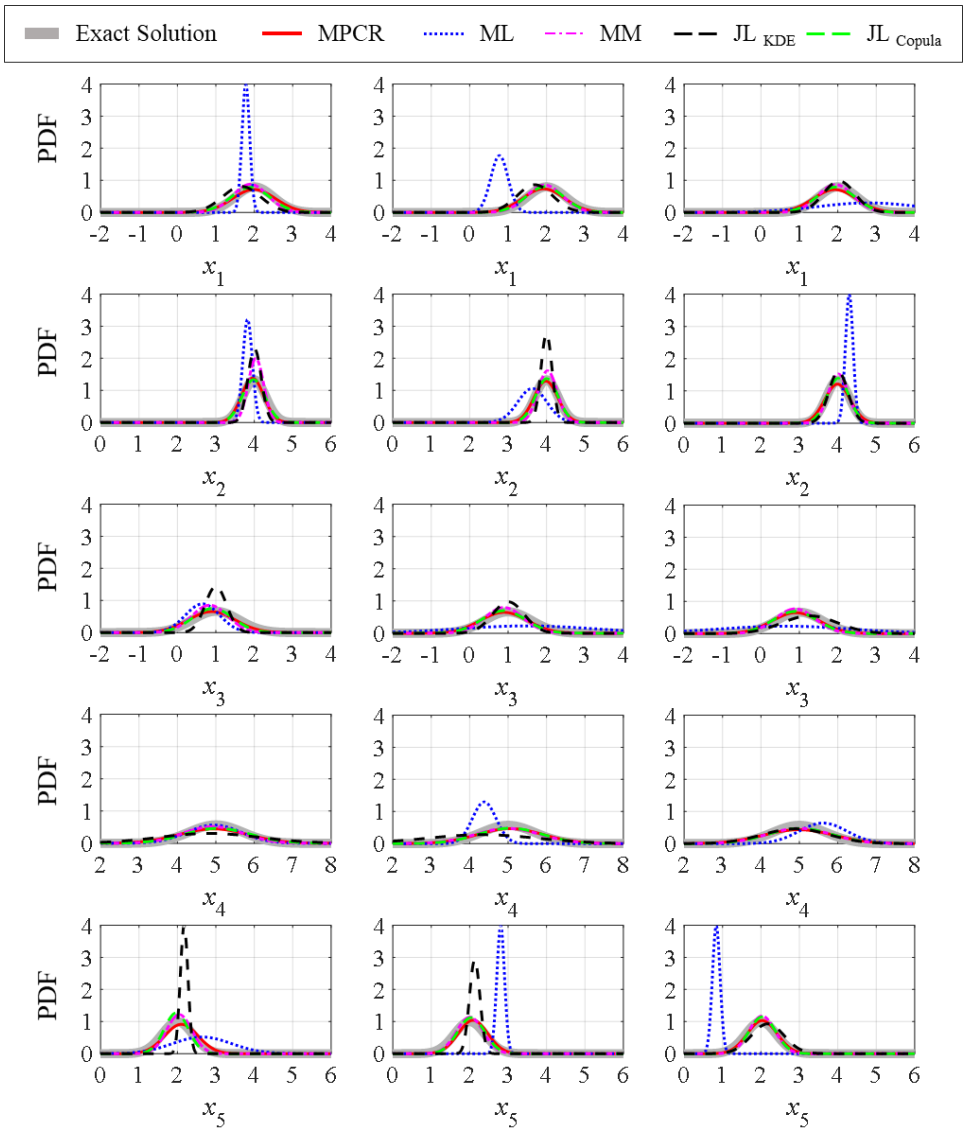

Figure 4-7 Calibrated marginal PDFs of the input variables with the number of MCS runs of: (a) 100, (b) 1,000, and (c) 10,000 (mathematical example 2)

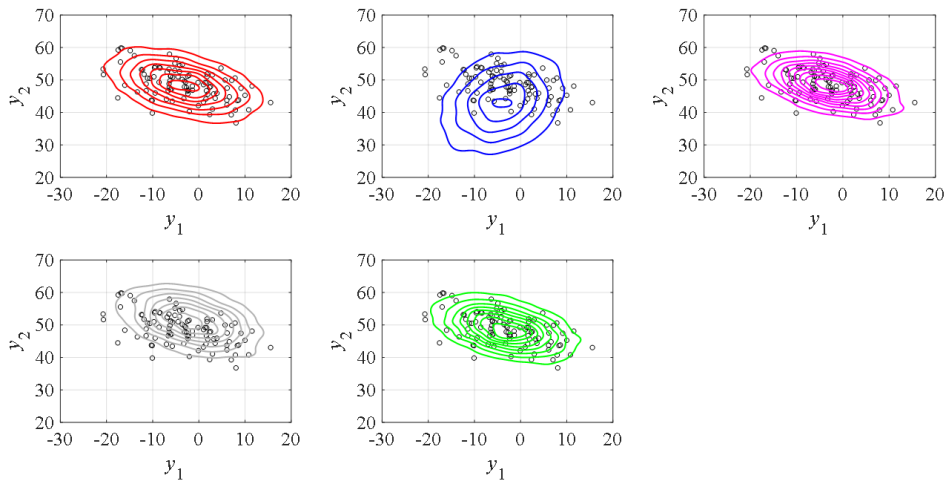

(a) The join PDF and scatter plot of y_1 and y_2

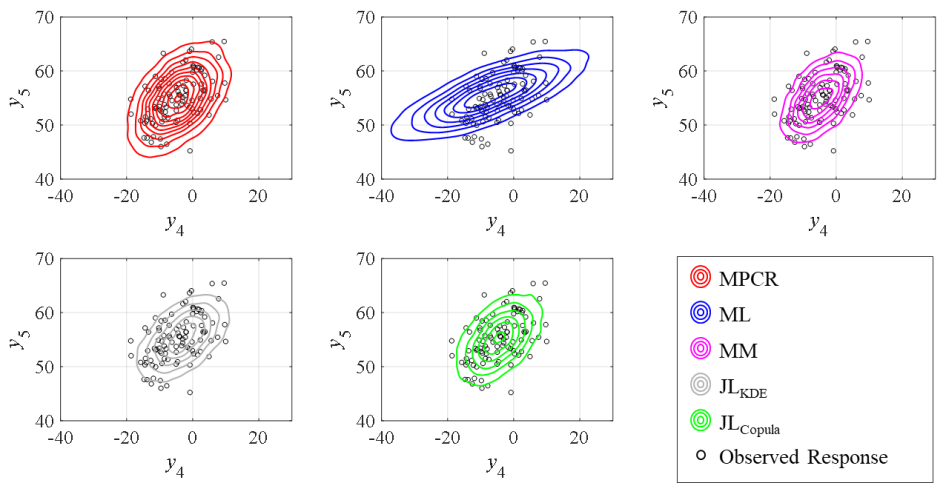

(b) The join PDF and scatter plot of y_4 and y_5

Figure 4-8 Calibrated joint PDFs of the output responses (mathematical example 2)

Table 4-2,4-2 and 4-3 summarize the estimated calibration parameters, relative errors, iterations, and function call for optimization-based statistical model calibration, which depend on the number of MCS runs. The relative error of the estimated calibration parameters by using the ML are not acceptable regardless of

the number of MCS runs. In addition, the relative errors of the JL_{KDE} decrease, as the number of MCS runs increases. The relative errors of the MPCR, JL_{Copula}, and MM are less than 40 %, regardless of the number of MCS runs. Even though the function call of the MPCR is relatively high compared to the other calibration metric, it can lead to an accurate solution regardless of the number of MCS runs in this example.

Table 4-2 The estimated calibration parameters, relative errors, iterations, and function calls (Mathematical example 2: the number of MCS runs is 100)

Calibration metric		Calibration parameters										Iterations	Function calls
		μ_1	σ_1	μ_2	σ_2	μ_3	σ_3	μ_4	σ_4	μ_5	σ_5		
Exact solution		2.00	0.50	4.00	0.30	1.00	0.60	5.00	0.70	2.00	0.40	-	-
MPCR	Estimate	1.99	0.56	3.96	0.29	0.89	0.61	4.94	0.89	2.10	0.44	58	725
	Error (%)	-0.40	11.48	-1.09	-3.78	-10.50	1.62	-1.20	27.36	5.19	8.99		
ML	Estimate	1.78	0.10	3.83	0.12	0.65	0.45	4.95	0.70	2.64	0.77	37	511
	Error (%)	-10.98	-80.00	-4.36	-58.60	-34.60	-25.77	-0.96	0.67	32.05	92.05		
MM	Estimate	1.90	0.45	4.04	0.20	0.84	0.47	4.92	0.77	2.05	0.33	53	701
	Error (%)	-5.06	-9.06	1.04	-33.26	-16.04	-22.12	-1.52	10.52	2.29	-18.08		
JL (KDE)	Estimate	1.67	0.49	4.01	0.17	1.00	0.28	4.83	1.30	2.18	0.10	38	522
	Error (%)	-16.54	-1.52	0.22	-41.94	0.04	-53.62	-3.42	85.85	8.76	-75.00		
JL (Gaussian copula)	Estimate	1.90	0.51	3.98	0.30	0.92	0.53	5.04	0.86	1.97	0.31	51	664
	Error (%)	-4.88	2.26	-0.51	-0.35	-8.43	-11.54	0.74	23.14	-1.38	-21.43		

MPCR: Marginal probability correlation residual
ML: Marginal likelihood metric
MM: Moment matching metric
JL: Joint likelihood metric
Error $= 100 \times (s - \hat{s})/s$ (%), s is the exact value and $\hat{s}$ is an estimate

Table 4-3 The estimated calibration parameters, relative errors, iterations, and function calls using (Mathematical example 2: the number of MCS runs is 1,000)

Calibration metric		Calibration parameters										Iterations	Function calls
		μ_1	σ_1	μ_2	σ_2	μ_3	σ_3	μ_4	σ_4	μ_5	σ_5		
Exact solution		2.00	0.50	4.00	0.30	1.00	0.60	5.00	0.70	2.00	0.40	-	-
MPCR	Estimate	1.92	0.54	3.98	0.31	0.89	0.62	5.06	0.86	2.09	0.38	50	646
	Error (%)	-3.81	8.33	-0.39	2.86	-10.84	2.57	1.13	22.33	4.35	-4.20		
ML	Estimate	0.77	0.23	3.63	0.38	1.49	1.76	4.38	0.31	2.81	0.10	54	702
	Error (%)	-61.25	-54.90	-9.25	25.63	49.20	192.64	-12.39	-56.02	40.38	-75.00		
MM	Estimate	1.95	0.47	4.03	0.25	0.89	0.50	5.00	0.84	2.01	0.35	42	593
	Error (%)	-2.45	-6.56	0.66	-17.32	-10.87	-16.53	-0.07	20.59	0.29	-12.42		
JL (KDE)	Estimate	1.70	0.46	4.00	0.14	1.01	0.41	4.33	1.44	2.13	0.14	44	584
	Error (%)	-15.13	-7.56	-0.01	-51.79	0.65	-31.61	-13.35	105.90	6.58	-65.80		
JL (Gaussian copula)	Estimate	1.96	0.50	4.01	0.29	0.88	0.57	5.06	0.83	2.04	0.36	33	478
	Error (%)	-2.22	-0.51	0.15	-2.40	-11.59	-5.00	1.12	19.01	1.91	-11.15		

MPCR: Marginal probability correlation residual
ML: Marginal likelihood metric
MM: Moment matching metric
JL: Joint likelihood metric
Error $= 100 \times (s - \hat{s})/s$ (%), s is the exact value and $\hat{s}$ is an estimate

Table 4-4 The estimated calibration parameters, relative errors, iterations, and function calls using (Mathematical example 2: the number of the MCS is 10,000)

Calibration metric		Calibration parameters										Iterations	Function calls
		μ_1	σ_1	μ_2	σ_2	μ_3	σ_3	μ_4	σ_4	μ_5	σ_5		
Exact Solution		2.00	0.50	4.00	0.30	1.00	0.60	5.00	0.70	2.00	0.40	-	-
MPCR	Estimate	1.92	0.56	3.99	0.33	0.91	0.61	4.98	0.92	2.03	0.39	55	688
	Error (%)	-3.95	12.09	-0.21	9.69	-9.40	2.30	-0.32	31.49	1.64	-3.25		
ML	Estimate	2.80	1.34	4.30	0.10	0.62	1.73	5.62	0.62	0.84	0.10	39	514
	Error (%)	40.02	167.85	7.46	-66.67	-38.21	188.15	12.33	-10.99	-58.15	-75.00		
MM	Estimate	1.94	0.46	4.01	0.26	0.89	0.52	5.00	0.84	2.03	0.34	49	666
	Error (%)	-2.87	-8.10	0.27	-12.66	-10.94	-13.40	-0.02	20.20	1.43	-15.05		
JL (KDE)	Estimate	2.03	0.41	4.01	0.25	1.27	0.72	4.91	0.86	2.18	0.43	40	546
	Error (%)	1.73	-18.39	0.36	-16.68	27.43	20.52	-1.84	23.50	8.79	7.39		
JL (Gaussian copula)	Estimate	1.95	0.50	4.01	0.29	0.89	0.58	5.01	0.84	2.03	0.35	54	713
	Error (%)	-2.68	0.74	0.14	-4.16	-11.09	-3.56	0.13	20.42	1.72	-13.00		

MPCR: Marginal probability correlation residual
ML: Marginal likelihood metric
MM: Moment matching metric
JL: Joint likelihood metric
Error $= 100 \times (s - \hat{s})/s$ (%), s is the exact value and $\hat{s}$ is an estimate

4.3.3 Engineering example 1: Modal analysis of a beam structure with uncertain rotational stiffness boundary conditions (Scale issue)

The boundaries of beam structures can be theoretically described as simply-supported or fixed conditions. However, in practice, the boundaries of beam structures might be clamped with joining processes, such as bolting, welding, or riveting. In this situation, the boundary condition of a beam structure cannot be exactly described as either having a simply-supported or a fixed condition. Therefore, the stiffness of the boundary conditions is uncertain, and decreases with time due to wear and/or looseness. In this example, optimization-based statistical model calibration is performed to infer the unknown statistical parameters of the rotational stiffness of the boundary condition of a beam structure.

The beam structure, which consists of six elements and seven nodes, was described in Figure 4-9. The boundary condition of the beam structure is modeled as the rotational stiffness connected between the rigid wall and the boundary nodes. The displacement in the *y*-direction is fixed at the end nodes 1 and 7. In Figure 4-9, k_r and k_l denote the rotational stiffness at the left and right ends of the beam, respectively. In this study, the bivariate output responses include the 3rd natural frequency of the beam, and the 3rd mode shape value ratio in the *y*-direction of the 4th and 6th nodes. In real experiments, the natural frequency and corresponding mode shape can be measured by a modal test. In this study, a computational model using a finite element method (FEM) was constructed to perform modal analysis. The Euler-Bernoulli beam theory is incorporated into the FEM to simulate the behavior of the beam.

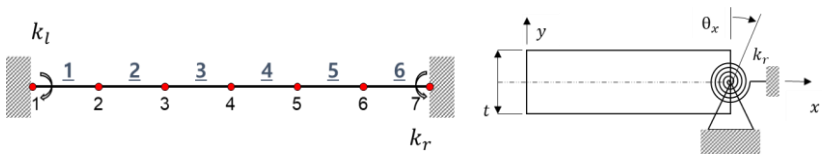

Figure 4-9 Schematic representation of the beam structure

The displacement of the Euler-Bernoulli beam can be mathematically described by a partial differential equation (PDE) as:

$$u = -y\frac{dv}{dx} \tag{4.25}$$

where u and v denote the displacement in the x- and y-directions, respectively. Based on the FEM, the equation of motion can be expressed as:

$$\mathbf{M}_a\ddot{\mathbf{U}} + \mathbf{K}_a\mathbf{U} = \mathbf{F} \tag{4.26}$$

where $\mathbf{M}_a$ and $\mathbf{K}_a$ denote the assembled mass and stiffness matrices, respectively; and the **U** and **F** denote the state (degree of freedom) and force vectors, respectively. The state and force vectors of the *i*th element are defined, respectively, as:

$$\mathbf{u}_i = \begin{Bmatrix} v_i \\ \theta_i \\ v_{i+1} \\ \theta_{i+1} \end{Bmatrix}, \qquad \mathbf{f}_i = \begin{Bmatrix} f_i \\ m_i \\ f_{i+1} \\ m_{i+1} \end{Bmatrix} \quad (i = 1, \dots, 6) \tag{4.27}$$

The beam element mass and stiffness matrices are defined, respectively, as:

$$\mathbf{M}_e = \frac{\rho_d Al}{420}\begin{bmatrix} 156 & 22l & 54 & -13l \\ 22l & 4l^2 & 13l & -3l^2 \\ 54 & 13l & 156 & -22l \\ -13l & -3l^2 & -22l & 4l^2 \end{bmatrix}, \qquad \mathbf{K}_e = \frac{EI}{l^3}\begin{bmatrix} 12 & 6l & -12 & 6l \\ 6l & 4l^2 & -6l & 2l^2 \\ -12 & -6l & 12 & -6l \\ 6l & 2l^2 & -6l & 4l^2 \end{bmatrix} \tag{4.28}$$

where E denotes the Young's modulus; ρ_d denotes the density; I and A denote the moment of inertia and cross-sectional area of the beam, respectively; and l denotes the beam length. In this example, it is assumed the beam is made of

aluminum (E = 70 GPa and ρ_d = 2760 kg/m^3). The width, thickness, and length of the beam are 15 mm, 1.5 mm, and 240 mm, respectively; the shape of the cross-section is rectangular.

It is assumed that the rotation spring constant at the left and right ends of the beam, denoted by k_l and k_r, follow normal distributions. Here, the calibration parameter is the normalized statistical parameter ($\boldsymbol{\theta}/k_r$), where $k_{r,0}$ is the nominal value of the rotational stiffness ($k_{r,0}$ = 400 N·m). The true statistical parameters of the input variables, denoted by $\boldsymbol{\theta}^*$, is that [μ_1, σ_1, μ_2, σ_2] = [$0.10k_{r,0}$, $0.05k_{r,0}$, $0.70k_{r,0}$, $0.03k_{r,0}$]. The observed bivariate output responses are given with 100 samples, as shown in Figure 4-10. It should be noted that there is a scale difference between the 3rd natural frequency and the mode shape value ratio.

The number of MCS runs was 10,000 in this example. The marginal PDFs of the predicted output responses after optimization-based statistical model calibration are estimated using the KDE with 10,000 samples, as shown in Figure 4-11. For the remaining three different calibration metrics, excepting the ML and MM, the marginal PDFs of the predicted output responses after optimization-based statistical

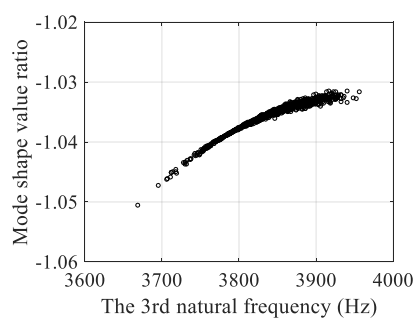

Figure 4-10 Observed correlated bivariate output responses (engineering example 1)

model calibration are in a good agreement with the histograms of the observed ones.

For both k_l and k_r, the predicted marginal PDFs of the input variables calibrated by the MPCR (red color) are in a very good agreement with the exact ones, as shown in Figure 4-12. However, both the ML and MM failed to correctly estimate the calibration parameters. As explained in Section 4.1.2, the MM requires the weighting matrix and vector to aggregate the mean vector and covariance matrix differences as one scalar value. In this example, the weighting matrix and vector were set as the identity matrix and ones-vector, respectively. However, the weighting matrix and vector should be carefully chosen when the output responses have a different unit and scale. Therefore, since there is a scale difference between the 3rd natural frequency and mode shape value ratio, the MM provided inaccurate calibration results. For the rotation spring constant at the left k_l, the JL_{KDE} and JL_{Copula} provide valid calibration results. However, for the rotation spring constant at the right k_r, the predicted marginal PDF calibrated by the JL_{Copula} is inaccurate, especially in terms of standard deviation. The JL_{Copula} is formulated with an assumption that the output responses follow Gaussian distributions. In this example, even though the input variables follow a Gaussian distribution, the bivariate output responses do not; thereby, the calibration result of the JL_{Copula} for k_r is not valid. This issue is related to the flexibility of the Gaussian copula.

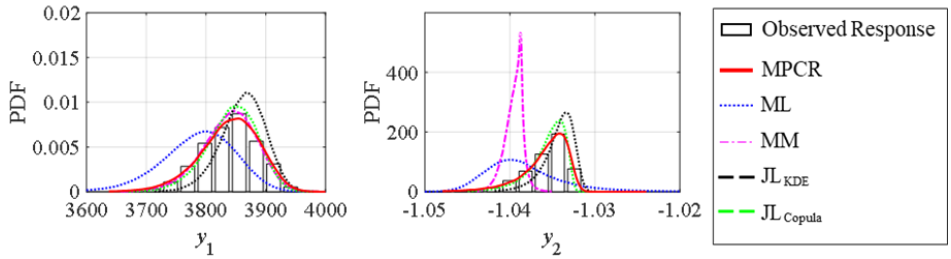

Figure 4-11 Calibrated marginal PDFs of the output responses (engineering example 1)

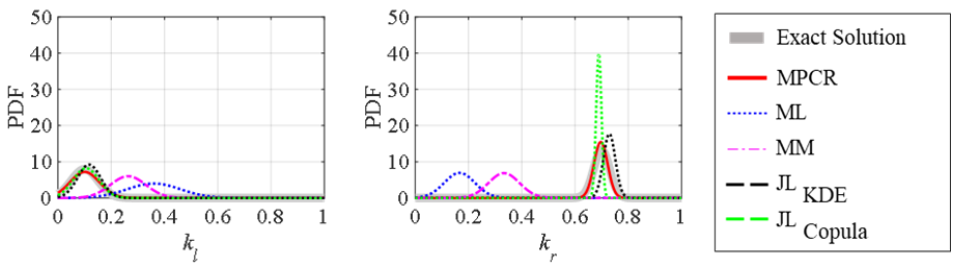

Figure 4-12 Calibrated marginal PDFs of the input variables (engineering example 1)

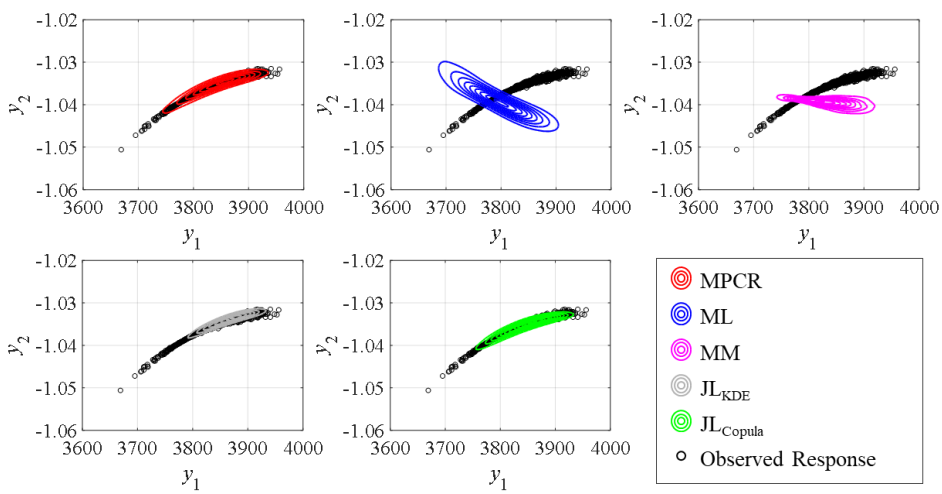

Figure 4-13 Calibrated joint PDFs of the output responses (engineering example 1)

The joint PDF contours of the predicted output responses were drawn in Figure 4-13. The joint PDF contours were obtained by using the multivariate KDE from

10,000 samples. The scatters indicate the observed output response. The predicted joint PDFs calibrated by the MM and ML are somewhat distorted and have opposite statistical correlation, as compared to the scatters. It can be thus concluded from the results that it is better to normalize a calibration metric to avoid the scale issue while considering the statistical correlation.

Table 4-5 The estimated statistical parameters, relative errors, iterations, and function calls (Mathematical example 1)

Calibration metric		Calibration parameters				Iterations	Function calls
		$\frac{\mu_1}{k_{r,0}}$	$\frac{\sigma_1}{k_{r,0}}$	$\frac{\mu_2}{k_{r,0}}$	$\frac{\sigma_2}{k_{r,0}}$		
Exact solution		0.10	0.05	0.70	0.03	-	-
MPCR	Estimate	0.10	0.06	0.70	0.03	17	119
	Error (%)	0.01	10.67	-0.47	-14.02		
ML	Estimate	0.36	0.10	0.17	0.06	15	119
	Error (%)	259.84	100.12	-76.23	91.65		
MM	Estimate	0.26	0.07	0.33	0.06	8	82
	Error (%)	163.26	32.71	-52.39	93.45		
JL (KDE)	Estimate	0.12	0.04	0.73	0.02	15	121
	Error (%)	16.83	-13.53	4.12	-24.94		
JL (Gaussian copula)	Estimate	0.11	0.05	0.69	0.01	17	108
	Error (%)	5.37	-3.09	-1.52	-66.67		

MPCR: Marginal probability correlation residual
ML: Marginal likelihood metric
MM: Moment matching metric
JL: Joint likelihood metric
Error $= 100 \times (s - \hat{s})/s$ (%), s is the exact value and $\hat{s}$ is an estimate

Table 4-5 shows the estimated calibration parameters, relative errors, iterations, and function call for optimization based statistical model calibration. It is worth pointing out that the relative errors of the estimated calibration parameters obtained by the proposed MPCR is the smallest compared to the other calibration metrics.

4.3.4 Engineering example 2: Crashworthiness of vehicle side impact (High dimensional & nonlinear problem)

In this example, a model for crashworthiness analysis of vehicle side impact [86] is statistically calibrated, which is high dimensional and nonlinear problem. The predictive capability of a model for crashworthiness analysis is important in reliable vehicle design. Statistical model calibration can be used to improve the credibility of crashworthiness analysis. In this study, it is assumed that the multivariate output responses can be measured by sensor attached to a dummy and a vehicle during side impact testing. The multivariate output responses include the abdomen load (y_1); the upper, middle, and lower rib deflections (y_2, y_3, y_4); the upper, middle, and lower viscous criteria (y_5, y_6, y_7); the public symphysis force (y_8); the velocity of the B-pillar (y_9); and the velocity of the front door (y_{10}). Due to the expense of a full-vehicle FE structural model, this study used the global response surface model generated using the quadratic backward-Stepwise Regression (SR), which was employed by Youn at el [] as:

$$y_1 = 1.16 - 0.3717x_2x_4 - 0.00931x_2x_{10} - 0.484x_3x_9 + 0.01343x_6x_{10} \quad (4.29)$$

$$y_2 = 28.98 + 3.818x_3 - 4.2x_1x_2 + 0.0207x_5x_{10} + 6.63x_6x_9 \\ -7.7x_7x_8 + 0.32x_9x_{10} \quad (4.30)$$

$$y_3 = 33.86 + 2.95x_3 + 0.1792x_{10} - 5.057x_1x_2 - 11.0x_2x_8 - 0.0215x_5x_{10} - 9.98x_7x_8 + 22.0x_8x_9 \quad (4.31)$$

$$y_4 = 46.36 - 9.9x_2 - 12.9x_1x_8 + 0.1107x_3x_{10} \quad (4.32)$$

$$y_5 = 0.261 - 0.0159x_1x_2 - 0.188x_1x_8 - 0.019x_2x_7 + 0.0144x_3x_5 + 0.0008757x_5x_{10} + 0.08045x_6x_9 + 0.00139x_8x_{11} + 0.00001575x_{10}x_{11} \quad (4.33)$$

$$y_6 = 0.214 + 0.00817x_5 - 0.131x_1x_8 - 0.0704x_1x_9 + 0.03099x_2x_6 - 0.018x_2x_7 + 0.0208x_3x_8 + 0.121x_3x_9 - 0.00364x_5x_6 + 0.0007715x_5x_{10} - 0.0005354x_6x_{10} + 0.00121x_8x_{11} \quad (4.34)$$

$$y_7 = 0.74 - 0.061x_2 - 0.163x_3x_8 + 0.001232x_3x_{10} - 0.166x_7x_9 + 0.227x_2^2 \quad (4.35)$$

$$y_8 = 4.72 - 0.5x_4 - 0.19x_2x_3 - 0.0122x_4x_{10} + 0.009325x_6x_{10} + 0.000191x_{11}^2 \quad (4.36)$$

$$y_9 = 10.58 - 0.674x_1x_2 - 1.95x_2x_8 + 0.02054x_3x_{10} - 0.0198x_4x_{10} + 0.028x_6x_{10} \quad (4.37)$$

$$y_{10} = 16.45 - 0.489x_3x_7 - 0.843x_5x_6 + 0.0432x_9x_{10} - 0.0556x_9x_{11} - 0.000786x_{11}^2 \quad (4.38)$$

where x_1 to x_7 denote the thickness of B-pillar inner (x_1), B-pillar reinforce (x_2), Floor side inner (x_3), Cross member (x_4), Door beam (x_5), Door belt line (x_6), and Roof rail (x_7), respectively; x_8 and x_9 denote the Young's modulus of B-pillar inner (x_8), and floor side inner (x_9), respectively; x_{10} and x_{11} denote barrier height (x_{10}), and hitting position (x_{11}), respectively. he input variables, x_1 to x_7 are assumed to follow lognormal distributions, while x_8 and x_9 are assumed to follow normal distributions. Then, the statistical parameters (the mean and standard deviation) of x_1 to x_9 are assigned to be calibration parameters in optimization-based statistical model calibration. The true statistical parameter vector of the input variables, denoted by θ^*, is that [μ_1, σ_1, μ_2, σ_2, μ_3, σ_3, μ_4, σ_4, μ_5, σ_5, μ_6, σ_6, μ_7, σ_7, μ_8, σ_8, μ_9, σ_9] = [0.51, 0.22, 1.42, 0.19, 0.49, 0.17, 1.34, 0.30, 0.69, 0.22, 1.49, 0.32, 0.50, 0.11, 0.36, 0.06, 0.20, 0.06]. Table 4-6 summarizes the information of the input variables, x_1 to x_9. In this

study, x_{10} and x_{11} are considered as known input variables with uniform distributions. The mean and standard deviation of x_{10} and x_{11} are defined as [μ_{10}, σ_{10}, μ_{11}, σ_{11}] = [0.00, 1.00, 0.00, 1.00].

The number of MCS runs was 10,000 in this example. The marginal PDFs of the predicted output responses after optimization-based statistical model calibration are estimated by using the KDE with 10,000 samples, as shown in Figure 4-14. For the remaining four different calibration metrics excepting the MM, the marginal PDFs of the predicted output responses after optimization-based statistical model calibration are in a good agreement with the histograms of the observed ones.

The predicted marginal PDFs of the input variables calibrated by the MPCR (red solid line) and JL_{Copula} (green dashed line) are in a very good agreement with the exact ones, as shown in Figure 4-15. However, the ML, MM, and JL_{KDE} fail to correctly estimate the calibration parameters due to their own limitation, as explained

Table 4-6 Information of the input variables of the vehicle side impact model

Category (Unit)	Input Variables	Vehicle Component	Distribution Type
Thickness (mm)	x_1	B-pillar inner	Lognormal
	x_2	B-pillar reinforce	Lognormal
	x_3	Floor side inner	Lognormal
	x_4	Cross member	Lognormal
	x_5	Door beam	Lognormal
	x_6	Door belt line	Lognormal
	x_7	Roof rail	Lognormal
Young's modulus (GPa)	x_8	B-pillar inner	Normal
	x_9	floor side inner	Normal

in Sections 4.1.1 and 4.1.2. the ML does not consider the statistical correlation between the multivariate output responses; the JL_{KDE} suffers from curse of dimensionality that causes the inaccurate estimation of the joint PDF in high dimensional problems; the MM could lead to an inaccurate solution when there is large scale difference in multivariate output responses. Table 4-7 summarizes the estimated calibration parameters, relative errors, required iterations, function calls, and computation time for calibration. It is worth noticing that the relative errors of the estimated calibration parameters by the MPCR are relatively small, compared to the other calibration metrics.

The joint PDF contours of the first and second predicted output responses (y_1, y_2) after calibration were drawn in Figure 4-16. The joint PDF contours were obtained by using the multivariate KDE from 10,000 samples. The scatters indicate the observed output response. The predicted joint PDFs calibrated by the MM is somewhat distorted, compared to the scatters.

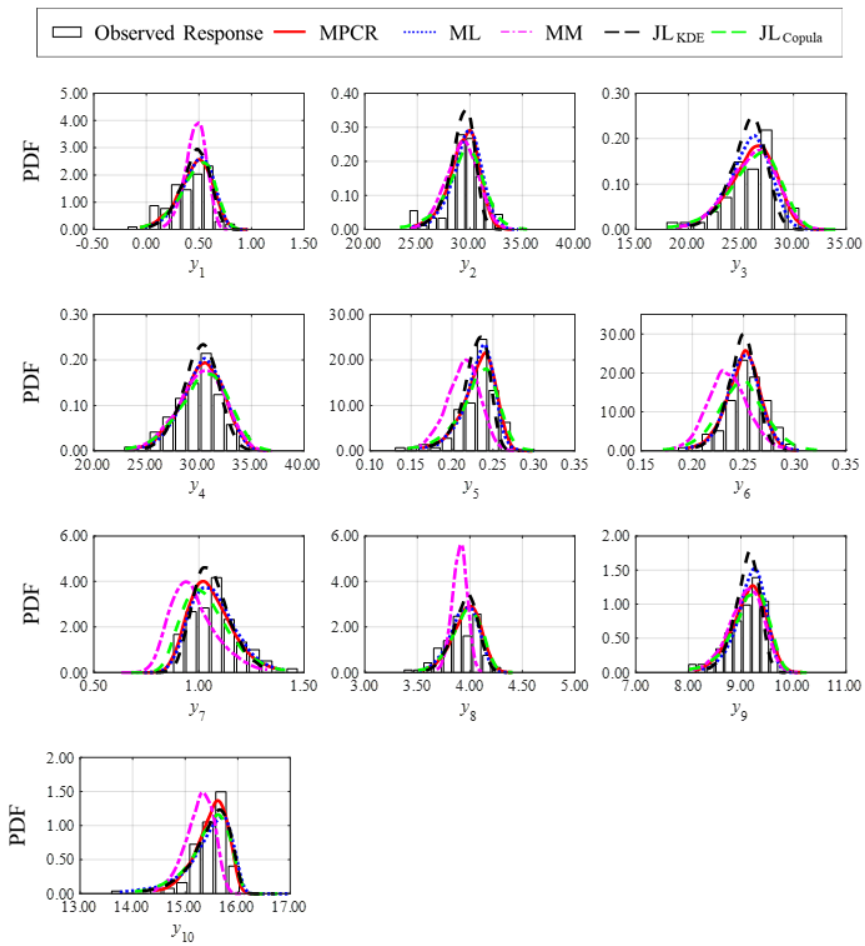

Figure 4-14 Calibrated marginal PDFs of the output responses (engineering example 2)

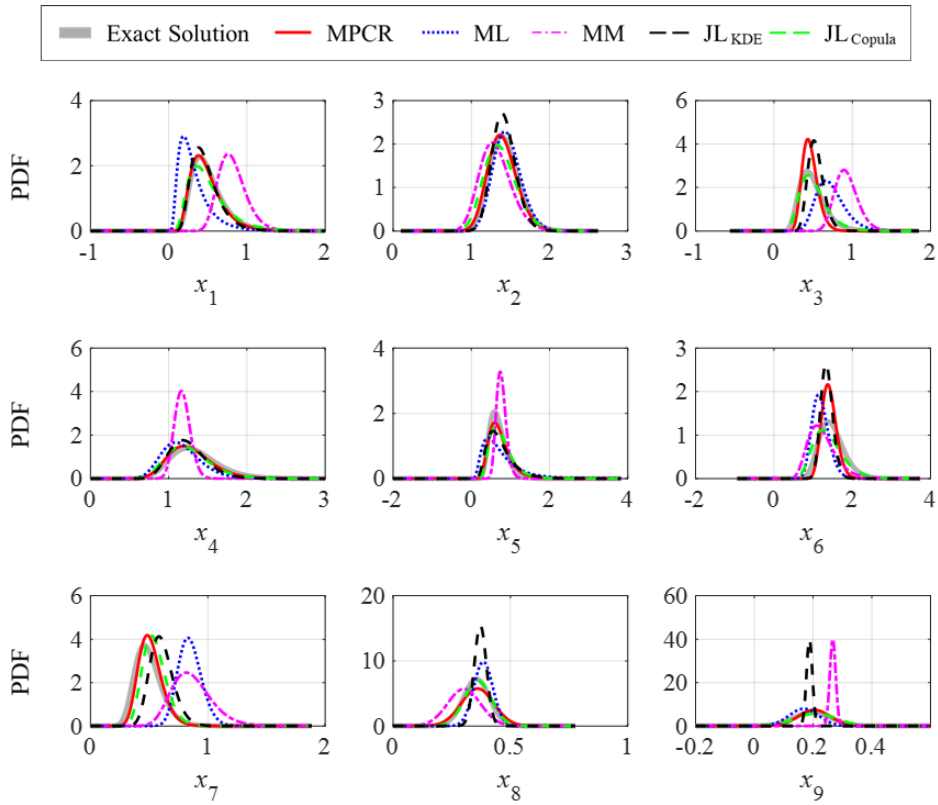

Figure 4-15 Calibrated marginal PDFs of the input variables (engineering example 2)

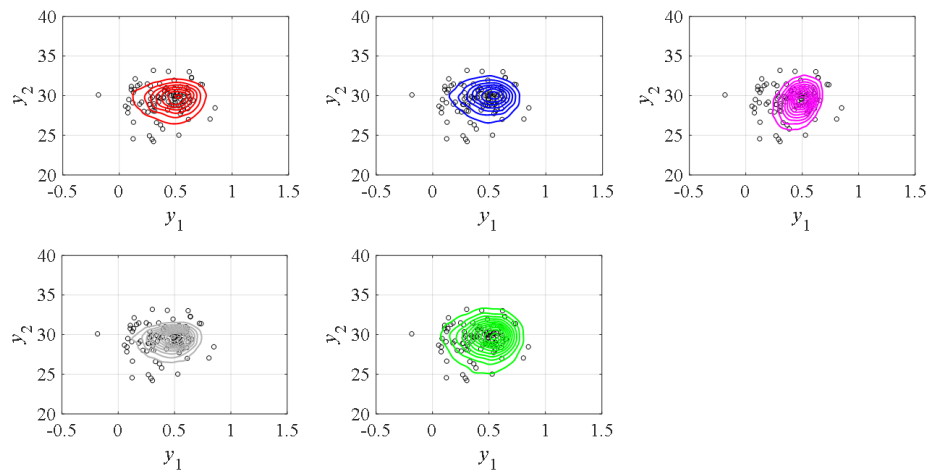

(a) The join PDF and scatter plot of y_1 and y_2

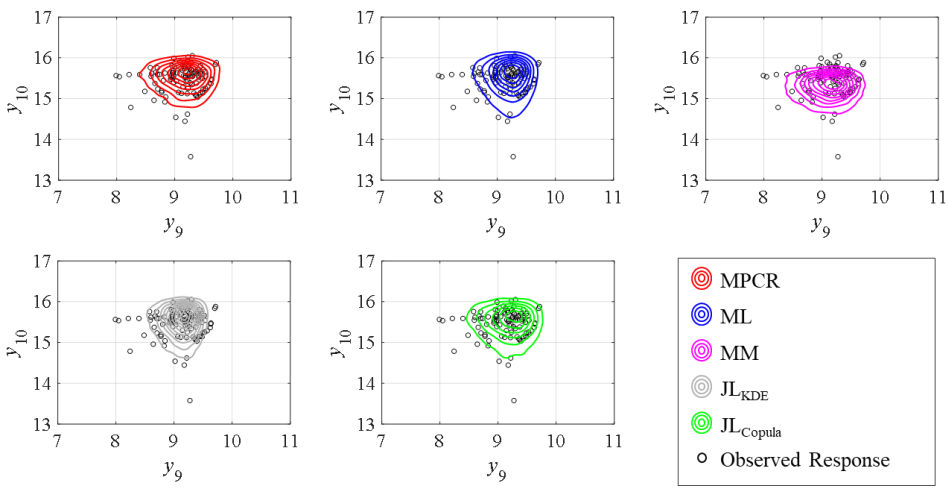

(b) The join PDF and scatter plot of y_9 and y_{10}

Figure 4-16 Calibrated joint PDFs of the output responses (engineering example 2)

Table 4-7 The estimated calibration parameters, relative errors, iterations, and function calls (Engineering example 2)

Calibration metric		Calibration parameters																		Iter.	F.C
		μ_1	σ_1	μ_2	σ_2	μ_3	σ_3	μ_4	σ_4	μ_5	σ_5	μ_6	σ_6	μ_7	σ_7	μ_8	σ_8	μ_9	σ_9		
Exact solution		0.51	0.22	1.42	0.19	0.49	0.17	1.34	0.30	0.69	0.22	1.49	0.32	0.50	0.11	0.36	0.06	0.20	0.06	-	-
MPCR	Estimation	0.49	0.21	1.40	0.18	0.46	0.10	1.28	0.28	0.73	0.27	1.41	0.19	0.51	0.10	0.36	0.07	0.20	0.05	52	1107
	Error (%)	-3.30	-1.31	-1.47	-1.32	-6.43	-39.59	-4.42	-6.71	6.40	25.60	-5.04	-41.65	3.35	-12.73	1.27	25.77	3.72	-15.55		
ML	Estimation	0.33	0.22	1.46	0.18	0.73	0.19	1.17	0.25	0.76	0.51	1.19	0.22	0.85	0.10	0.38	0.04	0.17	0.05	83	1811
	Error (%)	-35.84	0.38	2.63	-4.98	47.46	12.86	-12.83	-16.16	10.70	133.48	-19.66	-33.30	71.15	-12.73	8.14	-26.79	-14.54	-21.35		
MM	Estimation	0.82	0.18	1.31	0.20	0.93	0.15	1.17	0.10	0.77	0.13	1.24	0.36	0.87	0.17	0.30	0.07	0.27	0.01	56	1242
	Error (%)	60.04	-17.22	-7.68	8.21	87.41	11.47	-12.30	-66.98	12.25	-42.52	-16.69	12.17	74.60	48.52	-15.00	26.68	35.51	-84.30		
JL (KDE)	Estimation	0.47	0.19	1.42	0.15	0.54	0.10	1.25	0.24	0.75	0.35	1.35	0.15	0.61	0.10	0.37	0.03	0.19	0.01	42	983
	Error (%)	-7.12	-13.62	-0.36	-19.95	8.47	39.59	-7.01	-21.84	9.34	61.32	-8.91	-52.34	22.56	-12.73	4.58	-53.13	-4.82	-84.30		
JL (Gaussian copula)	Estimation	0.52	0.27	1.38	0.21	0.52	0.18	1.26	0.28	0.77	0.30	1.40	0.39	0.55	0.10	0.36	0.06	0.21	0.07	46	1080
	Error (%)	1.85	25.91	-3.23	10.94	4.60	8.61	-6.06	-6.28	12.14	35.57	-5.76	20.60	10.40	-12.73	1.59	4.12	6.67	9.48		

MPCR: Marginal probability correlation residual
ML: Marginal likelihood metric
MM: Moment matching metric
JL: Joint likelihood metric
Iter.: Iteration
F.C.: Function calls
Error $= 100 \times (s - \hat{s})/s$ (%), s is the exact value and $\hat{s}$ is an estimate

4.4 Summary and Discussion

This study proposed a new calibration metric, namely Marginal Probability and Correlation Residuals (MPCR), to properly consider the statistical correlation between multivariate output responses in optimization-based statistical model calibration. The foundational idea of the proposed MPCR metric is to decompose a multivariate joint probability distribution into multiple marginal probability distributions, while considering the statistical correlation between output responses. Two mathematical and two engineering examples were demonstrated to verify the effectiveness of the MPCR metric. It can be concluded from the results that even though the predicted marginal PDF of the output response after calibration matches well with the observed one, inaccurate solutions may be obtained if the statistical correlation between the output responses is not properly considered when formulating a calibration metric.

The MPCR metric has many favorable properties as a calibration metric, such as 1) marginalization, 2) normalization, and 3) boundedness. Owing to marginalization, the MPCR metric does not suffer from curse of dimensionality, since it incorporates the univariate KDE into the modeling of the marginal PDF. Owing to normalization, the MPCR metric can provide accurate calibration results even when there is a scale difference between the output responses. In addition, since the value of the MPCR metric is bounded, it can directly inform the statistical similarity or dissimilarity between the predicted and observed output responses. It is thus believed that the proposed MPCR metric will be very helpful for improving the accuracy and robustness of optimization-based statistical model calibration when the multivariate output responses are statistically correlated.

Sections of this chapter have been published or submitted as the following journal articles:

1) **Wongon Kim,** Heonjun Yoon, Guesuk Lee, Taejin Kim, and Byeng D. Youn, "A New Calibration Metric that Considers Statistical Correlation: Marginal Probability and Correlation Residuals," *Reliability Engineering & System Safety* , Vol. 195, 106677, 2020.

Chapter 5

Hybrid Model Calibration and Updating For Estimating System Failure

In Chapter 4, the statistical correlation in output response was taken to estimate the uncertainty in the model input parameter. The predictive capability of the digital twin approach is improved by considering uncertainties in manufacturing and test conditions using statistical model calibration. Maintaining the high predictive capability of a digital twin model under system failure is of great concern to the engineers who make design decisions at the early stages of product development. The physics-based digital twin can give a physical intuition such as prognosis and diagnosis of system failure. However, it hard to apply the physics-based digital twin approach to estimate system failure by the computational cost and lack of information. There is thus an urgent need to develop hybrid digital twin approach for evaluating system failure under physical uncertainty.

Crack initiation and growth are common failure mechanisms in engineered products. To verify the structural reliability and durability of engineered products,

engineers have tried to predict fatigue characteristics using an empirical crack growth model [87], [88] and advanced physics-based simulation [8], [10] in engineering product development. However, the predictive capability of a simulation model can be degraded by physical uncertainty in model formulation and test conditions. The digital twin approach, which is updated in this research to consider these uncertainties, can be an attractive substitute for conventional simulation models.

This study proposes a hybrid digital twin approach to estimate uncertain crack initiation and growth. The proposed improved digital twin approach for estimating fatigue crack initiation and growth can be used in a variety of product development settings. The proposed idea takes advantage of hybrid digital twin approaches, using both data-driven and physics-based approaches. The proposed approach for estimating fatigue crack initiation and growth is based on two techniques; (i) statistical model calibration and (ii) probabilistic element updating. In statistical model calibration, statistical parameters of input variables are estimated based on the observed response related to the crack initiation condition. Further, probabilistic analysis using estimated statistical parameters can predict possible critical elements that indicate crack initiation and growth. In probabilistic element updating procedures, the possible crack initiation and growth element is updated based on the observed response related to the crack growth condition. The validity of the proposed method is demonstrated using a case study of an automotive sub-frame fatigue test. The proposed idea is applied to estimate crack initiation and growth in the fatigue test. From the results, we conclude that the proposed digital twin approach can accurately estimate crack initiation and growth of an automotive structure under

uncertain loading conditions and material properties.

Chapter 5 is organized as follows. Section 5.1 provides a brief review of digital twin approach for estimating crack initiation and growth. The proposed hybrid digital twin approach is explained in Section 5.2. The application of the proposed method is demonstrated in Section 5.3. Finally, the conclusions of this work are outlined in Section 5.4.

5.1 Brief Review of Digital Twin Approaches for Estimating Crack Initiation & Growth

Crack initiation and growth are common failure mechanisms in engineered products. To verify the structural reliability and durability of engineered products, engineers have tried to predict fatigue characteristics using an empirical crack growth model [87], [88] and advanced physics-based simulation [8], [10] in engineering product development. However, the predictive capability of a simulation model can be degraded by physical uncertainty in model formulation and test conditions. For example, the geometry and boundary conditions in the model formulation may differ from the physical test conditions. In addition, the manufacturing tolerance and uncertain nonlinear effects during crack initiation in the physical test condition are also difficult to consider in the model analysis. The effects of physical uncertainty in model formulation and test conditions thus have to be taken into account to improve the predictive capability of simulation models. The digital twin approach, which is updated in this research to consider these uncertainties, can be an attractive

substitute for conventional simulation models.

A digital twin combines the observed response from a physical system in real space with a simulation model in cyberspace to support engineering decisions. In digital twin approaches, the simulation model must be improved using the observed response. Simulation models used in digital twin approaches can be categorized into 1) data-driven and 2) physics-based models. Data-driven models, such as relevance vector machine [3] and artificial neural networks [1], have been proposed to estimate crack initiation and growth using an experimentally observed response. Data-driven approaches rest on past experimental data to predict fatigue behavior. However, these methods require enough data to predict the fatigue crack behavior of the engineered product of interest. Further, the results of data-driven models are less interpretable than those from physics-based models. Physics-based models, such as finite element based models [89]–[92] and material models [93], [94], have been used to simulate the physical process of crack initiation and growth. However, due to the uncertainties in modeling and simulation, it is challenging to predict fatigue behavior with high accuracy using simulation models. In addition, expensive computational cost is a constraint of physics-based models. The proposed hybrid digital twin approach uses both data-driven and physics-based models simultaneously to capitalize on the advantages of each approach, while minimizing the disadvantages of each method. Hybrid approaches seek to estimate structural health monitoring and crack growth accurately and efficiently.

Li and Mahadevan et al. (2017) proposed a hybrid digital twin approach for aircraft wing health monitoring based on a dynamic Bayesian network and a physics-based model without crack geometry [48]. Their proposed method integrates

heterogeneous information – including test data, mathematical models, and expert opinions – to estimate crack length using a Bayesian network. However, their method requires past crack length data in various conditions; further, it is inefficient for construction of a crack growth model for each initiation point. Eder et al. (2020) proposed a hybrid digital twin approach using an FEA model with crack geometry based on the Virtual Crack Closure Technique (VCCT) [95]. This method was applied for predicting the fatigue cracks in the adhesive trailing edge joint of a full 3D finite element wind turbine blade model. The results show a robust and computationally efficient prediction by decoupling the computationally demanding finite element analysis from the discrete fatigue crack growth analysis. However, use of VCCT with a deterministic crack growth criterion makes it difficult to estimate the uncertain crack growth. The crack growth simulation needs to be probabilistically conducted to estimate the uncertain crack growth of the physical system. In other work, M. Karve et al. (2020) proposed a digital twin approach for performing mission optimization under uncertainty, aimed at ensuring system safety with respect to fatigue cracking [96]. In the Karve et al. study, a Bayesian damage diagnosis method was proposed by fusing homogeneous sources of data, including piezo-sensor data and a physics-based model. This method did not take uncertain crack initiation and growth into account.

Therefore, to consider both the initiation and growth of fatigue cracks, the present work takes advantage of hybrid digital twin approaches that utilize both data-driven and physics-based approaches. The proposed approach includes two techniques: (i) statistical model calibration using a data-driven model and (ii) probabilistic element updating using a physics-based model. In statistical model

calibration, statistical parameters of input variables can be estimated based on the observed response related to the crack initiation and growth condition. Further, the probabilistic analysis using estimated statistical parameters can predict possible critical elements that indicate crack initiation and growth. In the probabilistic element updating procedures, the possible crack initiation and growth element is updated based on the observed response. The three-fold novel aspects of this study include:

- This study proposes a hybrid digital twin approach to estimate uncertain crack initiation and growth, by incorporating two techniques: (i) statistical model calibration using a data-driven model and (ii) probabilistic element updating using a physics-based model.

- The validity and efficiency of the proposed methodology is verified through digital twin updating of an automotive sub-frame, by using the observed response related to crack initiation and growth from a fatigue test.

- The updated model, which is validated quantitatively and qualitatively, is compared with fatigue test results, such as displacements and fatigue crack initiation and growth points.

5.2 Proposed Digital Twin Approach : Hybrid Model Calibration & Updating

This section outlines the proposed hybrid digital twin approach. Figure 5-1 describes the procedure for the proposed hybrid digital twin approach. The first step is data-driven statistical model calibration. In statistical model calibration, the unknown input variables of a data-driven model, representing uncertainties in experiments and manufacturing, are estimated using the observed response. The data-driven model relieves the computational cost of a physics-based twin in the

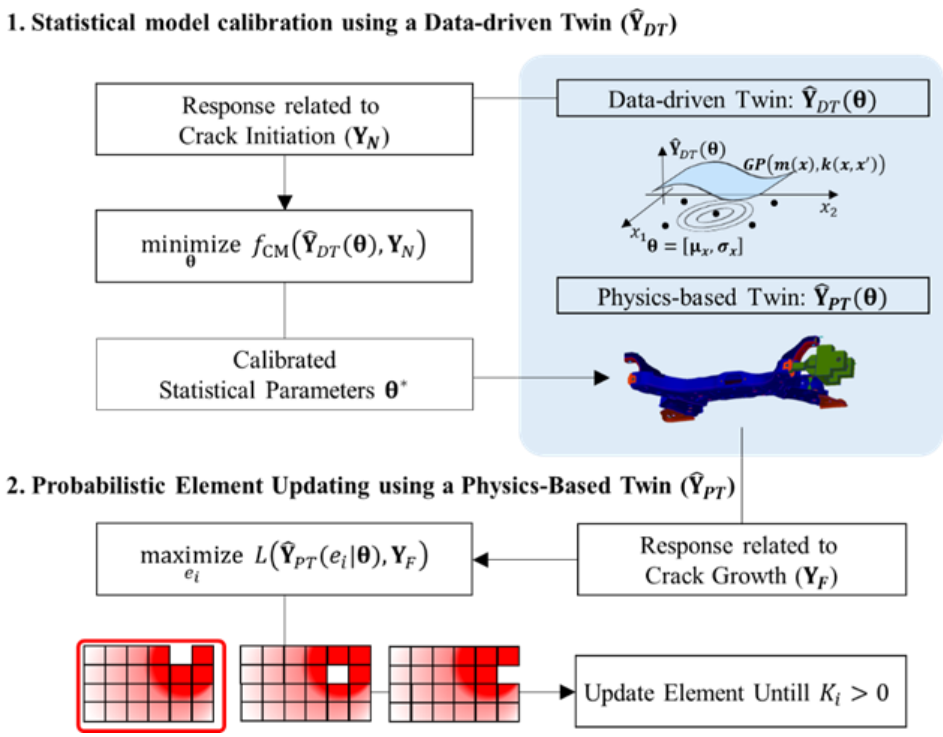

Figure 5-1 Procedure for the proposed hybrid-digital twin approach to estimate fatigue initiation and growth

model calibration. The estimated input variables of a data-driven model in the model calibration step can improve model prediction accuracy and validity of the physics-based twin in element updating. The second step is the probabilistic element updating. In element updating, the critical element of the physics-based model representing crack initiation and propagation is estimated using observed responses related to the crack initiation and growth condition. The proposed method can be applied to estimate uncertain and unidentifiable crack initiation and growth that arise because of the uncertainties in the manufacturing and test conditions. To help readers understand the proposed method, section 5.2.1 will explain optimization-based statistical model calibration procedures using a data-driven twin and section 5.2.2 will introduce element updating procedures using a physics-based twin.

5.2.1 Statistical Model Calibration using a Data-driven Twin

A physics-based model is necessary for virtual fatigue analysis in product development. However, it is not easy to use simulation models to predict physical behavior with high accuracy. Most input variables in physics-based models have a certain amount of physical uncertainty, such as inherent variability in material properties, manufacturing tolerances, and operating (loading) conditions. This input variable can be assumed as a random variable ($\mathbf{X}_{\text{unknown}}$) that is defined by the type of distribution and statistical parameter ($\boldsymbol{\theta}$).

To estimate an uncertain crack initiation point, probabilistic analysis that considers uncertainty in model formulation and test conditions is required. The proper statistical parameters of the input variables are needed for probabilistic

analysis. However, it is not easy to fully quantify the variability in the input variables due to limited resources (e.g., time, budget, and facilities); thereby, the statistical parameters of the model input variables are often unknown. Statistical model calibration is thus of great importance as a strategy to improve the predictive capability of a digital twin model [97], [98]. Representative methods for statistical model calibration include Bayesian approaches, maximum likelihood estimation (MLE)-based model updating approaches, Markov Chain Monte Carlo (MCMC) approaches, and optimization-based statistical model calibration approaches [19], [20], [97], [99]. Optimization-based model calibration can be an excellent strategy to calibrate a digital twin, considering the correlated output response [100].

However, it is hard to effectively calibrate these models because most physics-based analysis is computationally expensive. A data-driven twin ($\widehat{\mathbf{Y}}_{\mathrm{DT}}$) can be used in statistical model calibration as a surrogate model [101], [102]. Figure 5-2 describes the procedure of statistical model calibration using a data-driven twin. The study described in this paper uses a Gaussian process model to substitute for the physics-based model. The Latin-hyper-cube sampling method is applied to construct the design of experiment (DoE) for data-driven twin construction.

To estimate the input variables in a physics-based model, optimization-based statistical model calibration can be formulated as:

$$\underset{\boldsymbol{\theta}}{\text{minimize}} \quad f_{\mathrm{CM}}\left(\widehat{\mathbf{Y}}_{DT}(\boldsymbol{\theta}), \mathbf{Y}_{\mathrm{obs},N}\right) \tag{5.1}$$

where $\boldsymbol{\theta}$ denotes a statistical parameter vector of unknown input variables and f_{CM} denotes a calibration metric that quantifies the statistical dissimilarity between the

predicted ($\widehat{\mathbf{Y}}_{DT}(\boldsymbol{\theta})$) and observed ($\mathbf{Y}_{\mathrm{obs},N}$) output responses related to crack initiation. Monte Carlo simulation (MCS) is applied as an uncertainty propagation (UP) approach to quantify the output response uncertainties for a given statistical parameter ($\boldsymbol{\theta}$), using the constructed data-driven model. In optimization-based statistical model calibration, the calibration metric, which is defined as an objective function, must be formulated considering the statistical correlation between multivariate output responses. Kim et al. proposed the Marginal Probability Correlation Residual (MPCR) as a calibration metric to consider statistical correlation [100]. The MPCR is adopted as a calibration metric in this study for this same purpose. The kernel density estimation (KDE) estimates the probability density function of the response using the sets of responses from the Monte Carlo simulation.

After statistical model calibration, physics-based analysis can statistically predict possible crack initiation points where the maximum stress occurs. The calibrated model can be quantitatively and qualitatively validated. A hypothesis test using an area-metric is used as a quantitative method and crack initiation points are also validated qualitatively.

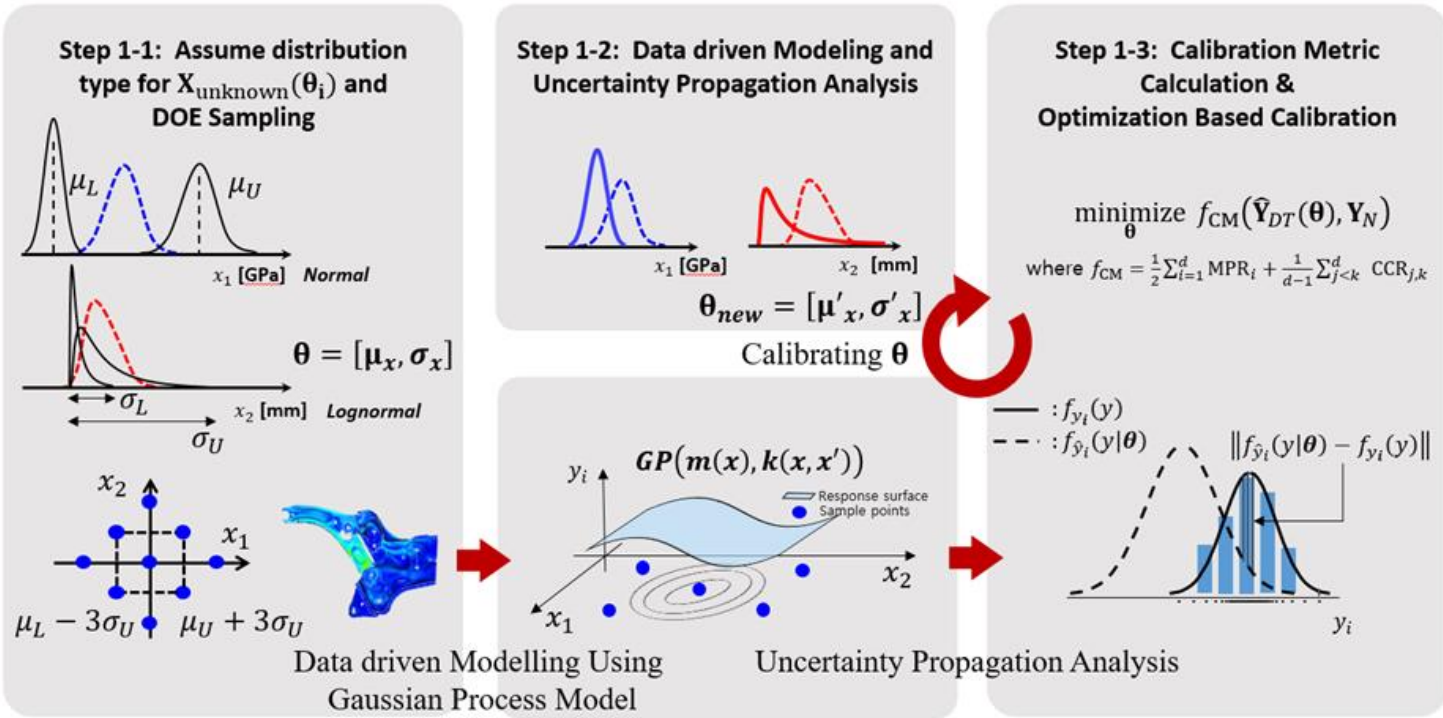

Figure 5-2 Statistical model calibration using a data-driven twin

5.2.2 Probabilistic Element Updating with a Physics-based Twin

Statistical model calibration can improve the model prediction accuracy of the physics-based twin using the observed response. The calibrated physics-based twin can predict possible critical elements where a crack is initiated. Crack initiation and growth in a physical system induce a transition of the observed response. In the digital twin approach, the digital twin needs to be updated to represent the fault state of a physical system in real space. In this study, probabilistic element updating is used to estimate crack initiation and growth of real physical entities, based on the observed response. Figure 5-3 represents the proposed element updating procedures.

- Step 2-1. Physics-based analysis using calibrated statistical parameters is used to estimate possible state transition, considering various uncertainties in test conditions. The candidate elements where maximum von-misses stress occurs are selected as deletion candidates (e_n).
- Step 2-2. UP analysis, with deletion of each candidate element, is conducted to construct the probability density function of the response transition ($\Delta\widehat{\mathbf{Y}}_{crack}$). The most probable deletion element among candidates is selected based on the likelihood evaluation with observed response transition in a fault state ($\Delta\mathbf{Y}_{\mathrm{obs},F}$).
- Step 2-3. The Bayes factor, which is an updating criterion, is calculated as the maximum likelihood ratios between the current and previous step from among candidate elements. The elements are deleted until the Bayes factor is positive. If the Bayes factor is negative, stop the iteration.

Simulation strategies have been developed to predict crack initiation and

growth, including finite element based methods like Virtual Crack Closure Techniques (VCCT), Cohesive Zone Model (CZM), and the element deletion method [7], [8], [10], [92]. However, VCCT requires a specified crack initiation point and mesh correction around the crack tip. CZM requires traction-separation law for specified crack interface elements, which need to be specified for each different material. The element deletion method can be utilized to simulate crack initiation and growth without mesh correction and a defined crack interface [103]–[105]. However, sophisticated element deletion criteria are required to simulate crack initiation and growth [105]. The likelihood function based on the observed response can be used as an updating (element deletion) criterion to overcome this issue. The likelihood of physics-based analysis with this *n*-th candidate element (e_n) deletion based on a fault-observed response at the *i*-th updating iteration is found by:

$$L_i(e_n) = \sum_{j=1}^{n_{exp}} log_{10}\ f_{\Delta\widehat{\boldsymbol{Y}}_{Crack}}\left(\Delta \boldsymbol{Y}_{j,Fault} | e_n\right) \tag{5.2}$$

where $\Delta\mathbf{Y}_{j,Fault}$ denotes the *j*-th observed response transition vector in a fault state and $f_{\Delta\widehat{\mathbf{Y}}_{Crack}}(.|e_n)$ denotes the joint PDF of the predicted response transition ($\Delta\widehat{\mathbf{Y}}_{Crack}$) with the *n*-th candidate element ($e_{n,i}$) deletion. The response transition is formulated as:

$$\Delta\widehat{\mathbf{Y}}_{Crack}(e_n) = \widehat{\mathbf{Y}}_{Crack}(\mathbf{X}(\boldsymbol{\theta}^*)|e_n) - \widehat{\mathbf{Y}}_{Normal}\left(\mathbf{X}(\boldsymbol{\theta}^*)\right) \tag{5.3}$$

where $\widehat{\mathbf{Y}}_{\boldsymbol{Crack}}(\mathbf{X}(\boldsymbol{\theta}^*)|\boldsymbol{e_n})$ denotes the predicted response with *n*-th candidate element (e_n) deletion and $\widehat{\mathbf{Y}}_{\boldsymbol{Normal}}(\mathbf{X}(\boldsymbol{\theta}^*))$ denotes the predicted response without element updating. The most probable elements from among the candidates can be selected based on the likelihood function. The model updating criterion using the

Bayes factor can be formulated as:

$$K_i = log \frac{\underset{n}{max}\, L_i(e_n)}{\underset{n}{max}\, L_{i-1}(e_n)} \tag{5.4}$$

where $\underset{n}{max}\, L_i(e_n)$ denotes the maximum likelihood function value from among deletion candidates at the *i*-th iteration; the Bayes factor (K_i) is the likelihood ratio between the current and previous updating iteration. A positive value of the Bayes factor indicates that the updated element model is more agreeable than the previous model, based on the observed response in the crack growth condition. Thus, the updating procedures are continued until the Bayes factor changes into a negative value.

Element size and density of the computation model affects computation cost of element updating and accuracy of digital twin analysis. G, Ljustina et al. showed the Johnson-Cook (JC) dynamic failure model results depending on element size [106]. Even though dense and fine mesh can represent detailed crack progress in real systems, the computation cost is incrased by a larger system matrix and matrix computation.

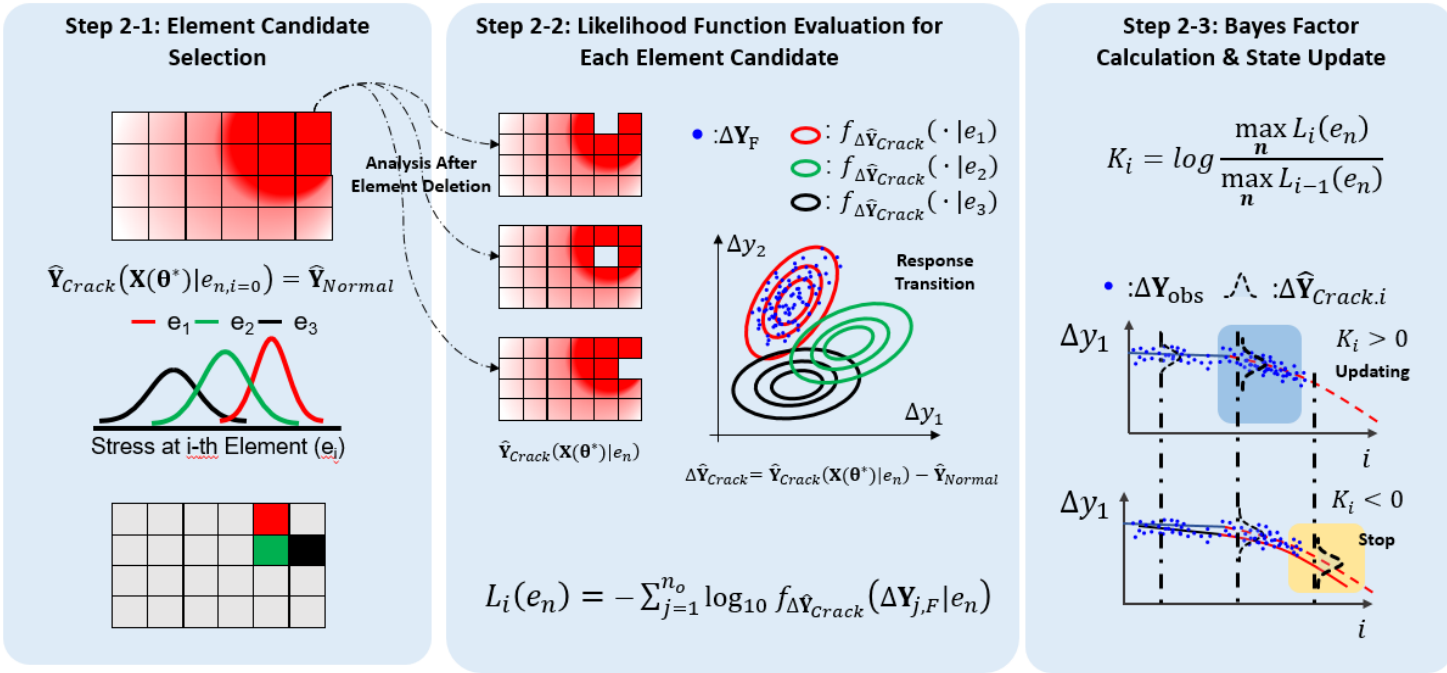

Figure 5-3 Probabilistic element updating with a physics-based twin

5.3 Case Study: Automotive Sub-Frame Structure

An automotive sub-frame is a structural component of a vehicle that sustains the wheels and tires during acceleration, driving, and deceleration. Fatigue characteristics of the sub-frame affect the ride comport of a car. The proposed method is applied to estimate the sub-frame's fatigue crack initiation and growth using the experimentally observed response. The commercial finite element analysis tool, Nastran, was used for the physics-based digital twin analysis.

5.3.1 Experimental Fatigue Test

In the experiments, the specimen is the suspension member that sustains a lower arm. The experiment aims to measure the displacement and principal strains during the quasi-static and cycling loading test. In this section, the test setups and results are described.

The sub-frame consists of a suspension member and a control arm. The load is applied to the suspension member at a joint connected to a control arm in the experiments. The principal strains were measured by attaching tri-axial strain gauges at the top surface of the structure. Strain measurement locations were selected based on sensitivity analysis with respect to the unknown input variables. The four measured strain points were selected as shown in Figure 5-4 (a). The specimen was fixed at four points and a load applied with the MTS Model 252-25G-01 fatigue test rig, as shown in Figure 5-4 (b).

Two types of loading conditions: 1) quasi-static and 2) cyclic load, are

considered, as shown in Figure 5-5. In the quasi-static load test, the principal strains were observed in four points under twelve load steps. The maximum magnitude of the quasi-static load was 14.7 kN. Three specimens were tested to evaluate the physical uncertainty and the manufacturing errors. The cyclic load was applied to one of the specimens in the fatigue test until a visually identifiable crack occurred. The maximum magnitude of cyclic load was 17.64 kN.

In the cyclic loading test, the measured strain in the cyclic load test showed a significant change at around 20,670 cycles, as shown in Figure 5-5 (c). Even with the response transition, there was no visible change in the specimen. It was found that the change was caused by an invisible internal crack. The observed deformation

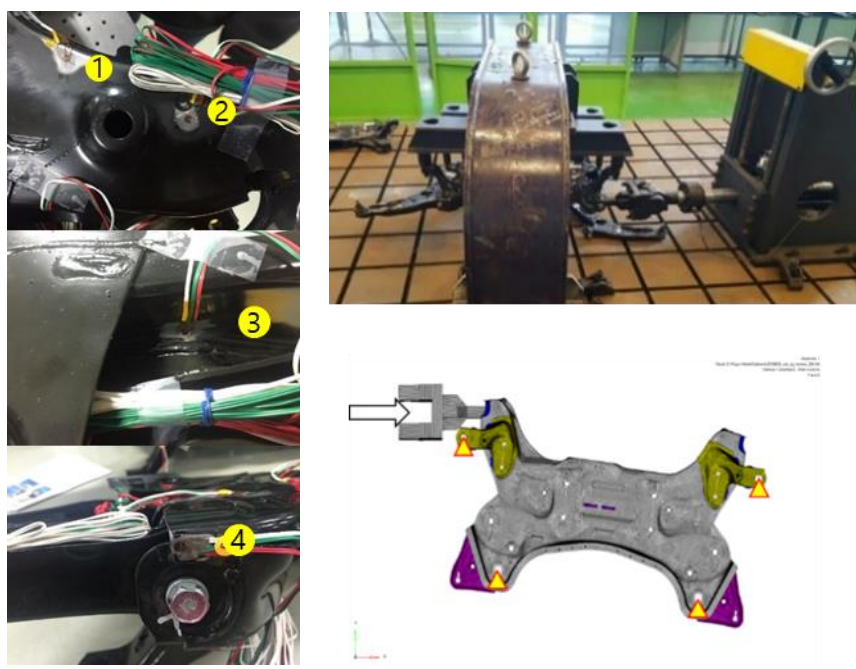

(a) (b)

Figure 5-4 Experimental condition : (a) strain measured points, (b) test rig

was assumed as the linear elastic phenomenon. The principal strain and displacement under twelve different load steps from quasi-static loads were linearly extrapolated at a maximum level of cyclic load, as shown in Figure 5-6.

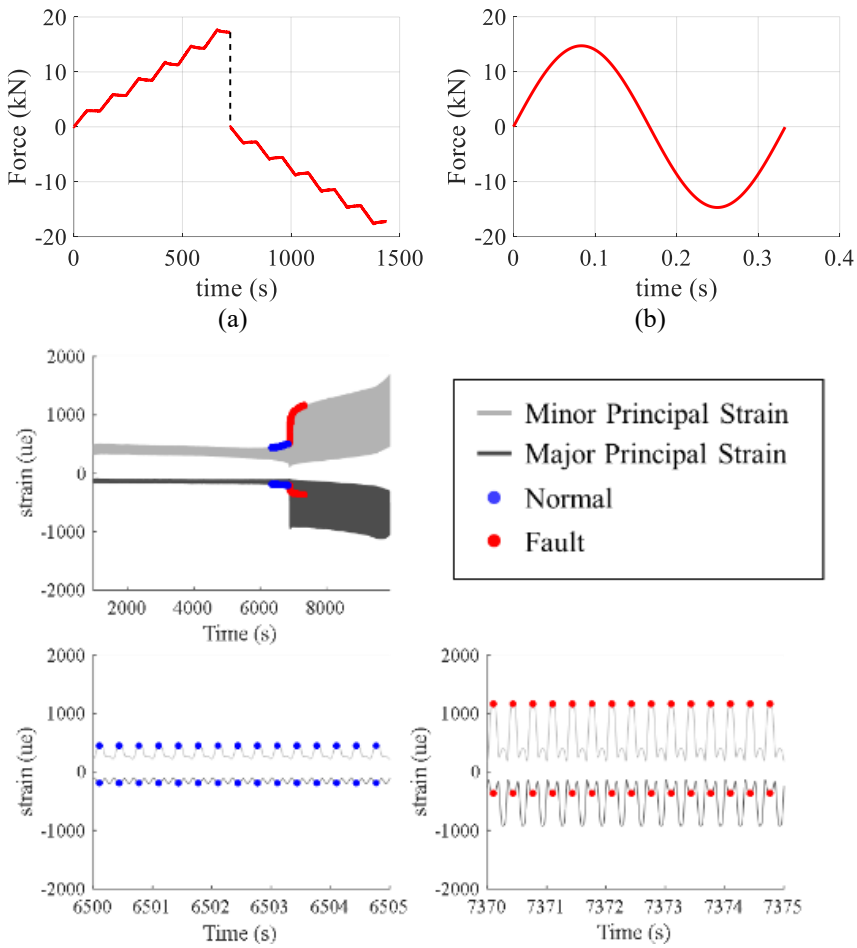

Figure 5-5 Loading condition : (a) quasi-static load, (b) cyclic load, (c) observed principal strain during cyclic load test

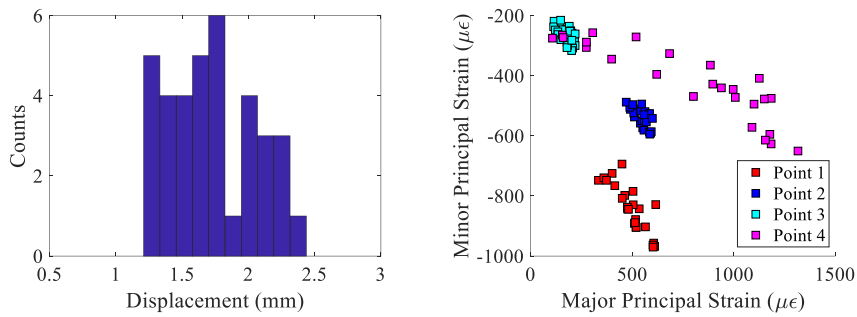

(a) (b)

Figure 5-6 Extrapolated experimental output response: (a) displacement (b) principal strains

5.3.2 Statistical Model Calibration using a Data-driven Twin

5.3.2.1. Physics-based Model of Suspension Members

The physics-based model was constructed with shell elements to evaluate the suspension member. The jig is connected to the suspension member using a rigid body element (RBE2) at the joint node. The load was applied to the point where a ball joint connects the actuator. The loading condition and boundary condition are shown in Figure 5-7 (a). The analysis was conducted using a commercial FE solution, Nastran. The steel plates with different metal properties are connected by three different weld types. Figure 5-7 (b) shows finite elements consisting of the physics-based model. The numeric value of the material properties is described as a non-dimensional value normalized by the initial reference value.

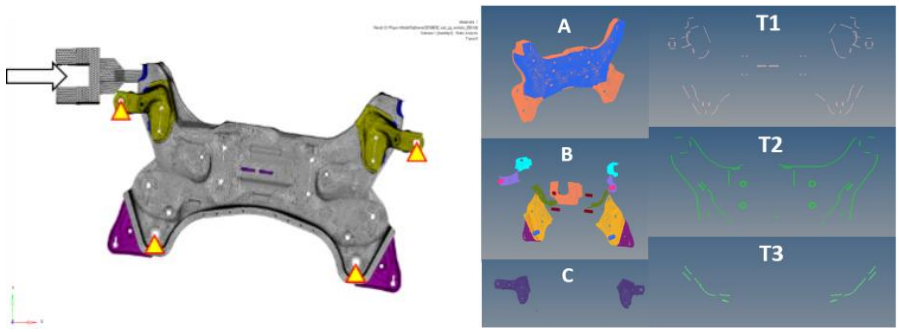

(a) (b)

Figure 5-7 Analysis condition: (a) loading and boundary conditions (b) model components

5.3.2.2. Unknown Input Variables

The suspension member consists of plates connected by welds. The welds are divided into three types (T1, T2, and T3) depending on the bead size. During the welding procedure, various defects are generated due to residual thermal stress and manufacturing tolerances. Therefore, the thicknesses of the weld components are considered as unknown input variables. The material properties of the plate also have uncertainty. In particular, Young's Modulus (E) is an important property of the elastomer, which defines the ratio between stress and strain. As the steel plates are deformed and machined, plastic deformation or an inner crack can occur during the manufacturing process. The defects can deteriorate or reinforce the stiffness of the plate by stress concentration or plastic hardening. Thus, the Young's Modulus values of the three different steel materials (A, B, and C) are considered as unknown input variables. The ball joints that connect the jig and actuator induce an uncertain loading direction; thus, the two loading direction parameters (θ_Z, θ_Y) are regarded as unknown input variables. Unknown model input variables and measured output responses are summarized in Table 5-1. In optimization-based statistical model

$\mathbf{X}_{\mathbf{unknown}}$	**Y**
Force Rotation Angle (x_1,x_2: θ_z, θ_Y)	Major/ Minor Principal Strain
Weld Thickness (x_3,x_4,x_5: T1, T2, T3)	@ Point 1 (y_1, y_2)
Young′ s Modulus (x_6,x_7,x_8:E_A, E_B, E_C)	@ Point 2 (y_3, y_4)
	@ Point 3 (y_5, y_6)
	@ Point 4 (y_7, y_8)

Table 5-1 Unknown model input variables and measured output responses

calibration, the distribution type of a random variable should be assumed based on prior information. The thickness value must have a positive value; thus, it is assumed that weld thickness follows a log-normal distribution. Further, it is assumed that the Young's Modulus and force direction parameters follow a normal distribution.

5.3.2.3. Calibration Problem Formulation using a Data-driven Twin

The calibration problem is formulated as

$$\begin{aligned} &\text{Find} && \boldsymbol{\theta} = [\boldsymbol{\mu}\ , \boldsymbol{\sigma}] \\ &\text{to minimize} && \mathbf{MPCR}\left(\mathbf{Y_{pre}}(\boldsymbol{\theta}), \mathbf{Y_{obs}}\right) \\ &\text{subject to} && \boldsymbol{\theta}^{\mathbf{L}} \leq \boldsymbol{\theta} \leq \boldsymbol{\theta}^{\mathbf{U}} \end{aligned} \tag{5.5}$$

where $\boldsymbol{\theta}$ denotes the statistical parameters of the unknown input variables; $\boldsymbol{\theta}$ consists of the mean and standard deviation vector, and; $\boldsymbol{\theta}^{\mathbf{L}}$ and $\boldsymbol{\theta}^{\mathbf{U}}$, respectively, denote the lower and upper bounds of the statistical parameters. The lower and upper bounds are summarized in Table 5-2.

	x_1	x_2	x_3 (mm)	x_4 (mm)	x_5 (mm)	x_6 (GPa)	x_7 (GPa)	x_8 (GPa)
μ_U	10°	10°	1.4A	1.4B	1.4C	1.4D	1.4E	1.4F
μ_L	-10°	-10°	0.4A	0.4B	0.4C	0.7D	0.7E	0.7F
σ_U	2°	2°	0.4A	0.4B	0.4C	0.04D	0.04E	0.04F
σ_L	0.01°	0.01°	0.001A	0.001B	0.001C	0.001D	0.001E	0.001F

Table 5-2 Lower and upper bounds of statistical parameters

The Gaussian process (kriging) based data-driven model was adopted to replace the expensive physics-based model; the design matrix of DOE was generated by the Optimal Latin Hypercube approach. A Gaussian process-based surrogate model was trained using the DOE. The accuracy of the surrogate model was validated before calibration. The Root Mean Squared Error (RMSE) of the kriging surrogate model was evaluated using one-hundred sample points. The value of error is less than 5% for each response model. The optimal parameter vector that minimizes the calibration metric was searched using a genetic algorithm. Monte-Carlo simulation with 10^4 sample points was run on the efficient surrogate model. Finally, kernel density estimation was used as PDF modeling.

5.3.2.4. Calibration Results

Table 5-3 summarizes the inferred statistical parameters of the unknown input variables. From the calibration results, the following observations are made. The force direction had bias and variability compared to the initial guess. In addition, the force rotation angle in the Z-axis has a negative bias. Further, the mean of Young's Modulus (E) changed up to 30% of the initial mean value. The thickness of the weld is divided into three types, depending on the bead size (T1, T2, and T3). Most of the

Unknown Input Variables		Initial		MPCR	
		Mean	Std.	Mean	Std.
θ_z		0	0	-4.70	1.97
θ_Y		0	0	-0.88	1.44
Weld Thickness	T1 (mm)	A	0.08A	0.45A	0.332A
	T2 (mm)	B	0.08B	0.45B	0.359B
	T3 (mm)	C	0.08C	1.21C	0.310C
Young's Modulus	E_A (GPa)	D	0.07D	1.03D	0.022D
	E_B (GPa)	E	0.07E	0.74E	0.024E
	E_C (GPa)	F	0.07F	1.29F	0.021F

Table 5-3 Calibration results of the automotive structural model

welds belong to two types of welds, specifically T1 and T2. The mean values of T1 and T2 were inferred as one-third of the original thickness mean value. This indicates that the weld stiffness was overestimated before calibration. Monte Carlo Simulation with 10^2 sample points was conducted using finite element analysis, rather than the kriging surrogate model. After calibration, the predicted output response had good agreement with the observed output response, as shown in Figure 5-8.

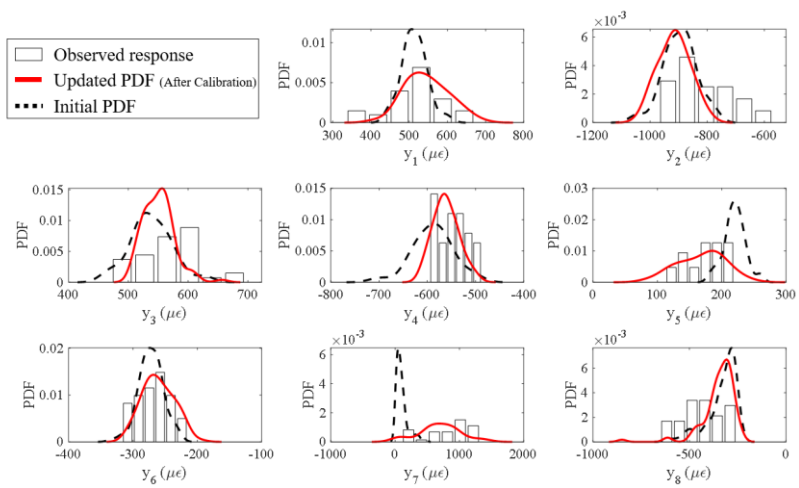

Figure 5-8 The updated output strain

5.3.2.5. Validity Check

The calibration results were validated quantitatively and qualitatively. The validity checks examine whether statistical calibration can improve the predictive capability of a physics-based model in an output response domain not used in calibration. In the quantitative validity check, the loading point displacement was used for validation. In this study, area metrics using the u-pooling method and hypothesis test were used as a validity check. The area metric measures the area difference between the cumulative distribution function (CDF) of the predicted output response and the empirical CDF of the experimental output response. As shown in Figure 5-9, the area metrics of the updated output response were smaller than the threshold (i.e., 0.1051) with a sample size of thirty-six and a significance level of 5.

The calibrated physics-based model analysis statistically predicts three possible crack initiation points, where the maximum von-Misses stress occurs, as shown in Figure 5-10 (a). The PDF of stress occurred in the possible crack initiation candidate shown in Figure 5-10 (b). Candidate 1 shows the most critical stress level compared to other candidates. After the cyclic loading test, an internal crack was found around the predicted possible crack initiation point. Thus, it can be concluded that statistical calibration can improve the predictive capability of a physics-based model.

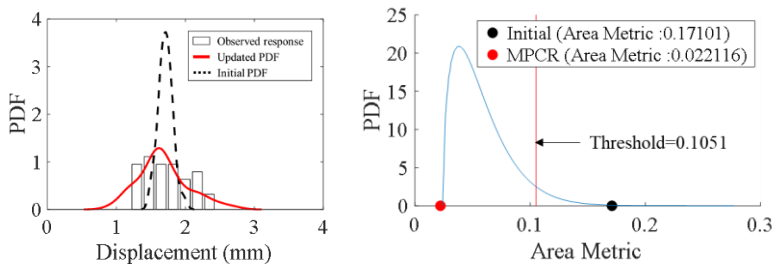

(a) (b)

Figure 5-9 (a) Displacement prediction after calibration (b) hypothesis testing using an area metric

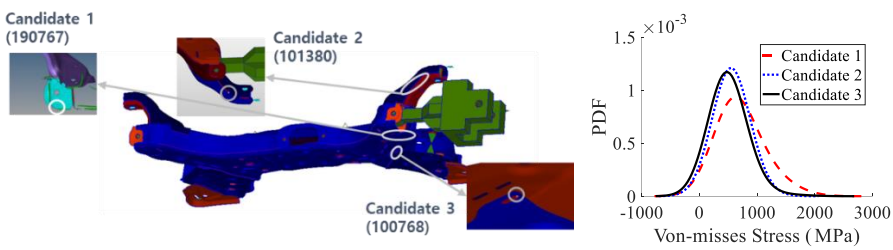

(a) (b)

Figure 5-10 (a) The candidates of crack initiation points (b) PDF of Von-misses stress at each candidate element

5.3.3 Element Updating with a Physics-based Twin

The UP analysis (MCS using a physics-based twin) with deletion of each candidate element was conducted and the response transition is as shown in Figure 5-11. The likelihood function for each candidate was calculated using the observed response transition ($\Delta\mathbf{Y}_{j,Fault}$), as shown in Table 5-4. The model prediction with candidate 1 gives a maximum likelihood compared to other candidate elements. The updating procedures were conducted based on the proposed methods.

At every element updating iteration, three candidate elements were selected based on the von-misses stress criterion. The most probable crack growth element was selected using the likelihood value. The Bayes factor, the likelihood ratio between the previous and current updated model, was calculated at each iteration. The updating procedure was continued until the Bayes factor changed into a negative value. The element updated models for each updating iteration are as shown in Figure 5-12. The updated model shows crack propagation as observed internal crack propagation in the fatigue test.

Figure 5-13 shows a transition of response in experiments and element updating. The response transition trend of the updated model follows well the observed response transition, except at point 1. Point 1 is far from the crack initiation points, and the response sensitivity is lower than other points in the model. The element deletion candidates predicted by the last updated model show good agreement with the observed external and internal cracks from the experiments, as shown in Figure 5-14 (a). The Bayes factor for each iteration was calculated, as shown in Figure 5-14 (b). The Bayes factor is exponentially decaying to a negative value. After the cyclic loading test, the internal crack is found around the predicted possible crack initiation and growth point, as shown in Figure 5-14 (c). It can be concluded that element updating can estimate crack initiation and growth.

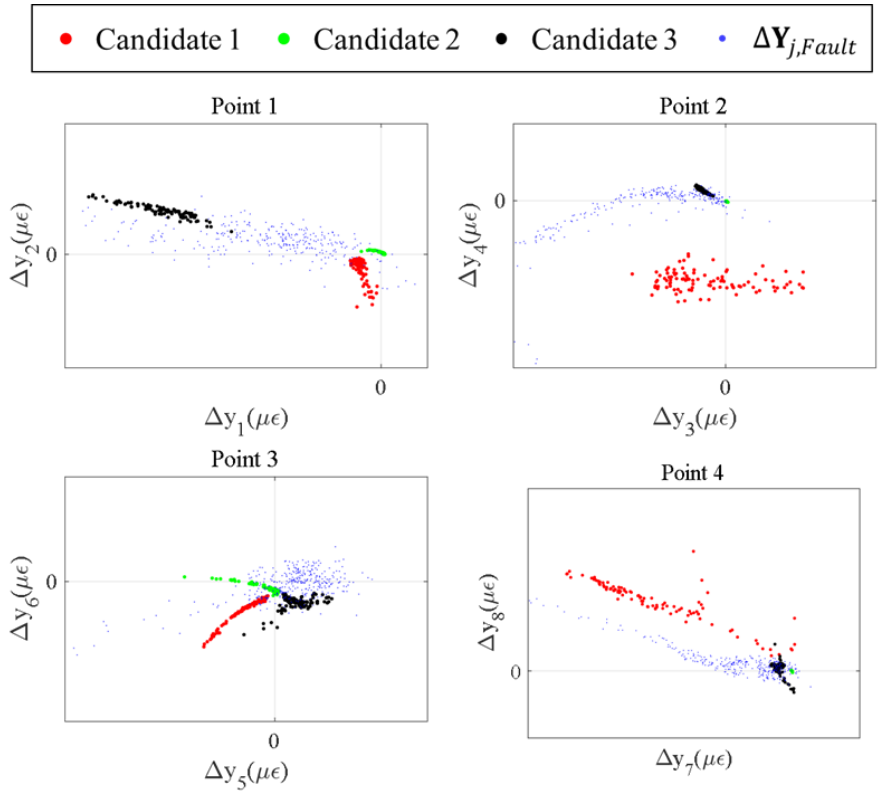

Figure 5-11 Response transition for each crack initiation candidate

$L_{i=1}(e_{n,i})$	Candidate 1 (190767)	Candidate 2 (101380)	Candidate 3 (100768)
$\sum_{j=1}^{n_{exp}} \log_{10} f_{\Delta\hat{Y}_{Crack}}(\Delta Y_{j,Fault}\|e_i)$	-3.2082e+10	-1.3775e+12	-1.7165e+14

Table 5-4 Likelihood evaluation for each candidate

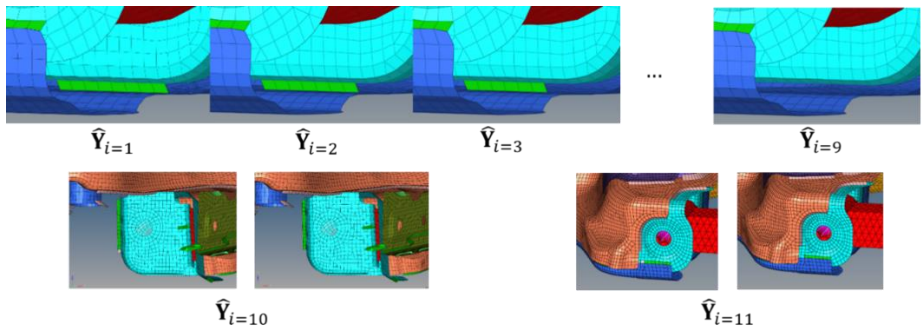

Figure 5-12 Updated models for each iteration

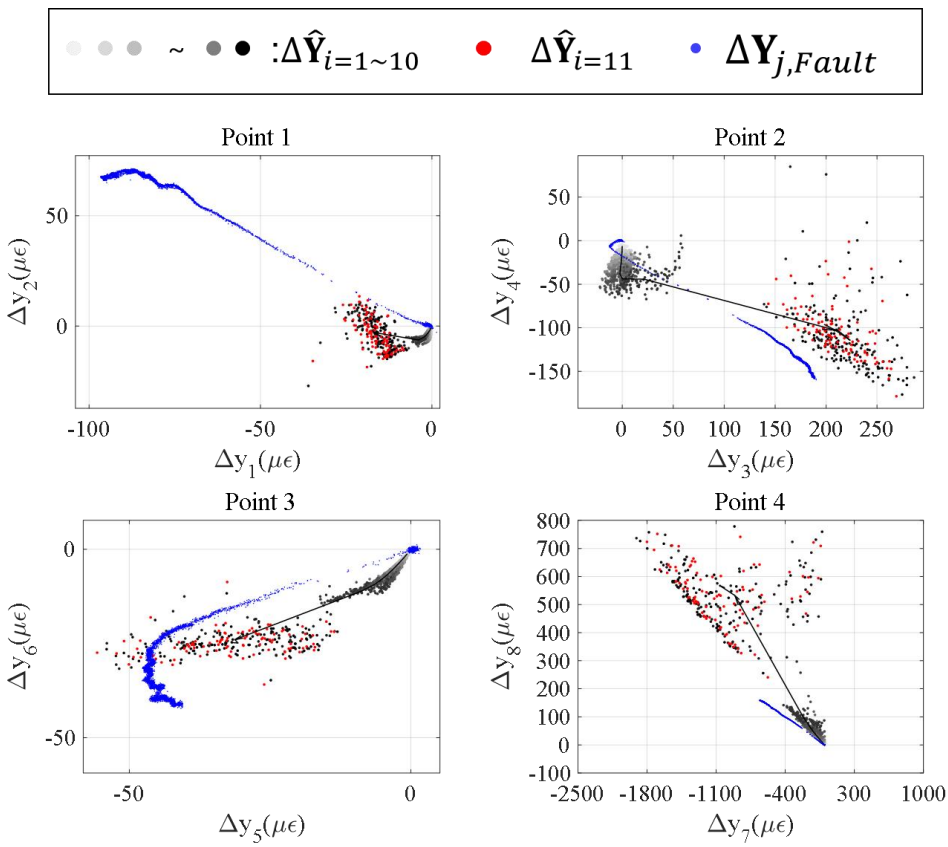

Figure 5-13 Transition of the updated and observed responses

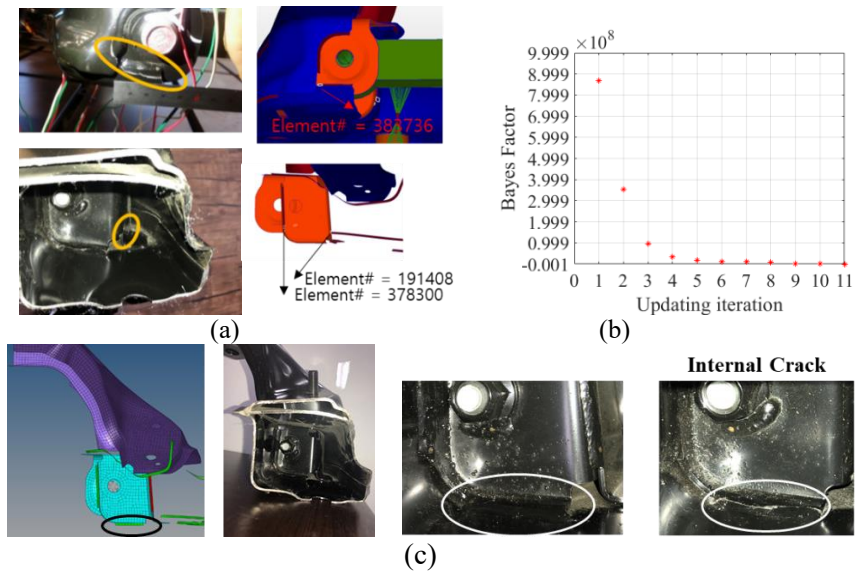

Figure 5-14 Element updating results : (a) candidate crack growth points (b) Bayes factor convergence plot (c) observed internal crack location

5.4 Summary and Discussion

In this study, a hybrid digital twin approach was proposed to estimate the crack initiation and growth using the observed response. The proposed digital twin approach is based on two techniques; (i) statistical model calibration using a data-driven twin and (ii) element updating with a physics-based twin. Marginal Probability & Correlation Residuals (MPCR) were selected as calibration metrics to consider the statistical correlation between output responses. The Gaussian process model was used as a data-driven model to substitute the physics-based twin for uncertainty propagation analysis using Monte Carlo simulation. Statistical model calibration can improve the validity of digital twins by considering uncertainty in the test conditions. Based on the observed response related to crack growth, the element

of the digital twin was updated using the element deletion method. The predicted critical elements that indicate crack initiation and growth were deleted to calculate the likelihood for each possible element. The Bayes factor, which is the updating criterion, was computed using the likelihood ratio at each updating iteration.

The proposed method was applied to an industrial problem to show the effectiveness of the method. In the experiments, the principal strains were measured on the surface of automotive structures at four points under quasi-static and cycling load. The statistical parameters of unknown input variables were inferred using observed output responses in a quasi-static load. The updated output response shows good agreement with the experimentally observed response. A validity check was quantitatively conducted to validate the calibration results. The crack initiation and growth in the fatigue test were predicted using element updating based on the observed response-related crack initiation and growth. The updated model was qualitatively validated by comparison with fatigue test results.

Sections of this chapter have been published or submitted as the following journal articles:

1) **Wongon Kim,** Guesuk Lee, Hyejeong Son, Hyunhee Choi, and Byeng D. Youn, "Estimation of Fatigue Crack Initiation and Growth in Engineering Product Development using a Digital Twin Approach," *Reliability Engineering & System Safety*, Submitted, 2021.

Chapter 6

Conclusions

6.1 Contributions and Significance

The proposed research in this doctoral dissertation aims at advancing model calibration and updating to build hybrid digital twin under insufficient prior information. This doctoral dissertation is composed of three research thrusts: (1) data-driven dynamic model updating for anomaly detection with an insufficient prior knowledge for modeling; (2) a new calibration metric formulation considering statistical correlation; and (3) hybrid model calibration and updating considering system failure. It is expected that the proposed research offers the following potential contributions and broader impacts in digital twin.

Contribution 1: Dynamic Model Updating Framework with Insufficient Prior Information for Physics-based and Data-driven Modeling

This doctoral dissertation proposes an dynamic model updating framework for anomaly detection under insufficient prior information for modeling. To the best of the author's knowledge, previous research has not addressed data driven dynamic

model updating to estimate uncertain operating condition under different noise level.

Contribution 2: Improving Optimization-based Statistical Model Calibration considering Statistical Correlation among Output Response

This study thoroughly examines what happens if the statistical correlation is neglected in model calibration. In addition, three existing calibration metrics (marginal likelihood, joint likelihood, and moment matching) are reviewed from the perspective of their ability to address the statistical correlation between multivariate output responses. To overcome the issues, a new calibration metric considering statistical correlation: Marginal Probability and Correlation Residual (MPCR) was proposed. MPCR metric has favorable properties including normalization, boundedness, and marginalization; thereby, limitations of three existing calibration metrics are overcome in this method. The proposed method allows consideration of the statistical correlation effectively; thus physically reasonable solutions can be confined. Consequently, accurate optimization-based statistical model calibration is enabled.

Contribution 3: A New Hybrid Digital Twin Approach to Estimate Fatigue Crack Initiation and Growth

To verify the structural reliability and durability of engineered products, engineers have tried to predict fatigue characteristics using an data-driven and physics-based

digital twin in engineering product development. However, the predictive capability of a digital twin model can be degraded by physical uncertainty in model formulation and test conditions. This work takes advantage of hybrid digital twin approaches that utilize both data-driven and physics-based approaches. The proposed approach includes two techniques: (i) statistical model calibration using a data-driven model and (ii) probabilistic element updating using a physics-based model. In statistical model calibration, statistical parameters of input variables can be estimated based on the observed response related to the crack initiation and growth condition. Further, the probabilistic analysis using estimated statistical parameters can predict possible critical elements that indicate crack initiation and growth. In the probabilistic element updating procedures, the possible crack initiation and growth element is updated based on the observed response. The validity and efficiency of the proposed methodology is verified through digital twin updating of an automotive sub-frame, by using the observed response related to crack initiation and growth from a fatigue test.

6.2 Suggestions for Future Research

Although the technical advances proposed in this doctoral dissertation successfully address some challenges in digital twin approach in both data-driven and physics-based approach, there are still several research topics that further investigations and developments are required to bring hybrid digital twin into an alternative solution for engineering decision support. Specific suggestions for future research are listed as follows.

Suggestion 1: Deep Learning-based Hybrid Digital Twin considering Modeling Error

As the relevant physical phenomena in an engineered system become more complex, a physics-based model needs to be more sophisticated. However, it is not easy to fully characterize the physics in the real system using a physics-based model due to limited resources (e.g., time, budget, and computation costs). The physics-based model with insufficient prior information includes various modeling errors. The engineering decisions should be made considering the error and uncertainties in the model. However, the model error and uncertainties are hard to be quantified using a small number of data and computation costs. To overcome the issue, the modeling errors can be quantified and formulated with a data-driven approach. Especially, the deep learning method can be used to integrate various error causes such as discretization and spatial and temporal uncertainty in modeling. Therefore, this issue highlights one research need of deep learning-based hybrid digital twin considering modeling error.

Suggestion 2: Experimental Design For Physically Feasible & Mathematically Unique Solution in Statistical Model Calibration

Most calibration solutions are questioned about solution uniqueness and physical feasibility. However, the model calibration, which is the inverse problem, cannot guarantee solution uniqueness and physical feasibility because of the ill-posedness

of an inverse problem. In this study, statistical correlation among output responses was considered to constraints the calibration solution. However, the solution's uniqueness and physical feasibility require a more sophisticated model calibration strategy. The sensitivity of response and uncertainty in data acquisition conditions can affect the solution convergence and uniqueness. Therefore, the experimental design for the sensor network and data acquisition should be considered to formulate statistical model calibration.

Suggestion 3: Hybrid Digital Twin Approach Including Non-linear Physics-based Model (Fluid, Battery)

As the relevant physical phenomena in an engineered system become more complex, a physics-based model includes non-linear analysis. The computation cost of non-linear analysis makes it hard to apply the digital twin approach for engineering systems with non-linear physics. Various engineering systems include non-linear physics such as a battery and energy facility with fluid flow, which must be operated and maintained using a digital twin approach. It is thus required to develop a hybrid digital twin approach including non-linear physics. Therefore, future work will include investigating the digital twin approach to deal with computationally expensive non-linear analysis while maintaining non-linear characteristics.

References

1. H. J. Lim, H. Sohn, and Y. Kim, “Data-driven fatigue crack quantification and prognosis using nonlinear ultrasonic modulation,” *Mech. Syst. Signal Process.*, vol. 109, pp. 185–195, 2018.

2. J. Guilleminot and J. E. Dolbow, “Data-driven enhancement of fracture paths in random composites,” *Mech. Res. Commun.*, vol. 103, 2020.

3. E. Zio and F. Di Maio, “Fatigue crack growth estimation by relevance vector machine,” *Expert Syst. Appl.*, vol. 39, no. 12, pp. 10681–10692, 2012.

4. Y. Xu, Y. Sun, X. Liu, and Y. Zheng, “A Digital-Twin-Assisted Fault Diagnosis Using Deep Transfer Learning,” *IEEE Access*, vol. 7, pp. 19990–19999, 2019.

5. W. Booyse, D. N. Wilke, and S. Heyns, “Deep digital twins for detection, diagnostics and prognostics,” *Mech. Syst. Signal Process.*, vol. 140, p. 106612, 2020.

6. M. S. Chowdhury, C. Song, and W. Gao, “Probabilistic fracture mechanics by using Monte Carlo simulation and the scaled boundary finite element method,” *Eng. Fract. Mech.*, vol. 78, no. 12, pp. 2369–2389, 2011.

7. X. Zhao, Z. L. Mo, Z. Y. Guo, and J. Li, “A modified three-dimensional virtual crack closure technique for calculating stress intensity factors with arbitrarily shaped finite element mesh arrangements across the crack front,”

Theor. Appl. Fract. Mech., vol. 109, no. June, p. 102695, 2020.

8. R. Krueger, “Virtual crack closure technique: History, approach, and applications,” *Appl. Mech. Rev.*, vol. 57, no. 1–6, pp. 109–143, 2004.

9. S. Rahman and J. S. Kim, “Probabilistic fracture mechanics for nonlinear structures,” *Int. J. Press. Vessel. Pip.*, vol. 78, no. 4, pp. 261–269, 2001.

10. M. Elices, G. V. Guinea, J. Gómez, and J. Planas, “The cohesive zone model: Advantages, limitations and challenges,” *Eng. Fract. Mech.*, vol. 69, no. 2, pp. 137–163, 2001.

11. P. Jain, J. Poon, J. P. Singh, C. Spanos, S. Sanders, and S. K. Panda, “A Digital Twin Approach for Fault Diagnosis in Distributed Photovoltaic System,” *IEEE Trans. Power Electron.*, 2019.

12. Y. Li, W. Jiang, G. Zhang, and L. Shu, “Wind turbine fault diagnosis based on transfer learning and convolutional autoencoder with small-scale data,” *Renew. Energy*, vol. 171, pp. 103–115, 2021.

13. O. San, A. Rasheed, and T. Kvamsdal, “Hybrid analysis and modeling, eclecticism, and multifidelity computing toward digital twin revolution,” *GAMM Mitteilungen*, vol. 44, no. 2, pp. 1–32, 2021.

14. Y. Wang, F. Tao, M. Zhang, L. Wang, and Y. Zuo, “Digital twin enhanced fault prediction for the autoclave with insufficient data,” *J. Manuf. Syst.*, vol. 60, no. March, pp. 350–359, 2021.

15. H.-S. Kim, S.-G. Jang, N.-H. Kim, and J.-H. Choi, “Statistical calibration and validation of elasto-plastic insertion analysis in pyrotechnically actuated devices,” *Struct. Multidiscip. Optim.*, vol. 54, no. 6, pp. 1573–1585, 2016.

16. K. Campbell, “Statistical calibration of computer simulations,” *Reliab. Eng. Syst. Saf.*, vol. 91, no. 10–11, pp. 1358–1363, 2006.

17. P. D. Arendt, D. W. Apley, and W. Chen, “Quantification of model uncertainty: Calibration, model discrepancy, and identifiability,” *J. Mech. Des.*, vol. 134, no. 10, p. 100908, 2012.

18. J. D. Christopher, N. T. Wimer, C. Lapointe, T. R. S. Hayden, I. Grooms, G. B. Rieker, and P. E. Hamlington, “Parameter estimation for complex thermal-fluid flows using approximate Bayesian computation,” *Phys. Rev. Fluids*, vol. 3, no. 10, p. 104602, 2018.

19. D. Higdon, J. Gattiker, B. Williams, and M. Rightley, “Computer model calibration using high-dimensional output,” *J. Am. Stat. Assoc.*, vol. 103, no. 482, pp. 570–583, 2008.

20. B. C. Jung, H. Yoon, H. Oh, G. Lee, M. Yoo, B. D. Youn, and Y. C. Huh, “Hierarchical model calibration for designing piezoelectric energy harvester in the presence of variability in material properties and geometry,” *Struct. Multidiscip. Optim.*, vol. 53, no. 1, pp. 161–173, 2016.

21. T. G. Trucano, L. P. Swiler, T. Igusa, W. L. Oberkampf, and M. Pilch,

"Calibration, validation, and sensitivity analysis: What's what," *Reliab. Eng. Syst. Saf.*, vol. 91, no. 10–11, pp. 1331–1357, 2006.

22. M. T. Wentworth, R. C. Smith, and B. Williams, "Bayesian model calibration and uncertainty quantification for an HIV model using adaptive Metropolis algorithms," *Inverse Probl. Sci. Eng.*, vol. 26, no. 2, pp. 233–256, 2018.

23. B. D. Youn, B. C. Jung, Z. Xi, S. B. Kim, and W. R. Lee, "A hierarchical framework for statistical model calibration in engineering product development," *Comput. Methods Appl. Mech. Eng.*, vol. 200, no. 13, pp. 1421–1431, 2011.

24. B. C. Jung, J. Park, H. Oh, J. Kim, and B. D. Youn, "A framework of model validation and virtual product qualification with limited experimental data based on statistical inference," *Struct. Multidiscip. Optim.*, vol. 51, no. 3, pp. 573–583, 2015.

25. H. Oh, H.-P. Wei, B. Han, and B. D. Youn, "Probabilistic Lifetime Prediction of Electronic Packages Using Advanced Uncertainty Propagation Analysis and Model Calibration," *IEEE Trans. Components, Packag. Manuf. Technol.*, vol. 6, no. 2, pp. 238–248, 2016.

26. S. Meraghni, L. S. Terrissa, M. Yue, J. Ma, S. Jemei, and N. Zerhouni, "A data-driven digital-twin prognostics method for proton exchange membrane fuel cell remaining useful life prediction," *Int. J. Hydrogen Energy*, vol. 46, no. 2, pp. 2555–2564, 2021.

27. Q. Wang, W. Jiao, and Y. M. Zhang, “Deep learning-empowered digital twin for visualized weld joint growth monitoring and penetration control,” *J. Manuf. Syst.*, vol. 57, no. August, pp. 429–439, 2020.

28. X. Li, W. Zhang, Q. Ding, and J. Q. Sun, “Intelligent rotating machinery fault diagnosis based on deep learning using data augmentation,” *J. Intell. Manuf.*, vol. 31, no. 2, pp. 433–452, 2020.

29. S. Shao, P. Wang, and R. Yan, “Generative adversarial networks for data augmentation in machine fault diagnosis,” *Comput. Ind.*, vol. 106, pp. 85–93, 2019.

30. K. Yu, T. R. Lin, H. Ma, X. Li, and X. Li, “A multi-stage semi-supervised learning approach for intelligent fault diagnosis of rolling bearing using data augmentation and metric learning,” *Mech. Syst. Signal Process.*, vol. 146, 2021.

31. B. Maschler, D. Braun, N. Jazdi, and M. Weyrich, “Transfer learning as an enabler of the intelligent digital twin,” *Procedia CIRP*, vol. 100, pp. 127–132, 2021.

32. D. Guivarch, E. Mermoz, Y. Marino, and M. Sartor, “Creation of helicopter dynamic systems digital twin using multibody simulations,” *CIRP Ann.*, vol. 68, no. 1, pp. 133–136, 2019.

33. P. Jain, J. Poon, J. P. Singh, C. Spanos, S. R. Sanders, and S. K. Panda, “A digital twin approach for fault diagnosis in distributed photovoltaic

systems," *IEEE Trans. Power Electron.*, vol. 35, no. 1, pp. 940–956, 2020.

34. L. E. Schwer, "An overview of the PTC 60/V&V 10: Guide for verification and validation in computational solid mechanics: Transmitted by L. E. Schwer, Chair PTC 60V&V 10," *Eng. Comput.*, vol. 23, no. 4, pp. 245–252, 2007.

35. W. L. Oberkampf and M. F. Barone, "Measures of agreement between computation and experiment: Validation metrics," *J. Comput. Phys.*, vol. 217, no. 1, pp. 5–36, 2006.

36. G. Han, T. J. Santner, and J. J. Rawlinson, "Simultaneous determination of tuning and calibration parameters for computer experiments," *Technometrics*, vol. 51, no. 4, pp. 464–474, 2009.

37. J. E. Mottershead, M. Link, and M. I. Friswell, "The sensitivity method in finite element model updating: A tutorial," *Mech. Syst. Signal Process.*, vol. 25, no. 7, pp. 2275–2296, 2011.

38. J. P. C. Kleijnen, "Validation of models," pp. 647–654, 1999.

39. W. L. Oberkampf and T. G. Trucano, "Verification , Validation , and Predictive Capability in Computational Engineering and Physics," *Found. Verif. Valid. 21st Century Work.*, pp. 1–74, 2002.

40. C. J. Roy and W. L. Oberkampf, "A complete framework for verification, validation, and uncertainty quantification in scientific computing (invited)," *48th AIAA Aerosp. Sci. Meet. Incl. New Horizons Forum Aerosp. Expo.*, no.

January, pp. 1–15, 2010.

41. C. J. Roy and W. L. Oberkampf, “A comprehensive framework for verification, validation, and uncertainty quantification in scientific computing,” *Comput. Methods Appl. Mech. Eng.*, vol. 200, no. 25–28, pp. 2131–2144, 2011.

42. S. P. Zhu, H. Z. Huang, W. Peng, H. K. Wang, and S. Mahadevan, “Probabilistic Physics of Failure-based framework for fatigue life prediction of aircraft gas turbine discs under uncertainty,” *Reliab. Eng. Syst. Saf.*, vol. 146, pp. 1–12, 2016.

43. I. Park and R. V. Grandhi, “A Bayesian statistical method for quantifying model form uncertainty and two model combination methods,” *Reliab. Eng. Syst. Saf.*, vol. 129, pp. 46–56, 2014.

44. W. Yao, X. Chen, W. Luo, M. Van Tooren, and J. Guo, “Review of uncertainty-based multidisciplinary design optimization methods for aerospace vehicles,” *Prog. Aerosp. Sci.*, vol. 47, no. 6, pp. 450–479, 2011.

45. S. Ferson, W. L. Oberkampf, and L. Ginzburg, “Model validation and predictive capability for the thermal challenge problem,” *Comput. Methods Appl. Mech. Eng.*, vol. 197, no. 29, pp. 2408–2430, 2008.

46. W. Li, W. Chen, Z. Jiang, Z. Lu, and Y. Liu, “New validation metrics for models with multiple correlated responses,” *Reliab. Eng. Syst. Saf.*, vol. 127, pp. 1–11, 2014.

47. X. Jiang and S. Mahadevan, “Bayesian wavelet method for multivariate model assessment of dynamic systems,” *J. Sound Vib.*, vol. 312, no. 4–5, pp. 694–712, 2008.

48. C. Li, S. Mahadevan, Y. Ling, L. Wang, and S. Choze, “A dynamic Bayesian network approach for digital twin,” in *19th AIAA Non-Deterministic Approaches Conference*, 2017, p. 1566.

49. M. Roohi, E. M. Hernandez, and D. Rosowsky, “Nonlinear seismic response reconstruction and performance assessment of instrumented wood-frame buildings—Validation using NEESWood Capstone full-scale tests,” *Struct. Control Heal. Monit.*, vol. 26, no. 9, pp. 1–22, 2019.

50. B. Wang, G. Zhang, H. Wang, J. Xuan, and K. Jiao, “Multi-physics-resolved digital twin of proton exchange membrane fuel cells with a data-driven surrogate model,” *Energy AI*, vol. 1, p. 100004, 2020.

51. M. Xia, H. Shao, D. Williams, S. Lu, L. Shu, and C. W. de Silva, “Intelligent fault diagnosis of machinery using digital twin-assisted deep transfer learning,” *Reliab. Eng. Syst. Saf.*, vol. 215, no. July, p. 107938, 2021.

52. J. Yu, Y. Song, D. Tang, and J. Dai, “A Digital Twin approach based on nonparametric Bayesian network for complex system health monitoring,” *J. Manuf. Syst.*, vol. 58, no. PB, pp. 293–304, 2021.

53. Y. Xiong, W. Chen, K.-L. Tsui, and D. W. Apley, “A better understanding

of model updating strategies in validating engineering models," *Comput. Methods Appl. Mech. Eng.*, vol. 198, no. 15–16, pp. 1327–1337, 2009.

54. S. Sankararaman, M. J. Daigle, and K. Goebel, "Uncertainty quantification in remaining useful life prediction using first-order reliability methods," *IEEE Trans. Reliab.*, vol. 63, no. 2, pp. 603–619, 2014.

55. E. Branlard, D. Giardina, and C. S. D. Brown, "Augmented Kalman filter with a reduced mechanical model to estimate tower loads on a land-based wind turbine: A step towards digital-Twin simulations," *Wind Energy Sci.*, vol. 5, no. 3, pp. 1155–1167, 2020.

56. J. T. Wang, C. J. Wang, and J. P. Zhao, "Frequency response function-based model updating using Kriging model," *Mech. Syst. Signal Process.*, vol. 87, pp. 218–228, 2017.

57. N. Bao and C. Wang, "A Monte Carlo simulation based inverse propagation method for stochastic model updating," *Mech. Syst. Signal Process.*, vol. 60, pp. 928–944, 2015.

58. S. Bi, S. Prabhu, S. Cogan, and S. Atamturktur, "Uncertainty Quantification Metrics with Varying Statistical Information in Model Calibration and Validation," *AIAA J.*, 2017.

59. P. D. Arendt, D. W. Apley, W. Chen, D. Lamb, and D. Gorsich, "Improving identifiability in model calibration using multiple responses," *J. Mech. Des.*, vol. 134, no. 10, p. 100909, 2012.

60. L. Zhao, Z. Lu, W. Yun, and W. Wang, “Validation metric based on Mahalanobis distance for models with multiple correlated responses,” *Reliab. Eng. Syst. Saf.*, vol. 159, pp. 80–89, 2017.

61. S. Eftekhar Azam, E. Chatzi, and C. Papadimitriou, “A dual Kalman filter approach for state estimation via output-only acceleration measurements,” *Mech. Syst. Signal Process.*, vol. 60, pp. 866–886, 2015.

62. A. Shrivastava and A. R. Mohanty, “Identification of unbalance in a rotor system using a joint input-state estimation technique,” *J. Sound Vib.*, vol. 442, pp. 414–427, 2019.

63. J. Seo, H. Ma, and T. K. Saha, “On savitzky-golay filtering for online condition monitoring of transformer on-load tap changer,” *IEEE Trans. Power Deliv.*, vol. 33, no. 4, pp. 1689–1698, 2018.

64. A. Hussain, S. J. Lee, M. S. Choi, and F. Brikci, “An expert system for acoustic diagnosis of power circuit breakers and on-load tap changers,” *Expert Syst. Appl.*, vol. 42, no. 24, pp. 9426–9433, 2015.

65. R. Duan and F. Wang, “Fault Diagnosis of On-Load Tap-Changer in Converter Transformer Based on Time-Frequency Vibration Analysis,” *IEEE Trans. Ind. Electron.*, vol. 63, no. 6, pp. 3815–3823, 2016.

66. E. F. Simas F, L. A. L. De Almeida, and A. C. Antonio, “Vibration monitoring of on-load tap changers using a genetic algorithm,” *Conf. Rec. - IEEE Instrum. Meas. Technol. Conf.*, vol. 3, no. May, pp. 2288–2293, 2005.

67. Q. Li, T. Zhao, L. Zhang, and J. Lou, “Mechanical fault diagnostics of onload tap changer within power transformers based on hidden Markov model,” *IEEE Trans. Power Deliv.*, vol. 27, no. 2, pp. 596–601, 2012.

68. J. Seo, H. Ma, and T. K. Saha, “A Joint Vibration and Arcing Measurement System for Online Condition Monitoring of Onload Tap Changer of the Power Transformer,” *IEEE Trans. Power Deliv.*, vol. 32, no. 2, pp. 1031–1038, 2017.

69. P. Kang, D. Birtwhistle, J. Daley, and D. McCulloch, “Noninvasive on-line condition monitoring of on load tap changers,” *2000 IEEE Power Eng. Soc. Conf. Proc.*, vol. 3, pp. 2223–2228, 2000.

70. J. J. Erbrink, E. Gulski, J. J. Smit, P. P. Seitz, B. Quak, R. Leich, and R. A. Malewski, “On-load tap changer diagnosis - An off-line method for detecting degradation and defects: Part 1,” *IEEE Electr. Insul. Mag.*, vol. 26, no. 5, pp. 49–59, 2010.

71. E. Rivas, J. C. Burgos, and J. C. García-Prada, “Vibration analysis using envelope wavelet for detecting faults in the OLTC tap selector,” *IEEE Trans. Power Deliv.*, vol. 25, no. 3, pp. 1629–1636, 2010.

72. J. Liu, G. Wang, T. Zhao, and L. Zhang, “Fault diagnosis of on-load tap-changer based on variational mode decomposition and relevance vector machine,” *Energies*, vol. 10, no. 7, 2017.

73. R. Yang, D. Zhang, Z. Li, K. Yang, S. Mo, and L. Li, “Mechanical Fault

Diagnostics of Power Transformer On-Load Tap Changers Using Dynamic Time Warping," *IEEE Trans. Instrum. Meas.*, vol. 68, no. 9, pp. 3119–3127, 2019.

74. C. AuYeung, R. M. Mersereau, and R. W. Schafer, "Maximum Entropy Deconvolution.," *ICASSP, IEEE Int. Conf. Acoust. Speech Signal Process. - Proc.*, vol. 16, pp. 273–276, 1986.

75. N. Sawalhi, R. B. Randall, and H. Endo, "The enhancement of fault detection and diagnosis in rolling element bearings using minimum entropy deconvolution combined with spectral kurtosis," *Mech. Syst. Signal Process.*, vol. 21, no. 6, pp. 2616–2633, 2007.

76. H. Endo and R. B. Randall, "Enhancement of autoregressive model based gear tooth fault detection technique by the use of minimum entropy deconvolution filter," *Mech. Syst. Signal Process.*, vol. 21, no. 2, pp. 906–919, 2007.

77. J. Park, Y. Kim, K. Na, and B. D. Youn, "Variance of energy residual (VER): An efficient method for planetary gear fault detection under variable-speed conditions," *J. Sound Vib.*, vol. 453, pp. 253–267, 2019.

78. Z. Liu, H. Zou, M. Hui, C. Dapeng, and G. Lin, "Dynamic Finite Element Model Updating for On-load Tap Changer based on Super-model," *MATEC Web Conf.*, vol. 256, p. 04001, 2019.

79. K. E. Tatsis, V. K. Dertimanis, C. Papadimitriou, E. Lourens, and E. N.

Chatzi, “A general substructure-based framework for input-state estimation using limited output measurements,” *Mech. Syst. Signal Process.*, vol. 150, p. 107223, 2021.

80. M. M. A. Al-subari, “Dedicated to my parents , siblings and my beloved ones,” no. January, 2018.

81. B. Feizifar and O. Usta, “A new arc-based model and condition monitoring algorithm for on-load tap-changers,” *Electr. Power Syst. Res.*, vol. 167, no. February 2018, pp. 58–70, 2019.

82. T. Duong, “Ks: Kernel density estimation and kernel discriminant analysis for multivariate data in R,” *J. Stat. Softw.*, vol. 21, no. 7, pp. 1–16, 2007.

83. P. L. Liu and A. Der Kiureghian, “Multivariate distribution models with prescribed marginals and covariances,” *Probabilistic Eng. Mech.*, vol. 1, no. 2, pp. 105–112, 1986.

84. T. Nagler and C. Czado, “Evading the curse of dimensionality in nonparametric density estimation with simplified vine copulas,” *J. Multivar. Anal.*, vol. 151, pp. 69–89, 2016.

85. K. Dehnad, “Density Estimation for Statistics and Data Analysis,” *Technometrics*, vol. 29, no. 4, pp. 495–495, 1987.

86. B. D. Youn, K. K. Choi, R. J. Yang, and L. Gu, “Reliability-based design optimization for crashworthiness of vehicle side impact,” *Struct. Multidiscip. Optim.*, vol. 26, no. 3–4, pp. 272–283, 2004.

87. S. C. Wu, C. H. Li, Y. Luo, H. O. Zhang, and G. Z. Kang, “A uniaxial tensile behavior based fatigue crack growth model,” *Int. J. Fatigue*, vol. 131, no. October 2019, 2020.

88. J. Hou, K. Tang, and H. Wu, “Short review on multiscale short fatigue crack growth model,” *Mater. Des. Process. Commun.*, vol. 2, no. 1, pp. 1–9, 2020.

89. A. Loghin and S. Ismonov, “Assessment of crack path uncertainty using 3D FEA and Response Surface Modeling,” no. January, pp. 1–17, 2020.

90. J. He, J. Yang, Y. Wang, H. Waisman, and W. Zhang, “Probabilistic model updating for sizing of hole-edge crack using fiber bragg grating sensors and the high-order extended finite element method,” *Sensors (Switzerland)*, vol. 16, no. 11, 2016.

91. J. Yang, J. He, X. Guan, D. Wang, H. Chen, W. Zhang, and Y. Liu, “A probabilistic crack size quantification method using in-situ Lamb wave test and Bayesian updating,” *Mech. Syst. Signal Process.*, vol. 78, pp. 118–133, 2016.

92. J. H. Song, H. Wang, and T. Belytschko, “A comparative study on finite element methods for dynamic fracture,” *Comput. Mech.*, vol. 42, no. 2, pp. 239–250, 2008.

93. T. J. Barrett, S. Takagi, N. Islam, T. Kuwabara, T. Hassan, B. L. Kinsey, M. Knezevic, and Y. P. Korkolis, “Material modeling and simulation of

continuous-bending-under-tension of AA6022-T4," *J. Mater. Process. Technol.*, vol. 287, no. May 2019, p. 116658, 2021.

94. P. Arora, M. K. Samal, S. K. Gupta, and J. Chattopadhyay, "Proposing an improved cyclic plasticity material model for assessment of multiaxial response of low C-Mn steel," *Int. J. Fatigue*, vol. 142, no. May 2020, p. 105888, 2021.

95. M. A. Eder and X. Chen, "FASTIGUE: A computationally efficient approach for simulating discrete fatigue crack growth in large-scale structures," *Eng. Fract. Mech.*, vol. 233, no. March, p. 107075, 2020.

96. P. M. Karve, Y. Guo, B. Kapusuzoglu, S. Mahadevan, and M. A. Haile, "Digital twin approach for damage-tolerant mission planning under uncertainty," *Eng. Fract. Mech.*, vol. 225, no. May 2019, p. 106766, 2020.

97. M. C. Kennedy and A. O'Hagan, "Bayesian calibration of computer models," *J. R. Stat. Soc. Ser. B (Statistical Methodol.*, vol. 63, no. 3, pp. 425–464, 2001.

98. G. Lee, W. Kim, H. Oh, B. D. Youn, and N. H. Kim, "Review of statistical model calibration and validation—from the perspective of uncertainty structures," *Struct. Multidiscip. Optim.*, vol. 60, no. 4, pp. 1619–1644, 2019.

99. B. A. Zárate, J. M. Caicedo, J. Yu, and P. Ziehl, "Bayesian model updating and prognosis of fatigue crack growth," *Eng. Struct.*, vol. 45, pp. 53–61, 2012.

100. W. Kim, H. Yoon, G. Lee, T. Kim, and B. D. Youn, “A new calibration metric that considers statistical correlation: Marginal Probability and Correlation Residuals,” *Reliab. Eng. Syst. Saf.*, vol. 195, Mar. 2020.

101. G. Lee, W. Kim, H. Oh, B. D. Youn, and N. H. Kim, “Review of statistical model calibration and validation—from the perspective of uncertainty structures,” *Struct. Multidiscip. Optim.*, vol. 60, no. 4, pp. 1619–1644, Oct. 2019.

102. H. Son, G. Lee, K. Kang, Y. J. Kang, B. D. Youn, I. Lee, and Y. Noh, “Industrial issues and solutions to statistical model improvement: a case study of an automobile steering column,” *Struct. Multidiscip. Optim.*, vol. 61, no. 4, pp. 1739–1756, 2020.

103. H. C. Lee, J. S. Choi, K. H. Jung, and Y. T. Im, “Application of element deletion method for numerical analyses of cracking,” *Manuf. Eng.*, vol. 35, no. 2, pp. 154–161, 2009.

104. V. V. Saykin, T. H. Nguyen, J. F. Hajjar, D. Deniz, and J. Song, “Material characterization using finite element deletion strategies for collapse modeling of steel structures,” *Eng. Struct.*, vol. 147, pp. 125–133, 2017.

105. V. V. Saykin, T. H. Nguyen, J. F. Hajjar, D. Deniz, and J. Song, “The effect of triaxiality on finite element deletion strategies for simulating collapse of full-scale steel structures,” *Eng. Struct.*, vol. 210, no. August 2019, p. 110364, 2020.

106. G. Ljustina, M. Fagerström, and R. Larsson, “Rate sensitive continuum damage models and mesh dependence in finite element analyses,” *Sci. World J.*, vol. 2014, 2014.

국문 초록

융합 디지털 트윈을 위한 물리-데이터 기반 모델의 통계적 모델 보정 및 갱신 방법 연구

실제 운행중인 공학 시스템의 가상 디지털 객체를 구축하여 시스템의 관측 데이터를 기반으로 실제 시스템의 다양한 상황을 모사할 수 있는 디지털 트윈 기술은 설계, 제조 및 시스템 상태 관리와 같은 공학적 의사 결정을 지원할 수 있는 솔루션을 제공합니다. 디지털 트윈 접근 방식은 1) 데이터 기반 접근 방식, 2) 물리 기반 접근 방식, 3) 융합형 접근 방식의 세 가지 범주로 나눌 수 있습니다. 융합형 디지털 트윈은 데이터 기반 모델과 물리 기반 모델을 모두 활용하여 이 두 가지 접근 방식의 단점을 극복하기 때문에 관찰된 데이터를 바탕으로 신뢰할 수 있는 공학적 의사 결정을 가능하게 합니다. 그러나 이를 적용하기 위해 필요한 시스템에 대한 사전 정보들은 대부분의 공학 시스템에서 제한적으로 이용 가능합니다. 이러한 사전 정보에는 모델 입력 변수의 통계적 정보, 데이터 기반 혹은 물리 기반 모델링에 필요한 모델링 정보, 시스템 이상 상태에 대한 물리적 사전 지식이 포함됩니다.

많은 경우, 주어진 사전 정보가 충분하지 않은 상황에서 디지털 트윈을 활용한 의사 결정의 신뢰성 문제가 발생합니다. 통계적 모델

보정 및 갱신 방법은 불충분한 사전 정보 하에서 디지털 트윈 분석을 검증 및 고도화하는 데 사용할 수 있습니다. 본 박사 학위 논문은 사전 정보가 부족한 상황에서 융합형 디지털 트윈을 구축하기 위해 모델 보정 및 갱신에서 세 가지 필수 및 관련 연구 분야를 발전시키는 것을 목표로 합니다.

유효한 디지털 트윈 모델을 구축하기 위해서는 다양한 운행 조건에서 충분한 관측 데이터와 시스템 형상, 재료 속성, 작동 조건과 같은 사전 지식이 필요합니다. 그러나 복잡한 엔지니어링 시스템에서는 모델 구축을 위한 사전 정보를 얻기가 어렵습니다. 첫번째 연구에서는 모델 구축에 필요한 사전 지식 부족 시에도 활용 가능한 데이터 기반 동적 모델 갱신 방법을 제안합니다. 제안된 신호 전 처리를 사용하여 관측된 신호에서 시스템 이상 감지를 위한 시간–주파수 영역 특성을 추출합니다. 다양한 작동 조건에서의 시스템 구동 상태를 예측하기 위해 부분 공간 상태 공간 시스템 식별 방법을 이용하여 상태 공간 모델을 구축합니다. 시스템 작동 조건은 시스템 모델의 매개변수화된 입력 신호로 정의됩니다. 다음으로, 신호 관측 시점에서의 시스템 작동 조건과 이상 상태를 추정하기 위해 입력 신호 매개변수는 기준 신호와 관측 신호의 오차를 최소화하도록 갱신됩니다.

모델 입력 변수의 통계적 정보 부족할 경우 최적화 기반 통계 모델 보정을 통해 미지 입력 변수를 추정하여 모델의 예측 능력을 향상시킬 수 있습니다. 최적화 기반 통계 모델 보정은 가상 모델의 예측 응답과 실제 시스템의 관측 응답 간의 통계적 유사성을 최대화하여 모델에 존재하는 미지 입력 변수의 통계적 모수를 추정하는 최적화 문제로 공식화 됩니다. 이때 보정 척도는 통계적 유사성을 정량화하는 목적 함수로 정의됩니다. 두 번째 연구에서는 모델 보정의 정확도와 효율성을

높이기 위해 통계적 상관관계를 고려한 새로운 보정 메트릭인 Marginal Probability and Correlation Residual (MPCR)을 제안합니다. MPCR의 기본 아이디어는 출력 응답 간의 통계적 상관 관계를 고려하면서 다변량 결합 확률 분포를 수치적 계산 비용이 낮은 다중 주변 확률 분포로 분해하는 것입니다.

디지털 트윈을 이용하여 고장 상태에 대한 사전 지식 부재한 공학 시스템의 고장 상태를 예측하기 위해, 제조 및 실험 조건의 불확실성들이 고려되어야 합니다. 세 번째 연구 방향은 고장 상태에 대한 사전 지식이 부재한 시스템의 피로 균열 시작 및 성장을 추정하기 위한 융합형 디지털 트윈 접근 방식을 제안하였습니다. 본 연구에서는 피로 균열의 시작과 성장을 추정하기 위해 두 가지 기술: (i) 통계적 모델 보정과 (ii) 확률적 요소 갱신을 제안합니다. 통계 모델 보정에서는 균열 시작 조건과 관련된 관찰된 응답을 기반으로 제조 및 실험 조건의 불확실성을 나타내는 입력 변수의 통계적 매개변수를 추정합니다. 통계적 보정을 통해 불확실성을 고려한 확률론적 물리 기반 해석을 통해 균열 시작 및 성장을 나타내는 주요 취약 요소를 예측할 수 있습니다. 확률적 요소 갱신에서는 시스템의 피로 균열 시작 및 성장을 추정하기 위해 균열 성장 조건에서 관찰된 응답을 이용한 최대 우도 법을 갱신 기준으로 모델을 갱신합니다.

주요어: 디지털 트윈
모델 검증 및 보증
최적화 기반 통계적 모델 보정
변수 추정

학 번: 2015-22710